Alma Mater Studiorum – Università di Bologna

DOTTORATO DI RICERCA IN

Biologia Cellulare e Molecolare

Ciclo XXX

Settore Concorsuale di afferenza: 05/E1

Settore Scientifico disciplinare: BIO/10

TITOLO TESI

Biochemical characterization and validation of a novel cell model for dominant optic atrophy.

Presentata da: Mario Fogazza

Coordinatore Dottorato
Prof. Giovanni Capranico

Relatore
Prof.ssa Michela Rugolo

Correlatore
Dott.ssa Claudia Zanna

Esame finale: Bologna, Aprile 2018

ABSTRACT

Mutations in the *OPA1* gene, encoding the mitochondrial dynamin-like GTPase OPA1, are well known to cause Dominant Optic Atrophy (DOA), the most common inherited optic neuropathy. The missense variants, envisaged to exert a dominant-negative effect, are associated with high risk to develop the severe multisystem disorder (DOA "plus"), characterized by extra-ocular features, including sensorineural deafness, ataxia, myopathy, chronic progressive external ophthalmoplegia, and peripheral neuropathy. Primary skin fibroblasts derived from patients bearing OPA1 mutations represent the cell model for studying DOA pathophysiology, although they often reveal a mild phenotype, as a consequence of the autosomal genetic transmission of DOA. Other genetically modified cellular models characterized by a phenotype strikingly different from wild-type, are therefore desirable.

In this study we describe a novel cell model obtained from Opa1-/- MEFs, where human OPA1 isoform 1 bearing *OPA1* mutations was expressed. Under this setting, all OPA1 protein is mutated, ruling out the effect of the wild-type allele. We present here a detailed molecular and biochemical analysis in parallel of fibroblasts and MEFs bearing three known *OPA1* pathogenic mutations (I382M, G439V, R445H) and a novel one (D603H), selected on the basis of their clinical phenotypes, ranging from very mild associated with pure optic atrophy to more detrimental causing severe syndromic forms. The results indicate that MEFs bearing *OPA1* mutations are a model useful to predict the pathogenicity of new mutations. In fact, according with the severity of the clinical phenotype of patients, the MEFs exhibit an increased number of mitochondrial dysfunctions.

In addition, we propose this cell model as a suitable tool to test drugs with potential therapeutic effect on mitochondrial diseases associated with *OPA1* mutations. Indeed, in a preliminary study we were able to to confirm the efficacy of few molecules previously identified in a yeast hight throuput screening as able to revert the pathological phenotype of a mutant Mgm1-OPA1 yeast chimera.

INTRODUCTION

Historic overview

OPA1 (Optic Atrophy 1) is a nuclear gene, first mapped in the 3q28-qter region (1), that encodes for a dynamin-related protein localized in the inter-membrane space (IMS) of mitochondria, anchored to the mitochondrial inner membrane (IMM) (2,3). The name derives from Dominant Optic Atrophy (DOA), a disease caused by mutations in this gene (4,5), disease firstly described in 1959 (6) and characterized by degeneration of the retinal ganglion cells (RGCs) and optic nerve atrophy.

OPA1 is a conserved dynamin-related GTPase, its expression is ubiquitous, but quantitatively variable depending to the organ or tissue examined. High mRNA expression levels are present in retina, brain, liver, heart and pancreas (4,7,8).

OPA1 was initially associated with the mechanism of fusion of the IMM (9), but as time went on OPA1 has been recognized to be implicated also in other important mitochondrial functions, such as the maintenance of the complex architecture of *cristae* (10), which in turn controls the onset of apoptotic process by regulating the release of the cytochrome c from the *cristae* into the cytoplasm. OPA1 was also shown to be able to directly interacts with some respiratory complexes, thus stabilizing the oxidative phosphorylation system (11). It is also required for the supramolecular organization of respiratory supercomplexes, which is strictly linked to energetic efficiency (12), and, finally, it contributes to maintenance of the mitochondrial DNA stability, probably by anchoring this genome to the IMM (13).

From the gene to the function

OPA1 gene and protein

Mapped by linkage studies short tandem repeat polymorphisms (1), in 2000, using different approaches, two European groups simultaneously identified the first mutations in the OPA1 gene (4,5) the human of yeast ortholog Mgm1p/Msp1p.

The gene spans more than 100kb and is composed of 31 exons, and the alternative splicing of the exons 4, 4b and 5b generate 8 different isoforms with a great variability of expression between them in different human tissues, suggesting a fine regulation of OPA1 mRNAs. All OPA1 isoforms are ubiquitously expressed, nevertheless splicing variants containing exon 4 are consistently more represented. In the brain the exons 4 and 4b, alone or combined, are predominant. The exon 4 is evolutionarily conserved, while the exons 4b and 5b are both specific to vertebrates (8,14).

The eight OPA1 mRNA splice forms encode proteins of 924–1014 aminoacids, presenting at the N-terminus an amphiphilic mitochondria targeting sequence (MTS) followed by a transmembrane domain (TM), acting as a stop transfer signal, anchoring the protein at the IMM and leaving most of it in the IMS (2), and the three alternate spliced exons 4, 4b and 5b (8). While apparently the exon 4 does not include any noteworthy domain, exon 4b and 5b encode two additional hydrophobic domains, TM2a and TM2b. The 5b exon also presents a coiled-coil domain (CC0). The following portion of the protein contains the conserved dynamin regions: the GTPase domain, with a coiled-coil domain (CC1), the middle domain, whose function is unknown, and the C-terminus GTPase effector domain (GED) also presenting a coiled-coil domain (CC2) (8,15).

The two main coiled-coil domains, CC1 and CC2, exhibited only the capacity to self-interact to form homo-oligomers, without showing the ability to cross-interact with other peptides. In support of this, mutations known to cause DOA located on the CC2 were shown to abolish its capacity of self-interact. Conversely, the analysis of the CC0 domain supported the hypothesis of a hetero-interaction with CC1 domain on the same OPA1 protein, rather than an homo-interaction (16).

After import of the precursors through the mitochondrial membranes and cleavage of the MTS by the mitochondrial processing peptidase (MPP), OPA1 may be further processed at two N terminus cleavage sites, named S1 and S2, located on exons 5 and 5b respectively. The proteolytic cleavage is carried out by the two IMM peptidases YME1L and OMA1 to

produce a defined combination of membrane-anchored long forms (l-forms) and short forms (s-forms) soluble in the IMS, which can be peripherally attached to the IMM or diffuse in the IMS and associate to the OM (17). Furthermore, the four isoforms including the exon 4b are completely cleaved into the short forms (18).

Finally YME1L and OMA1 are reciprocally degraded in response to distinct types of cellular stress, thus modulating the proteolytic processing of OPA1 (19).
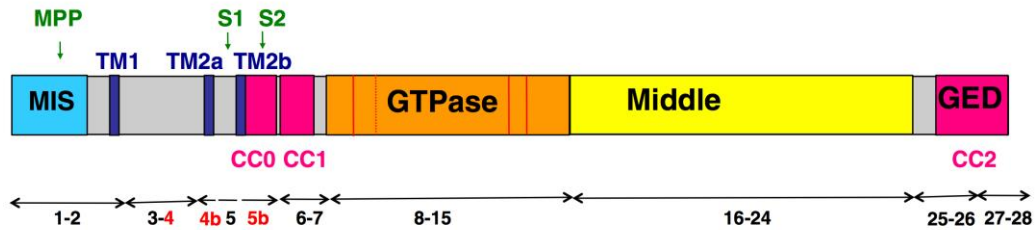
Figure 1. Schematic representation of OPA1 protein domains. Cleavage sites are highlighted in green, trans-membrane domains in blue, coiled-coil domains in pink, the three alternatively spliced exons in red (from Belenguer et all., 2013)

.

The role of the eight isoforms

As mentioned above, eight isoforms of OPA1 exist, formed by different combinations of the three alternatively spliced exons 4, 4b and 5b. Thus, question has been raised whether each of these exons were associated with a specific OPA1 function, to assess which each of the three alternative exons has been selectively silenced in HeLa cells. Since the variants including the exon 4 represents ~90% of the total protein, its silencing provoked a drastic decrease of OPA1 level, causing mitochondria network fragmentation and depolarization, without signs of cytochrome c release or apoptosis, whereas the silencing of exons 4b and 5b provoked apoptosis, with a slow cytochrome c release, only minor *cristae* modifications and without mitochondrial fission or depolarization (8).

Later, the same group proved how silencing of the exon 4b, but not the others, caused significant mtDNA depletion and an uneven distribution of the nucleoprotein complexes or nucleoids throughout the mitochondrial network. Furthermore, the N-terminal OPA1 peptide including the and exon 4b, released after the proteolytic cleavage, was shown to physically interact with mitochondrial transcription factor A (TFAM) and DNA polymerase gamma (POLG), the main protein components of nucleoids, and with mtDNA. It was therefore proposed that exon 4b containing OPA1 variants may promote mtDNA

4

stability by anchoring the nucleoids to the IMM, which in turn guarantees mtDNA replication, nucleoids abundance and proper distribution along the network (13).

It seems therefore that specific mitochondrial functions may be associated with the three differentially spliced exons of OPA1, i.e. the exon 4 containing variants could be responsible for fusion of the IMM, the exon 5b variants could preserve the tightness of the cristae junctions, preventing the release of cytochrome c, and the exon 4b variants could promote the mtDNA stability, but these data give us no indication about the need of having eight different isoforms.

Thus, in order to evaluate whether a single OPA1 isoform is specifically associated with a definite mitochondrial function, we carried out a detailed molecular and biochemical analysis in a murine cellular model where OPA1 was deleted, the Opa1-null murine embryonal fibroblasts (MEFs), where every individual OPA1 splice form has been stably expressed alone. Our analysis highlighted that every isoform was able to recover the major phonotypes affected by Opa1 depletion, such as mtDNA content, *cristae* organization and energetic competence (20). However, the completely fragmented mitochondrial network observed in Opa1-/- MEFs was only in part rescued by mRNA splice forms generating both long and short forms, in accord with a previous report (18). Using two different approaches, co-expressing different couples of isoforms in Opa1-/- MEFs, and co-silencing with different combinations two out of the three alternatively spliced exons in HeLa cells, we concluded that to fully recover even the mitochondrial network morphology, both an adequate amount of OPA1 protein and at least two isoforms with a defined long/short forms ratio are needed (20).

We therefore sustain the presence of a hierarchy in the mitochondrial features the cell first needs to recover, being mtDNA, *cristae* organization and energetic competence equally important to restore the cellular metabolic efficiency and strictly related one with each other. We proved that every OPA1 isoform has, alone, the capacity to recover these main features, apparently in contrast with transient silencing experiments results, but actually, the two models give us different information. In fact, while the "chronic" model, with the stable expression of any single isoform, reveals that each isoform has the potential to recover those features, the "acute" model, with the transient silencing, suggests that in a physiological context each variant, moreover expressed at different levels, can carry out preferentially a specific function (20).

Thus, each OPA1 isoform is not specifically associated with a definite mitochondrial function, but rather the redundancy of their potentials provides mitochondria of the

necessary flexibility to withstand and adapt to different metabolic and stress conditions in highly specialized tissues.

Transcriptional regulation

OPA1 expression is ubiquitous, but its regulation is still not fully understood, although it seems to lay downstream several pathways.

Together with MFN2, OPA1 is reported to be upregulated during bone marrow progenitor differentiation and to promote the migration of immature dendritic cells (21).

Novel *in vitro* evidence indicates that TNFR2 activation upregulates OPA1 expression, with the acetylation of STAT3 at lysine 370 and/or 383 by p300 playing an essential role, enabling the interaction of STAT3 with RelA to bind to the promoter region of OPA1 and enhance transcription. TNFR2 activation in an *in vivo* transverse aortic constriction-induced heart failure mouse model exerted beneficial effects on OPA1 expression, improving mitochondrial morphology and respiratory activity, leading to improved cardiac function and survival rate (22).

Treatment of cardiomyocytes *in vitro* and *in vivo* with insulin also increased Opa-1 protein levels, ameliorating mitochondrial functions as fusion, membrane potential, ATP levels and oxygen consumption. This has been achieved through the Akt-mTOR-NF-κB signaling pathway, highlighting the existence of a link between mitochondrial morphology and insulin signaling in cardiac and skeletal muscle cells and potentially with the onset of insulin resistance (23). It is known that under stress condition, OPA1 is transcriptionally upregulated via NF-kB-responsive promoter elements for maintenance of mitochondrial integrity and protection from stress-induced cell death.

Some studies suggest that this is due to parkin recruitment to the linear ubiquitin assembly complex and increases linear ubiquitination of NF-kB essential modulator (NEMO), which is essential for canonical NF-κB signaling. Accordingly, linear ubiquitination of NEMO, activation of NF-κB and upregulation of OPA1 are significantly reduced in response to TNF-a stimulation in parkin-deficient cells (24).

In contrast to this, a more recent study proposes that the protective effect of parkin may rather be related to the ubiquitination of Bax impairing its mitochondrial translocation. Indeed this study shows that the absence of IKKα, with or without IKKβ, has an impact on OPA1 expression and mitochondrial network morphology, pointing out a role of the

nonclassical NF-κB pathway rather than the canonical one, in the regulation of mitochondrial dynamics and OPA1 expression (25)

Another recent study displays that T-cell intracellular antigens (TIA1b/TIARb) and Hu antigen R (HuR) exert antagonistic roles in regulating expression of mitochondrial shaping proteins. In particular, while HuR functions as a translational activator increasing steady-state levels of the protein, TIARb operates as a translational repressor, both in a 3'-UTR-dependent manner on the OPA1 mRNA. Moreover, TIA1 and TIAR modulate alternative splicing of OPA1 pre-mRNA, promoting exon 4b inclusion and exon 5b skipping, facilitating the production of short OPA1 forms (26).
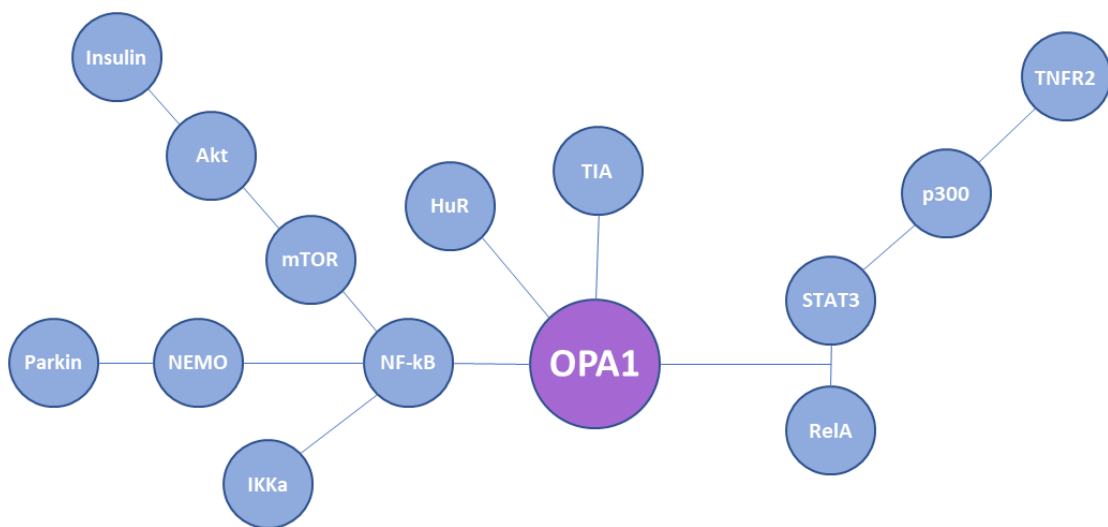
Figure 2. Schematic representation of factors known to be involved in the transcriptional and post-transcriptional regulation of OPA1 mRNA.

Proteolytic processing

The primary sequence of OPA1 presents two cleavage sites, S1, present in all the isoforms and located at exon 5, and S2, present only in the isoforms containing exon 5b. Thus, each mRNA splice form can generate a long form, produced by cleavage with MPP, and one or more short isoforms (produced by cleavage at S1 or S2). But, as mentioned above, OPA1 isoforms containing exon 4b are totally processed into short forms (18,27).

Several and sometimes discordant studies have identified different proteases recognizing the two cleavage sites of OPA1 in human cells. The presilin-associated rhomboid-like protease (PARL) seems to be involved in the generation of a soluble short form of OPA1 in the IMS (28). The m-AAA proteases, are present in the IMM as AFG3L2 homo-

oligomers or AFG3L2-paraplegin hetero-oligomeric complexes (29). Overexpression of paraplegin induces the accumulation of short forms of OPA1 by cleavage at S1 (27). Down-regulation of AFG3L2 decreased the stability of long OPA1 forms (30). Nevertheless, neither PARL nor paraplegin are involved exclusively in OPA1 processing. Indeed, knocking them down/out does not alter the long/short forms ratio (27).

Down-regulation of ATP-independent protease OMA1 lightly decreased the levels of OPA1 short forms, generated by cleavage at S1 site and accumulated at low levels in MEFs (30,31). The cleavage at S2 is ascribed to the ATP-dependent AAA+ protease YME1L (18,32). The MEFs OMA1- and YME1L- double knockout contained only long forms of OPA1 (33). OMA1 and YME1L have many independent functions but cooperate to regulate their differential processing of OPA1. Moreover, these two proteases are reciprocally degraded in response to insults that depolarize mitochondria in a process dictated by cellular energetic status. OMA1 is degraded through a YME1L-dependent mechanism following insults that depolarize mitochondria. Alternatively, YME1L is degraded in response to insults that depolarize mitochondria and deplete cellular ATP through a mechanism involving OMA1. This differential degradation alters their proteolytic processing of OPA1 (19).

Moreover, even prohibitins are involved in the processing of OPA1 Indeed, their deletion results in selective loss of long forms of OPA1 and concomitant increase of the short forms (34,35), although the mechanism underlying the effect of prohibitins is not known.

Post-translational regulation of OPA1 comprises, in addition to proteolytic processing, also other modifications that take part in the regulation of other proteins involved in the mitochondrial dynamics. In this respect, the deacetylation of OPA1 lysines 926 and 931 by SIRT3 has been shown to increase OPA1 GTPase activity and to recover mitochondrial functions in OPA1 -/- cells (36). Moreover, OPA1 has been demonstrated to be the substrate of the leucine-rich repeat kinase 2 (LRRK2, PARK8), whose mutations are commonly associated with autosomal dominant familial Parkinson's disease. In this regard, mutations in the kinase domain of LRRK2 proved to reduce the steady-state levels of short forms of OPA1 in human Parkinson's brain (37).


Protein structure

OPA1 is a member of a family of highly conserved GTPases related to dynamin, has the same domain architecture as the dynamin-like proteins, compared to the classical dynamins

lack of the prolin-rich domain, but has an additional amino-terminal mitochondrial import sequence that is followed by a transmembrane and coiled-coil sequence (38). While the primary structure of the protein, in every of its isoform, is well known, the information we have about the upper level structure are fragmentary because the three-dimensional structure of OPA1 has not be resolved by experimental procedures such as NMR and X-ray crystal analysis and there is little information on the structure of the complex between OPA1 and GTP.

First attempt to obtain a structural homology model of the OPA1 GTPase domain yielded the Dictyostelium dynamin A GTPase domain as the most similar structure (39). After manual refinement, OPA1 and Dictyostelium dynamin A GTPase domains could be superposed, showing that the resolved G1, G3 and G4 signatures, involved in the coordination of GDP/GTP and the Mg^{2+} ion, essential for GTP hydrolysis, could be structurally and functionally mirrored in the OPA1 GTPase domain model (40).

Later, bacterial dynamin like protein (BDLP) was identified as the most significant hit in a profile–profile sequence searches with a sequence identity of 13% in the C terminal region of OPA1 (residues 220–960), thus the BDLP coordinates (41) were used as a template for modelling the OPA1 structure. The model obtained was used to map some missense mutations found in DOA patients, most of which reside in the highly conserved GTPase domain. These missense mutations (A357T, G439V, R445H, S545R) affect the GTPase domain just adjacent to its active site potentially interfering with nucleotide binding and altering the affinity and hydrolysis rate of the GTPase domain. The only missense mutation differently located (V910D) resides at the interface of the two effector domains performing the conformational change (42).

Recently, homodimer structural models of wild-type and mutant OPA1 were predicated. Molecular modeling was performed with a region containing the GTPase domain and part of the middle domain of the dimer crystal structure of human Dynamin 1 (43) as a template. The analyses predicted decreased dimer formation of OPA1 and decreased GTP binding as the causes of the disease symptoms associated with these mutations (44). Indeed, dynamin-related proteins are known to homo- and hetero-oligomerize (45).
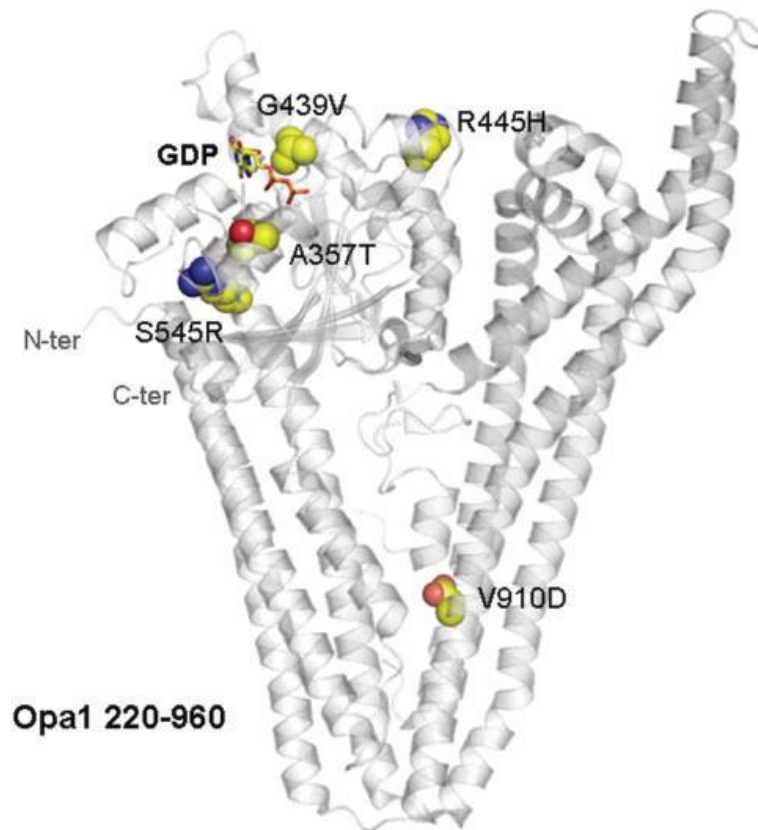
Figure 3. Human OPA1 homology model from residue 220 to 960. GDP depicted in sticks, DOA mutations depicted in spheres. (from Amati-Bonneau et al., 2008)

Oligomerization and interactors

Peptide analysis of the OPA1 protein demonstrated specific self-interaction of two coiled-coil domains, the CC1 in the GTPase domain and CC2 in the C-terminal GED domain, while the CC0 in the exon 5b could only hetero-interact with the CC1. Being so near to the TM domain, the CC1 domain of the long forms may be sterically hampered from interaction because of the membrane bound, while their CC2 domain could still interact with other OPA1 molecules in the IMS. Instead, the processing to short forms would allow free interaction even of the CC1 domain supporting the formation of larger aggregates via both coiled-coil domains. However, in short forms of isoforms bearing the exon 5b could only a dimer formation via CC2, because of the presence of CC0, which blocks CC1 interaction. (16)

First evidence that of OPA1 can form oligomers of different molecular weight in the IMS came by experiments where mitochondria isolated from HeLa cells were solubilized with 1% Triton X-100 and subjected to gel filtration. Western blots of each fraction revealed

that the long and the short forms of OPA1 were eluted at distinctly different peak with apparent molecular weight of 440 and 158 kDa, respectively, with the short form being found in a broad molecular weight range, approximately from 400 to 150 kDa. This analysis could not clarify if these complexes were homo- or hetero-oligomers. Given their differential sub-mitochondrial localization, since OPA1 long forms were found associated to the IMM and the short one both in the IMS and associated with OMM, these different molecular mass complexes should consist of different proteins (3).

Similar results have been obtained in purified mitochondria isolated from different mouse tissues by using the same purification protocol, but with milder detergents to avoid aberrant migration. OPA1 was detected in fractions, corresponding to the apparent molecular weight of 285 and 184 kDa, respectively. In all tissues the peak levels of long forms and the short forms without the 5b were found in fractions corresponding to the 285 kDa complexes. Whether the different isoforms form individual homomeric complexes or interact in one large heteromeric complex remains to be elucidated. In contrast, the highest peak intensity for short form with the exon 5b was observed in the fraction corresponding to the small complex of 184 kDa (16)

Another group identified by chemical crosslinking an ~290 kDa OPA1 immunoreactive band that disappeared when *cristae* membranes were separated by osmotic swelling. Using tagged versions of long and short forms of OPA1, they demonstrated that this oligomer contained both. The size of the OPA1 oligomer suggested the presence of at least a trimer comprising two long and one short form of OPA1. They also found OPA1 in a ~230 to ~180 kDa fraction after *in vitro* treatment of mitochondria with cleaved p7/p15 BID (cBID), suggesting that OPA1 can associate with other proteins during apoptosis. (10). During apoptosis, these oligomers are early targets of BID, BIM-S, and BNIP3, the latter being proved to co-immunoprecipitate with OPA1, as well as of intrinsic death stimuli, with their disruption being associated with *cristae* remodeling (10,46,47).

Further analysis by western blot of blue native gel electrophoresis (BNGE) of mitochondrial proteins revealed four major OPA1-containing complexes, the heavier of which, ~720 kDa molecular weight complex, rapidly disappeared upon treatment with cBID (12). Accordingly, the OPA1 oligomers targeted by cBID to trigger *cristae* remodeling and cytochrome c redistribution were stabilized in Opa1 isoform1-overexpressing mice mitochondria. All together, these data show that mild OPA1 overexpression hampers apoptotic cristae remodeling *in vivo* (48).

A fraction of OPA1 was found to co-immunoprecipitated with MIC60 (49) and MIC25 (50), core proteins of the mitochondrial contact site and *cristae* organizing system (MICOS). Moreover, a ~180–190 kDa complex stabilized by crosslinking was found to be immunoreactive for both OPA1 and MIC60, and this complex was also reduced in apoptotic cBID-treated mitochondria. Not only the ~720 kDa OPA1 but also complexes that partially overlap with it containing MIC60 and MIC19, another crucial MICOS component that regulate *cristae* junctions' biogenesis, were selectively destabilized during apoptotic *cristae* remodeling, data confirmed also by mass spectrometry analysis and quantitative proteomic analysis. All these evidence together show that OPA1 not only interact, but is also epistatic to MICOS in the regulation of *cristae* shape (49).

The list of the proteins proved to interact with OPA1 become longer over time, most of them being involved in the energy production or in apoptosis and mitophagy mechanisms. To the first category belong the RCSs. Indeed, it has been shown that, within the *cristae* membrane, OPA1 directly interacts with subunits of CI, CII, CIII (11) and CIV (51). Furthermore, recently two proteins involved in the GTP fueling of OPA1, NDPK-D (mitochondrial nucleoside diphosphate Kinase, also called nonmetastatic protein 23-H4 or Nm23-H4) and WBSCR16 (Williams-Beuren syndrome critical region 16), were found to physically interact with OPA1, being located in the IMS bound to the IM (52–54).

Both long and short forms of OPA1 co-immunoprecipitated even with SIRT4, a stress-responsive mitochondrial sirtuin that controls cellular energy metabolism in a NAD$^+$-dependent manner and is implicated in cellular senescence and aging. Only the enzymatically active SIRT4 triggered an unbalance of the long/short OPA1 ratio toward the long forms, and interacted with the long form of OPA1. This OPA1 long form stabilization could involve direct or indirect protein-protein interaction or even a mechanism of protection from stress-induced or protease mediated processing (55).

Among the proteins that proved to co-immunoprecipitate with OPA1, the reactive oxygen species modulator 1 (ROMO1), belong to the protein involved in the mitochondria quality control mechanisms, being a redox-regulated protein shown to be important for mitochondrial fusion activity and normal cristae morphology. Not only knockdown of ROMO1 promoted mitochondrial fission and led to an imbalance in OPA1 isoforms abundance that favored the accumulation of the short form of isoform 1, but ROMO1 also proved to be essential for the oligomerization of OPA1 (56).

It seems also that overexpression of Hypoxia-induced gene domain protein-1a (Higd-1a), a IMM protein that plays a role in cell survival under hypoxic conditions, directly inhibits

the processing of Opa1 induced by hypoxia and CCCP, finding also corroborated by the co-immunoprecipitation of Higd-1a with Opa1, and in particular only with the long forms of it. Indeed, the soluble short forms of Opa1 did not interact with Higd-1a at all, so the N-terminal domain of Opa1 appears essential for its interaction. Moreover, the deletion of a N-terminal portion of Higd-1a, a region that includes some highly conserved basic amino acids and is located in the IMS proximal to the TM domain, completely eliminated its interaction with Opa1 and its fusogenic activity. Thus, due to its position Higd-1a can approach the N-terminal domain of Opa1. Furthermore, even MFN1 can be co-immunoprecipitated together with OPA1 and Higd-1a, but the interaction with the latter seems to be indirect, because Opa1 knockdown or cleavage eliminated also the interaction of MFN1 with Higd-1a (57).

Another protein, involved in apoptosis and in the mitophagy mechanism, proved to co-immunoprecipitate with OPA1, is the FUN-14 domain containing protein 1 (FUNDC1), that is able to anchor OPA1 through its lysine 70 residue toward the inner face of OMM. Under mitochondrial stresses conditions, OPA1 is cleaved or even degraded, thus promoting mitochondrial fission, required for mitophagy (58).

Furthermore, OPA1 was found to co-immunoprecipitate also with Omi/HtrA2, a serine protease released as a pro-apoptotic factor from the IMS into the cytosol. The loss of this protein is known to cause nerve cell loss in mouse models and has been linked to neurodegeneration in Parkinson's and Huntington's diseases. In cells, loss of Omi/HtrA2 provoked a selective up-regulation of more soluble OPA1 protein. Interestingly, the accumulated long forms of OPA1 were degraded more rapidly upon proteinase K digestion. Also, an increase of the small cytosolic pool of OPA1 in the Omi/HtrA2 KO cells has been found (59). The release of OPA1 were already been described upon disruption of OPA1 engagement in *cristae* junctions (10).

Finally, two of the already discussed post-translational regulators of OPA1, in particular SIRT3 and LRRK2, have been demonstrated to physically interact with OPA1 (36,37).
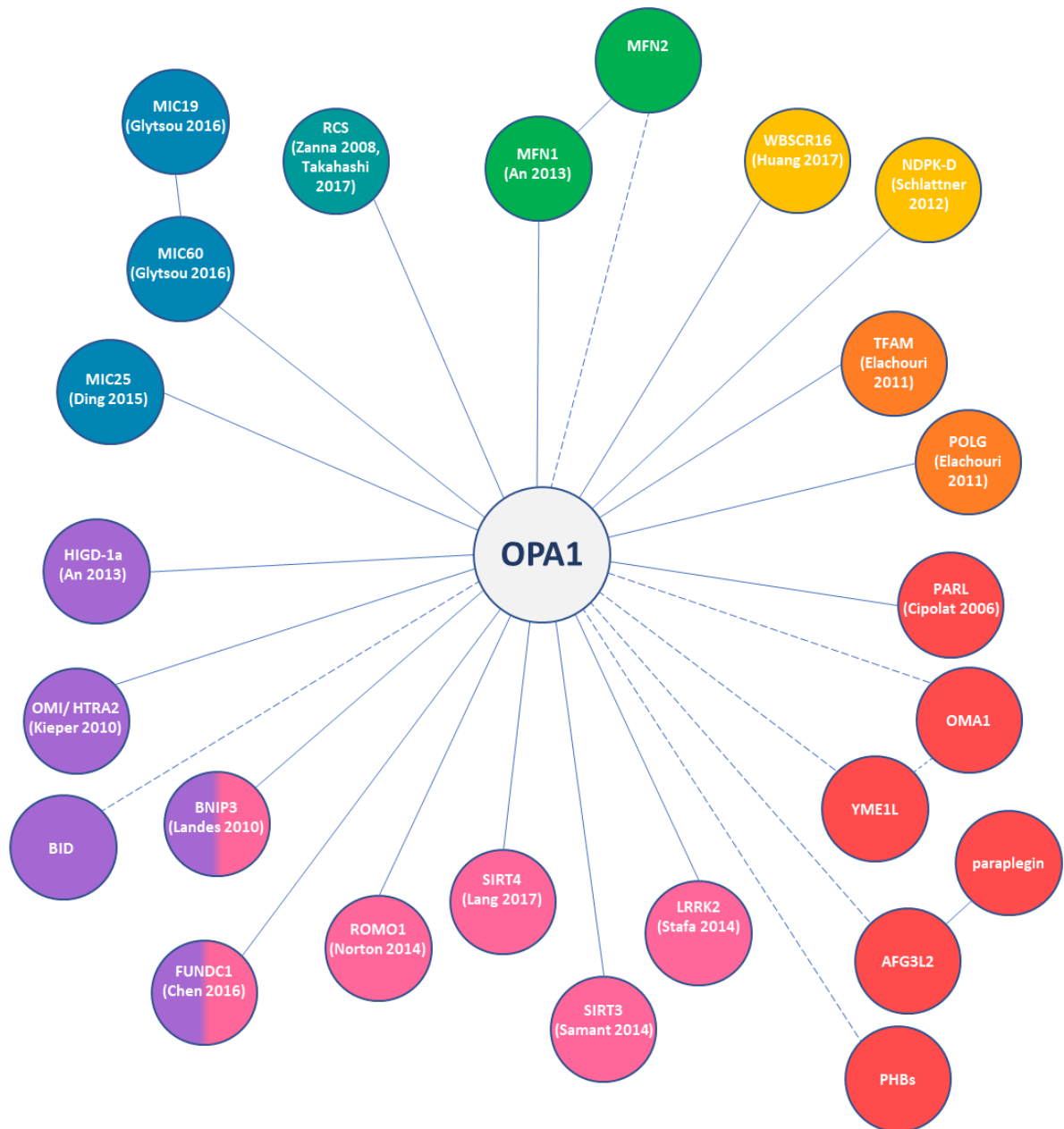
Figure 4. Schematic representation of all the proteins known (solid lines) or supposed (dashed lines) to physically interact with OPA1. The colors identified proteins involved in: green – mitochondrial fusion, petrol blue – energetics, blue – *cristae*, purple – apoptosis, pink – mitochondria quality control, red – proteases, orange – nucleoids, yellow – ATP/GTP exchange.

The functions in the mitochondrial landscape

Mitochondrial dynamics and long/short balance

When observed by live-cell imaging, mitochondria appear as an interconnected network that spreads through the cell. This structure is not static, being dynamically regulated by constitutively ongoing fusion and fission processes occurring at the two mitochondrial membranes. In mammals, the mitochondrial network dynamics involves four proteins, each playing a specific role: DRP1 is in charge of mitochondrial fission, MFN-1 and -2 and OPA1, are responsible for the fusion of OMM, and IMM, respectively.

The OPA1 orthologs in yeasts, Mgm1p and Msp1p, were initially identified for their involvement in the maintenance of mitochondrial genome, and only later associated with mitochondrial fusion. OPA1 was first identified by linkage studies, and from the beginning associated with mitochondrial dynamics. In agreement with its localization in the IMS, its primary function was demonstrated to be the fusion of the IMM. Indeed, several studies disclosed that OPA1 loss of function, by gene knock-out or knock-down, leads to a fragmented mitochondrial network (9,18,60–62). Noteworthy, the OPA1 overexpression in a physiological context also induces network fragmentation, whereas in cells where mitochondrial network was already fragmented the overexpression of OPA1 promotes its elongation (2,60). A mild OPA1 overexpression also inhibited apoptotic cristae remodeling and corrected the altered cristae shape and defective mitochondrial bioenergetics in mouse models of primary mitochondrial diseases (12,48,49,63).

The fusogenic activity has been initially ascribed to the OPA1 variants bearing the exon 4, as suggested by silencing experiments (8), but recently our and another group independently established that any isoform processed in both long and short forms has the capability to restore mitochondrial network morphology in Opa1-/- MEFs. (20,64). Moreover, both studies demonstrated that the expression of an un-cleavable isoform 1 in Opa1-/- MEFs allows for mitochondrial fusion, beside not being able to restore the interconnected network morphology (20,64). Indeed, is now clear that even if the mitochondrial fusion is indispensable to the network to be interconnected, the ability to fuse does not assure a filamentous and interconnected mitochondrial morphology. Thus, fusion capability and mitochondrial morphology have to be considered as distinct phenotypes.

The initial hypothesis was that the OPA1 long forms only were fusion competent, whereas short forms were unable to promote fusion (27). Indeed, *in vitro* experiments evidenced that a recombinant OPA1 short form was able to tubulate membranes, but could not induce membrane fusion (65). More recently, by using an *in vitro* fusion assay, the same group clearly demonstrated that OPA1 long forms on one membrane and cardiolipin on the other are the minimal components sufficient and necessary for the two membrane to fuse (66). Moreover, this study confirmed that the short forms are involved in the fusion process, but are not able to promote it without the long forms. Indeed, addition of the short forms to the minimal components accelerated the fusion process and promoted liposome binding, suggesting that the soluble short forms may act like a bridge between the two membranes, linking the long forms on one side and the cardiolipin on the opposite one (66).

Still, a residual fusogenic activity of short forms can be detected when expressed in Opa1-/- MEFs (20,64), whereas mutations that ablate the GTPase activity totally prevent fusion (20). Accordingly, the artificial anchoring of the short forms to the membrane via a lipid tail (66), or by fusion of the N-terminal portion of the IMM protein AIF (20), resulted in a significant increase in membrane fusion. Taken together, these results support the hypothesis that both the functional GTPase domain and the membrane anchoring are necessary to promote fusion, in accord with previous studies on Oma1 and Yme1l double knockout MEFs, where the formation of short forms is blocked, and long forms alone are sufficient to promote mitochondrial fusion (Anand et al., 2014).

Conversely, the role of the short forms is still debated. Anand and colleagues suggest that they are involved in mitochondrial fission, given that the expression of a chimeric AIF-short form did not modify the fusion rate while increasing mitochondria fragmentation in a GTPase activity dependent manner. Moreover the GTPase-inactive AIF-short form co-localizes with sites of mitochondrial division (33). Still, it must be noticed that the AIF domain of this chimaera contains a trans-membrane sequence that may compromise the solubility of this short form, resulting in a shorter membrane anchored form.

Thus, the long/short forms ratio seems to play a major role in the mitochondrial network morphology. In Opa1-/- MEFs, several studies pointed out that only the expression of the long and short forms together was able to elongate the mitochondrial network, whereas it remained completely fragmented after the expression of an uncleavable long version of the isoform 1, despite its proved fusogenic capability (18,20,64). Still, another group is discordant about the uncleavable form fragmentation recover, stating that that OPA1 processing is dispensable for the ability to maintain tubular interconnected mitochondria

(33). However, for a full recovery of the mitochondrial network morphology due to ablation of Opa1 in MEFs, only partially rescued by the expression of one isoform generating both long and short forms, the expression of at least two isoforms with a balanced long/short forms ratio is required (20).

Conversely, the overexpression of long form re-equilibrated the accumulation of OPA1 short forms in rat retinal cells exposed to ischemia-reperfusion injury, preventing fragmentation of mitochondrial network and cell death (67). Furthermore, in both Oma1 and Yme1l double knockout MEFs and cardiomyocytes, in which only the long forms are present, an interconnected mitochondrial network was observed (33,68).

These data are not necessarily in disagreement with each other, as they were obtained on different models, where the different multiplicity of OPA1 variants expression may be the keystone.

Cristae **structure and bioenergetics**

As already mentioned OPA1 is mainly found in the IMS of mitochondria, soluble or anchored to the IMM (2,7) with a small amount of the short soluble forms found to be associated with the OMM (3). Due to the presence of the narrow tubular *cristae* junctions (CJ), the IMM can be divided in two sub-compartments: the *cristae* membrane and the inner boundary membrane, that face the OMM (69). It was hypothesized that OPA1 sustain *cristae* architecture by acting as a dynamic intra-mitochondrial skeleton (70). Silencing experiments of OPA1 in HeLa cells showed drastically disorganized IMM structures with irregular *cristae* shape and fragmentation of the mitochondrial network, well before appearance of apoptosis hallmarks (2,61). Accordingly, the alteration of *cristae* shape was also described in several OPA1 deficiency mouse models, attesting the relevance of OPA1 in the maintenance of *cristae* architecture (71–74).

Opa1 genetic depletion also caused dramatic ultrastructural changes, such as mitochondrial swelling and loss of *cristae* organization (75), as well as energetic impairment, mirrored by severe perturbation of the respiratory chain supercomplexes (RCS) and complex V organization (20,64).

Similar ultrastructural defects were detected even in conditional Opa1 ablation mouse model, exhibiting altered mitochondrial network morphology, increased *cristae* width and reduced amount of assembled RCS, but without affecting mtDNA content or translation. In these studies the link between OPA1, *cristae* architecture and energetic features was further

corroborated by evidencing that a mild over-expression of Opa1 promoted *cristae* tightening, RCS assembly and mitochondrial energetic efficiency in the conditional Opa1 ablation mouse (12).

In this regard, it was reported that the protease PARL could generate a soluble OPA1 short form that, binding to the long forms, contribute to preserve the integrity of the CJ. Noticeably, in PARL−/− MEFs the loss of PARL reduced the levels of OPA1 short form, leading to faster apoptotic *cristae* remodeling and cytochrome c release due to proapoptotic stimuli (Cipolat et al., 2006).

Remarkably, in the absence of respiratory substrates, the level of OPA1 oligomers increased in parallel with significant narrowing of the *cristae* width, promoting ATP synthase assembly and granting the maintenance of mitochondrial functions in a fusion-independent manner (76). Accordingly, even starvation induced an increase in the density of *cristae* in mitochondria of both wildtype and MFN2-/- cells, but not in those of OPA1-/- cells (77).

Increased mitochondrial network fragmentation, cristae structure alterations and variable degree of energetic impairments have been often reported in several studies in fibroblast and lymphoblasts derived from DOA patients (8,42,78), highlighting lowered mitochondrial ATP synthesis and uncoupling of OXPHOS (79,80). Interestingly, as far as lymphoblasts from DOA patients with nonsense mutations concerns, OXPHOS dysfunction arise only in those with severe vision loss. Patients with relative preserved vision maintained a normal mitochondrial ATP production, likely compensating through increases in the distal complexes of the respiratory chain (81).

Our group showed that the mitochondria of fibroblasts derived from patients with different mutations causing haploinsufficiency displayed a significant reduction in the number and organization of *cristae*, which dramatically worsened when cells were forced to rely on OXPHOS only for ATP production. Moreover, in these fibroblasts the ATP synthesis driven by CI substrates was significantly impaired and the mitochondrial network much less interconnected. Furthermore, OPA1 was shown to interact with CI, CII and CIII, providing a potential direct link between OPA1 mutations and the energetic defects (11,78). Remarkably, defective OXPHOS was confirmed *in vivo* in muscle from DOA patients bearing several different OPA1 mutations (82,83).

The silencing of the alternate spliced OPA1 exons showed that the exon 4 was also involved with the $\Delta\Psi$m maintenance (8). Accordingly, even the depletion of OPA1 via RNAi in MEFs cells induced loss of membrane potential and drastic reduction of basal respiration,

unresponsive to uncoupler (84). In this regard OPA1 plays a role in transient matrix contraction coupling to mitochondrial depolarization (85) and is necessary for spontaneous mitochondrial depolarization induced matrix alkalinization (pH flash), a mechanism propose to electrically couple non fused mitochondria (86). OPA1 is supposed to stabilize RCS in a conformation that enables mitochondria respiration to compensate drops in mitochondrial membrane potential by an explosive pH flash (87)

It remains still unclear the respective role of long and short forms in maintaining the mitochondrial respiratory competence and *cristae* architecture.

While, when expressed in Opa1-/- MEFs, both long and short forms proved to be alone equally effective in maintaining the mitochondrial energetic competence, keeping the *cristae* density and width and CJ density (64), short forms proved to be more effective than the long ones in recovering bioenergetic features (20). Indeed, even if long forms have a similar mtDNA amount and *cristae* organization, nevertheless exhibited limited oxygen consumption rate (OCR) and reduced amount of assembled RCS (20). Contrarily, the *in vitro* manipulation of the mitochondrial proteases involved in OPA1 processing, result in a different outcome. In fact, while OMA1-/- cells show normally shaped *cristae*, YME1L-/- cells, that exhibit a decrease in the long/short forms ratio, display disorganized *cristae* morphology. Finally, the double KO cell model of OMA1 and YME1L, that present only the long forms of OPA1, present normal *cristae* morphology (33). Accordingly, even the knockdown of other proteins that perturb the long/short forms ratio causing an accumulation of the short one causes disorganization of *cristae* structure (30,35,56,57,88). In view of the above, we could speculate that, even if both long and short forms have the capability to organize the *cristae* structure, only the long ones are involved in the *cristae* maintenance.

Still, in these last models OPA1 long/short ratio variation may not be the cause of the observed *cristae* structure impairment, this being directly chargeable to the loss of the different proteins analyzed. In agreement with this, *in vivo* loss of OMA1 prevents brain atrophy in Phb2-knockout mice (89) and cardiomyopathy in heart-specific Yme1l-knockout mice (68) stabilizing the long forms of OPA1 but without restoring *cristae* morphology.

Our proposal is a model in which the short forms may act as a passive scaffold for the cristae to wrap on, anchoring the mtDNA and possibly interacting with components of MICOS complex (20), accordingly with other groups studies (50). Another model has been

proposed, with the short forms requiring prohibitins to furnish the congenial lipid environment, necessary for membrane binding and *cristae* maintenance (64)

mtDNA maintenance

The role carried out by Mgm1p in the mtDNA maintenance has been critical for its identification in yeast (90,91). As OPA1 deficiency alters IMM morphology and *cristae* architecture, it stands to reason it affects mtDNA stability too. Indeed mtDNA is known to be associated with proteins in nucleoids and to be anchored to IMM on the matrix side (92), regulating mtDNA replication and transcription (93). Thus, OPA1 depletion or mutation, impairing cristae morphology, could restrain mtDNA anchoring to the IMM and affect its properties. In alternative, altered mitochondrial fusion could hamper the mixing of intra-mitochondrial content which has the potential to dilute out the damaged components, thus repairing the damaged organelle through functional complementation (94). Thus OPA1 mutations could contribute to mtDNA instability, precluding in particular the repair of damaged mtDNA, which would perturb nucleoids abundance and distribution along the network (95).

The role of OPA1 in mtDNA stability was described for the first time in a multicenter clinical study revealing the accumulation of mtDNA multiple deletions in skeletal muscle biopsies of DOA patients bearing *OPA1* missense mutations (42,96). Another study reported, in the COX-negative fibers, a 2- to 4-fold increase in mtDNA copy number (97). Conversely, fibroblasts and lymphocytes from DOA patients failed to exhibit significant changes in the mtDNA copy number (11,98) or any deletion (78).

The differential silencing of the three exons involved in the alternative splicing showed that down-regulation of the isoforms bearing the exon 4b in HeLa cells leads to a reduction in the mtDNA content and replication as well as an altered distribution of nucleoids through the mitochondrial network. The reintroduction of the N-terminal portion of OPA1 containing the exon 4b, upstream the cleavage site, reverted the phenotype, and this peptide was also shown to colocalize with mtDNA. These findings led to propose that this N-terminal peptide containing the exon 4b might anchor the nucleoids to the IMM (13), similarly to what observed in yeast for the Mgm1p (99).
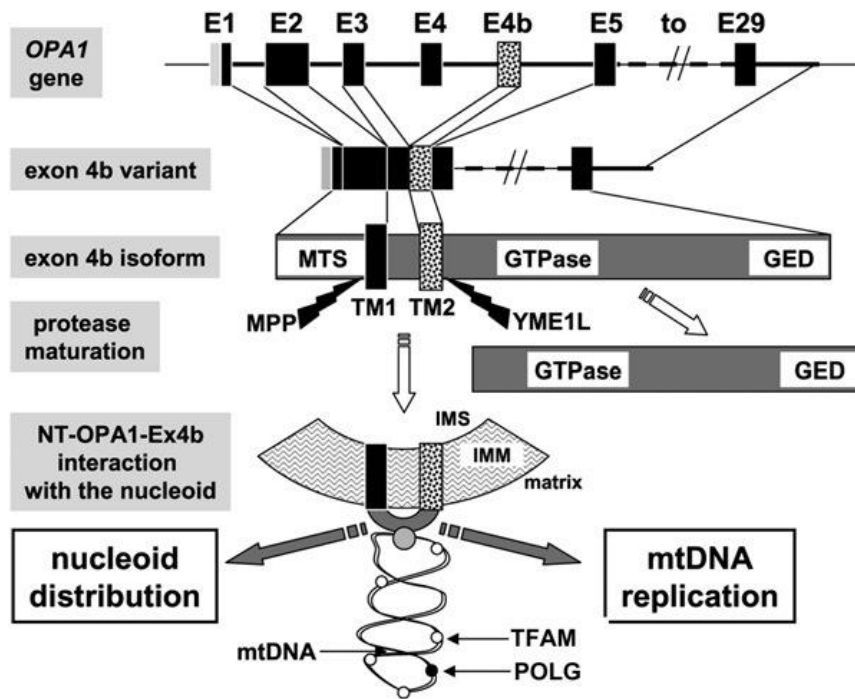
Figure 5. Schematic representation of the mechanism through the N-terminal OPA1 peptide, including the exon 4b, is proposed to anchor the nucleoids to IMM (from Elachouri et al., 2011)

Apoptosis

Another cellular function in which OPA1 is implicated, directly linked to its role in CJ organization, is apoptosis, as demonstrated by the increased sensitivity of cells to spontaneous and induced apoptosis following the down-regulation or expression of pathogenic mutants of OPA1 (9,100,101).

Indeed, the OPA1 role in the apoptotic process has to be searched in the *cristae* architecture organization and the following compartmentalization of the pro-apoptogenic factor cytochrome c (9,10). As previously stated, has been proposed that soluble short forms of OPA1, produced by PARL, may interact with the long one to maintain the CJ bottleneck, holding cytochrome c within the *cristae* volume and regulating its release during apoptosis (28). Expression of functional OPA1 is able to protect cells from death induced by intrinsic apoptotic stimuli independently from mitochondrial fusion, evidence given by the observation of apoptotic protection in MFN1−/− and double MFN1−/− and MFN2−/− cells (10).

Even the differential silencing of the three spliced exons confirmed the uncoupling of the fusogenic and antiapoptotic functions of OPA1. Indeed, silencing of isoforms bearing either exon 4b or exon 5b favored cytochrome c release without mitochondrial network

fragmentation or mitochondrial membrane depolarization. Furthermore, the overexpression of OPA1 isoforms bearing exon 5b seems to positively affect cytochrome c compartmentalization (8). Similarly, fibroblasts from a DOA patient with a mutation in the exon 5b of OPA1 displayed an increased susceptibility to apoptosis and minor mitochondrial respiration defects, but no augmented fragmentation of mitochondrial network (102).

During the apoptotic process, the BH3-only pro-apoptotic protein tBid induces a striking remodeling of IMM structure, with the opening of the CJ (103), by inducing the disassembly of OPA1 oligomers, and thus the release of cytochrome c (10,47).

Cristae architecture alterations and an increased susceptibility to external apoptotic stimuli have also been shown by our group in DOA patients fibroblasts (11). Moreover, the OPA1 oligomers disassembly in cytochrome c release from the *cristae* was highlighted in BNIP3-induced apoptosis. OPA1 and BNIP3 was proved to co-immunoprecipitate, ant their interaction is necessary to trigger Opa1 oligomers disassembly in a Bax- and/or Bak-dependent manner, inducing mitochondrial network fragmentation and apoptosis (104,105).

Another model to explain the anti-apoptotic role of OPA1 is based on the evidence that OPA1 is more efficient in binding liposomes that containing cardiolipin (65), an anionic phospholipid present predominantly in the IMM, to which cytochrome c is associated (106). Nonetheless, recent studies failed to confirm these hypotheses neither in human cells bearing OPA1 pathogenic variants nor in DOA animal models (107). Moreover deletion of Opa1 in MEFs was shown to delay staurosporine-induced apoptosis (108). Nevertheless, it cannot be ruled out that OPA1 dysfunctions may sensitize cells to alternative cell-death pathways such as autophagic cell death (109).

Autophagy and mitophagy

Autophagy belongs to cellular cytoprotective pathways. It consists in the recycling of cellular material, ensuring its lysosomal degradation. The selective degradation of damaged mitochondria by autophagy is referred to as mitophagy. In addition to cell survival, an autophagic type of cell death or type II cell death has also been described (110,111)

In DOA mouse models, autophagic vesicles were detected in RGCs and in other tissues, supporting the hypothesis of RGCs loss by programmed autophagic cell death (73,112).

Mitophagy alteration, together with imbalance of mitochondrial dynamics and respiratory chain function, has been associated with neurodegenerative disorders (113). The strict interplay between mitochondrial dynamics/energetics and the autophagic machinery ensures the maintenance of a cohort of healthy mitochondria, through fragmentation of the mitochondrial network, selective targetting of dysfunctional fragments and their delivery to autophagosomes for removal by lysosomes. Indeed, targetting damaged and depolarized mitochondria to lysosomes needs the mitochondrial reticulum to be fragmented (114). Conversely, its elongation by fission inhibition protected cells from autophagic degradation during starvation (77).

New evidence suggests that in the early stages of DOA pathogenesis, the down-regulation of OPA1 could lead to a reduction of BNIP3 and consequently of autophagy and mitophagy levels, contributing to desensitization of NGCs to acute or chronic stresses. With the disease progression, OPA1 down-regulation leads to a redox imbalance that cannot be compensated thus increasing ROS production, restoring the BNIP3 level, whose long-term expression has pro-apoptotic function (115).

Accordingly, a recent study in DOA patients' fibroblasts showed different alterations of mitochondrial functions and turnover in relation to the type of OPA1 mutation considered, with an intrisical activation of the autophagic machinery associated with dominant negative mutations but not with the haploinsufficient ones (116). Increased mitophagy levels and mitochondrial network fragmentation have been also found in DOA plus patients' fibroblasts carrying biallelic OPA1 mutations (117). Thus, alterations in OPA1 protein levels and pro-fusion activity may influence the autophagic and mitophagic response, in accordance with the evidence that mitophagy constitutes a pro-survival pathway through the up-regulation of OPA1 expression (24). Moreover, recently a coupling mechanism between mitochondrial dyamics and mitophagy has been found to involve FUNDC1. This protein interacts with OPA1 in the IMS in normal conditions, while the interaction is reduced under mitochondrial stress conditions, when it recruit the fission protein DRP1 toward mitochondria from its normal cytosolic localization (58).

Calcium homeostasis and glutamate excitotoxicity

OPA1 seems to be also implicated in calcium homeostasis, even if is still not clear if the disfunctions observed are part of the pathogenic process or rather a consequence of ATP level depletion. Indeed, it has been shown that after the knockdown of OPA1 in cells, an

increase in the rate and amplitude of mitochondrial $[Ca^{2+}]$ rise evoked with K^+ and histamine was registered, despite reduced mitochondrial membrane potential. Moreover, in permeabilized cells the rate of Ca^{2+} uptake by depolarized mitochondria was also increased in OPA1-silenced cells, suggesting the involvement of Na^+/Ca^{2+} and Ca^{2+}/H^+ antiporters, as indicated by pharmacological inhibitors of these carriers (118)

The same group therefore studied mitochondrial Ca^{2+} homeostasis in fibroblasts obtained from members of a DOA family. The ophthalmological parameters were inversely correlated to the evoked mitochondrial Ca^{2+} signals, indicating the importance of enhanced mitochondrial Ca^{2+} uptake as a pathogenic factor in the progress of DOA and the significance of OPA1 in the control of mitochondrial Ca^{2+} homeostasis (119)

Also, OPA1 loss by RNA interference in cell lines and RGCs results in reduced mitochondrial Ca^{2+} retention capacity. OPA1-depleted cells exhibit decreased histamine-evoked mitochondrial Ca^{2+} uptake and a reduction of NAD^+ to NADH. Although in this study OPA1 loss in RGCs has no apparent impact on mitochondrial morphology, it decreases buffering of cytosolic Ca^{2+} and sensitizes RGCs to excitotoxic injury (120) Moreover, treatment with CCCP on cells silenced for OPA1 during the recovery phase after high K^+ stimulation, shown how in the absence of a normal $\Delta\Psi m$ and of OPA1 activity, Ca^{2+} recapture is highly defective, leading to drastic impairment in Ca^{2+} clearance and ultimately to cell death. (121)

Neurons could suffer excitotoxic damage if glutamate, the principal excitatory transmitter within the vertebrate nervous system, is released in excess into the extracellular space, activating ionotropic and metabotropic receptors and resulting in toxic cytoplasmic Ca^{2+} accumulation. Glutamate excitotoxicity can alter mitochondrial dynamics in a process that could be mediated by oxidative stress. (122)

Besides, during acute glutamate exposure in cell culture models occurs a phenomenon known as delayed Ca^{2+} deregulation (DCD) (123,124) that leads to neuronal cell death (125) and is thought to be a consequence of mitochondrial Ca^{2+} overload-mediated injury (126). Remarkably, RGCs are known to be resistant to excitotoxicity in contrast to hippocampal neurons (127). However, when OPA1 is depleted, DCD becomes irreversible and leads RGCs to death. (120)

It's been reported that increased OPA1 expression restores mitochondrial morphology and promotes neuronal survival following excitotoxicity. (128)

Furthermore a study on the retina of a haploinsufficient mouse model showed that the expression of the glutamate NMDA receptors (NR1, 2A, and 2B) was significantly

increased, demonstrating that an imbalance in mitochondrial fission/fusion leads to NMDA receptor upregulation and oxidative stress and so proposing a new vicious cycle involved in neurodegeneration. (129)

On the other hand, as already mentioned, OPA1 mutations can cause ATP production impairment, which results in a diminished Na^+/K^+ exchange and more depolarized cell membrane potentials. In this situation the probability of the sodium and calcium voltage-dependent channels opening increases, and excitatory stimuli are more likely to fire action potentials. (130)

Also, this cell membrane partial depolarization will relieve the voltage-dependent magnesium block of NMDA receptor, allowing normal synaptic concentrations of glutamate to activate the NMDA receptor, which could initiate the excitotoxic cascade. (Stavrovskaya et al., 2005)

In MEFs reduced mitochondrial Ca^{2+} uptake was shown to be caused by the loss of the mitochondrial protein AFG3L2, component of the m-AAA proteases, due to the fragmentation of the mitochondrial network, secondary to respiratory dysfunction and the consequent processing of OPA1. The majority of mitochondria lose the connections to the ER and thus Ca^{2+} elevations, interfering with the proper Ca^{2+} diffusion along the mitochondrial network. The overexpression of OPA1 recover the mitochondrial fragmentation in Afg3l2-/- MEFs and rescues the impaired mitochondrial Ca^{2+} buffering, but fails in restoring respiration (131)

More recently, in presymptomatic 3-month old DOA mice, metabolomics analysis revealed a Opa1+/- related signature characterized by, among other molecules, the increased concentration of glutamate and carnosine in Opa1+/- optic nerves compared to controls. (132) The increased carnosine may be interpreted as a counteracting mechanism against the increased excitatory glutamate concentration since carnosine decreases neuronal cell death by targeting the glutamate system. (Ouyang L, 2016)

Other functions and implications

Being OPA1 implicated in process like apoptosis and autophagy, that regulate cells' destiny between life and death, it follows that it may also have a correlation with the process of aging. Indeed, some recent studies linked the protein to this process.

If it was known that in a OPA1 haploinsufficiency mouse model there was a dendritic degeneration with age, characterized by a selective loss of glutamatergic, but not

GABAergic, synaptic sites (74), it was recently proved that the activity reduction of CIV in mice with aging coincided with binding reduction of OPA1 to CIV (51).

Moreover, in humans OPA1, together with MFN1, has been proved to regulate a metabolic shift from glycolysis to mitochondrial respiration in old human fibroblasts during chronological lifespan (133), and an age-related decline of its levels has been associated with muscle loss sedentary but not active humans (134).

The regulation of the adipose tissue is another field in which OPA1 showed to have an implication, first seemed to be related to its fusogenic role. Indeed, adipocytes' mitochondrial morphology turn from filamentous to fragmented upon differentiation to adult adipocytes, with subsequent cellular triacylglycerol accumulation regulated, at least in part, by mitochondrial dynamics (135), and adrenergic stimulation was proved to induce brown adipocytes thermogenic activation by complete mitochondrial fragmentation, through DRP1 phosphorilation and OPA1 cleavage (136).

Still, more recently in this regard an extra-mitochondrial role has been proposed for OPA1, suggesting it may work as A-kinase anchoring protein (AKAP) on lipid droplets, so mediating the adrenergic control of lipolysis (137). Consistently with this hypothesis, the loss of the protease OMA1, known to alter OPA1 processing, has been showed to cause obesity and defective thermogenesis in mice (138).
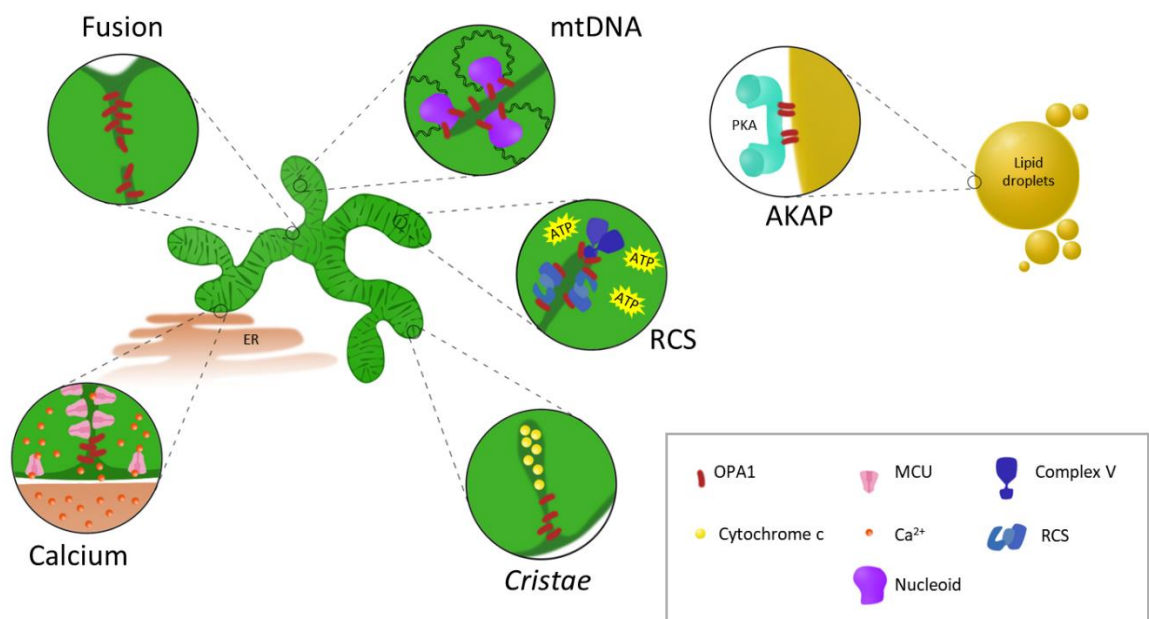
Figure 6. Schematic representation of OPA1 functions

OPA1 dysfunctions: mutations and pathophysiology

DOA pathophysiology

Autosomal dominant optic atrophy (DOA), also known as Kjer's type dominant optic atrophy or Kjer's disease (6), is the most common hereditary optic neuropathy, characterized by degeneration of the retinal ganglion cells and optic nerve atrophy, with a moderate to severe loss of visual acuity, blue-yellow dyschromatopsia and central scotoma. Usually the onset occur during the first two decades of life, with an estimated disease prevalence of 1:50000 worldwide, and is associated with mutations in nuclear genes encoding mitochondrial proteins, primarily the *OPA1* gene (4,5).

DOA has a manifestation extremely tissue-specific, limitated to RGCs and their axons, that form the optic nerve, with a preferential involvement of the small fibers in the papillomacular bundle that subserve central vision (139). The disease is characterized by a slowly progressive bilateral visual loss, associated with centrocaecal scotomata, impairment of color vision (usually acquired blue-yellow loss, or tritanopia, but also generalized nonspecific dyschromatopsia and rarely red-green defects), pallor of the optic discs temporally and relative preservation of the pupillary reflex (140,141). The onset is usual in school age, although it can manifest later and remain subclinical until early adult life. Visual impairment is irreversible, usually moderate, but can be encountered from subclinical manifestations to extreme severe (legal blindness) (141).

The two postmortem histologic studies available to date on DOA patients identified similar histopathologic changes, with the optic nerves, the optic chiasm and optic tracts showing diffuse atrophy of the RGC layer, an increased content of collagen tissue and a decreased number of neurofibrils and demyelination, situation extended to the lateral geniculate body, with massive loss of ganglion cells, fibrillary gliosis and a great quantity of fine granular lipid in the cytoplasm of the ganglion cells (Johnston et al., 1979; Kjer et al., 1983).

With the advent of optical coherence tomography (OCT), a non-invasive diagnostic and monitoring technology, has been clarify that DOA patients exhibit a general decreased retinal nerve fiber layer (RNFL) thickness with a averagely smaller optic disc size, with the peripapillary RNFL loss due to axonal degeneration (142–144). OCT measurements also showed that among patients with different OPA1 mutation, the ones with missense mutations displayed the most severe phenotype (143).

The mechanisms that lead to the degeneration of RGCs in DOA patients are still poorly understood, but the particular anatomic features of these cells may be the cause of their susceptibility. RGCs soma and dendrites are constantly exposed to high levels of light, which could enhance ROS production and aggravate the effect of mitochondrial dysfunction. Indeed, rat retinal cells' light exposure experiments showed an increase in the apoptotic response caused by cleavage and activation of caspase-3 by light (Lascaratos et al., 2007). As already discussed, DOA murine models exhibit and increased autophagy in the RGC layer, with early age-related like signs of optic nerve degeneration. Actually, an increased autophagy may contribute to RGCs loss and thus optic atrophy (White et al., 2009).

Furthermore, RGCs exhibit a particular uneven mitochondrial subcellular distribution. Indeed, mitochondria are more abudant in the unmyelinated portion of the axon and less in the myelinated one. This peculiar pattern mirrors the high-energy requirement of the unmyelinated section, making these cells potentially more vulnerable to energetic impairment. Moreover, due to the pronounced length of RGCs axons, more stringent energetic requirements and an adequate mitochondrial transport along these axons may be required. Thus, due to its role in mitochondrial dynamics and energetic functions, it stands to reason that OPA1 mutations may lead, directly or not, to an impairment of the cellular functions in tissue with high energetic demands (139,145).

Downregulation of OPA1 in cultured RGCs led to abnormal mitochondria aggregation in both the soma and neurites (Kamei et al., 2005). Moreover, from *in vitro* study of cortical neurons OPA1 seems to be essential for the neuronal maturation. In addition to the phenotypes seen in other models, OPA1 loss provoked reduced dendritic growth and synaptogenesis, which may be linked to impaired synaptic plasticity associated with other neurodegenerative diseases, and that could contribute to the pathogenic mechanism (146). Accordingly, the dendropathy of the RGCs has been shown to be the first morphologic evidence of the disease in OPA1-mutant mouse model, with an increase in the severity with the age. Together with impaired mitochondrial morphology and *cristae* ultrastructure, this model exhibited changes even in synaptic density and structure, suggesting that the dendritic atrophy could be driven by the synaptic atrophy (74,147).

OPA1 mutations: DOA and DOA "plus"

To date, the locus-specific database dedicated to OPA1 (http://opa1.mitodyn.org/) has listed a total of 414 OPA1 gene variants, of which more than the 60% are considered pathogenic. Among the variants more than two-thirds are in the coding sequence, and among them two out of three are in the dynamin and in the GTPases domain. The great part of the mutations are substitutions (290) and deletions (94), while only few duplications (20), insertions (5) and in/del (5) mutations have been annotated.

Even if mutations are mostly family-specific, some of them are extensively encountered. About 50% of the pathogenic mutations cause the introduction of premature stop codon(148), leading to the consequent truncation of the open reading frame and degradation of the mRNA, with the complete loss of function of the mutant allele and the decreased OPA1 protein amount. Thus, these variants share haploinsufficiency as pathological mechanism (149).

DOA was first described a disorder specifically affecting RCGs, only sometimes associated with deafness (150,151). Then it was proposed that a particular missense mutation, the R445H, in a high conserved residue in the GTPase domain, could be associated with the insurgence of a form of DOA with moderate progressive deafness (DOAD) (152,153) or in a more complex syndrome including DOA, deafness, ptosis, and ophthalmoplegia (154). This hypothesis has been the confirmed (79) and since then many other similar cases have been described (42,96), leading to conclude that up to 20% of OPA1-related disorders are syndromic (155).

The extraocular features characterizing this condition described as "DOA plus" or DOA+ syndrome, may include sensorineural deafness, ataxia, myopathy, chronic progressive external ophthalmoplegia, and peripheral neuropathy. Among these, progressive sensorineural hearing loss was shown to be the most common one, found in about 6% of all OPA1 patients (156).

Even if usually these extraocular feature set in during young adulthood after the occurrence of the optic neuropathy, some patients present these dysfunctions before or even in absence of optic neuropathy, thus making diagnosis even more difficult (157).

The grand part of patients with syndromic DOA carry missense mutations of OPA1 rather than nonsense, suggesting a dominant negative effect as pathogenic mechanism. Indeed, is proven that the risk of DOAD/DOA+ syndromes is significantly higher in the case of a missense mutation than that of a nonsense one (97).

OPA1 mutations: other neurological disorders

Over the years, the spectrum of neurological disorders associated with OPA1 mutations has become wider, and multiple sclerosis-like syndrome (155,158), spastic paraplegia (155), and Behr-like syndrome (159) first, and more recently syndromic parkinsonism and dementia (160) are part of this scenario.

Moreover, since 2011 a new early-onset severe neurological syndrome OPA1-related, distinct from those previously described, has been reported in a growing number of patients (161–164), a phenotype fully compatible with the Behr syndrome, occurring during the three first years of life. The important difference between this syndrome and the other previously described is that this have a bi-allelic mode of inheritance, with a combination of nonsense and missense OPA1 mutations.

Recently, a study identified novel compound heterozygous OPA1 mutations in a patient with an early-onset recessive severe optic atrophy, sensorimotor neuropathy, ataxia and congenital cataracts (165), while another one reported of two patients with early-onset Behr-like syndrome with Leigh-like neuroimaging features due to compound heterozygous and homozygous novel variant (166). Another group identify in two sisters presenting lethal infantile encephalopathy, hypertrophic cardiomyopathy and optic atrophy a novel homozygous mutation in the GTPase domain as causative genetic defect (167). Finally, a recent report provides evidence of bi-allelic OPA1 mutation in three patients: a boy showing an early-onset and severely progressive mitochondrial disorder, leading to early death because of multiorgan failure, and two girls showing a spastic ataxic syndrome associated with sensory motor peripheral neuropathy, resembling Behr syndrome. The first carried truncating and a missense mutations, the second carried a novel and an already known missense mutations, while the third patient carried an homozygous missense mutation (168)

AIMS

Mutations in the *OPA1* gene, encoding a mitochondrial GTPase, are the major cause of DOA, the most common hereditary optic neuropathy, and its syndromic form DOA "plus". Over 400 *OPA1* mutations have been identified so far, although their pathogenic mechanisms are not clear yet. Literature is plenty of papers that investigated the biochemical features of cells (usually fibroblasts or lymphocytes) derived from DOA patients. What comes up is that these cellular models always show a mild phenotype when compared to the severity of the clinical picture in patients and often these models are not predictive towards new mutations pathogenicity, this being due to the partial compensatory effect of the wild-type allele.

To highlight the pathogenic phenotype associated with different mutations, we developed a murine cell models, expressing the human OPA1 isoform 1 bearing different mutations in Opa1-/- MEFs.

The first aim of this study has been to characterize in detail these murine cell models bearing four OPA1 mutations, selected on the basis of their different clinical phenotypes, and make a comparison with patients' fibroblasts bearing the very same mutations. A wide array of biochemical and molecular analyses have been utilized to evaluate the energetic competence and network dynamics, allowing to establish the pathogenicity prediction capacity of this model against novel mutations.

Then, we took advantage of this model to investigate the efficacy of a few drug candidates, previously identified in a high-throughput screening carried out in an *ad hoc* generated yeast model of this disease. This preliminary study aims at validating this cell model in a therapeutic perspective for DOA.

MATERIALS AND METHODS

Cells culture conditions

Skin fibroblasts were derived, following informed consent, from five healthy donors, two DOA patients from two unrelated families with the c.1146A>G (p.I382M) mutation, one patient with the c.1316G>T (p.G439V) mutation, two related patients from the same family with the c.1334G>A (p.R445H) mutation and two related patients with the c.1807G>C (p.D603H) mutation. The localization of these mutations in the *OPA1* gene is reported in Table 1. All mutations were heterozygous and strictly co-segregated with individuals affected by optic atrophy in families with autosomal dominant inheritance.

The same mutations analyzed in patients' fibroblasts have been introduced in OPA1 isoform 1 cDNA and then stably expressed in Opa1-/- Mouse Embryonic Fibroblasts (MEFs), a kind gift from Prof. David Chan, Division of Biology, California Institute of Technology, Pasadena, CA, USA (84).

MEFs and fibroblasts were cultured in Dulbecco's Modified Eagle Medium containing 25mM glucose (DMEM, Gibco, Life Technologies) supplemented with 10% fetal bovine serum (FBS, South America, Gibco, Life Technologies), 2 mM L- glutamine, 100 units/mL penicillin, and 100μg/mL streptomycin, in an incubator with a humidified atmosphere of 5% CO_2 at 37°C. For some experiments, cells were incubated in glucose-free DMEM supplemented with 5mM galactose, 2 mM L-glutamine, 5 mM Na-pyruvate and 5% FBS (DMEM-galactose).

mtDNA mutation variant 1	Protein domain	Aminoacid change isoform 1	Disease
c.1146A>G	GTPase	p.I382M	DOA-modifier
c.1316G>T	GTPase	p.G439V	DOAplus
c.1334G>A	GTPase	p.R445H	DOAplus
c.1807G>C	Dynamin	p.D603H	DOA

Table 1. Characteristics of the *OPA1* mutations analyzed in this study.

Plasmid construction and retroviral transduction

Plasmid expressing the OPA1 isoform 1 was previously described (18). Isoform 1 was further mutagenized (I382M and D603H) and cloned into the pMSCV-puro vector, whereas the plasmids expressing isoform 1 bearing the mutations G439V and R445H were previously described (65). Retrovirus production and infection were performed as previously described (169). Plasmid (6µg/experiment) transfection of mouse embryonic fibroblasts (MEFs) was performed with Lipofectamine 3000 (Life Technologies) following the manufacturer's instructions.

Cellular ATP content

The amount of cellular ATP was measured by using the luciferin/luciferase assay according to (170) with minor modifications. Cells (3×10^5) were seeded onto 6-well plates, incubated in DMEM-glucose or in DMEM-galactose. At the times indicated, cells were trypsinized and resuspended in PBS, and one aliquot was used to determine the protein content (171). Aliquots of cellular suspension were incubated with 5% perchloric acid for 1min at 4°C and subsequently neutralized with 90mM Tris and 140mM K_2CO_3. After centrifugation at 10000g for 1min, ATP content in the supernatant was measured in duplicate by using the ATP monitoring kit (Sigma-Aldrich), according to manufacturer's instructions. An appropriate internal ATP standard was added to each sample for calibration. The measurement was performed using a Sirius L Berthold Luminometer.

Mitochondrial ATP Synthesis

The mitochondrial ATP synthesis rate was measured in digitonin-permeabilized cells as previously described (11), with minor modifications by using the luciferin/luciferase assay. Briefly, cells (10^6/mL) were incubated in 150 mM KCl, 25 mM Tris-HCl, 2 mM EDTA, 0.1% BSA, 10 mM potassiumphosphate, 0.1 mM $MgCl_2$ (pH 7.4), 0.1 mM P_1,P_5-di(adenosine-5) pentaphosphate (AP_5A, inhibitor of adenylate kinase), with 50 µg/mL digitonin. Aliquots of 3×10^5 cells were incubated in the same buffer in the presence of substrates of CI (1 mM malate plus 1 mM pyruvate) or CII (4 mM succinate plus 5 µM rotenone) or GPD (20 mM glycerol-3-phosphate plus 5 µM rotenone and 5 mM malonate).

After the addition of 80 µM ADP, chemiluminescence was determined as a function of time with a luminometer (Sirius L Berthold Luminometer). The chemiluminescence signal was calibrated with 10µM ATP, as internal standard, after the addition of 5µM oligomycin. The rates of ATP synthesis were normalized to protein contents (171) and citrate synthase (CS) activity (see below).

Citrate synthase activity

In order to determine the citrate synthase activity, 10µg of cells were diluted in the assay buffer (0,1% Triton X100, 125mM Tris-HCl, pH 8) and incubated with 0.3mM acetyl coenzyme A, 0.1mM DTNB and 0.5mM oxaloacetate. The rate of coenzyme A production by citrate synthase was determined at 30°C from the absorbance of DTNB at 412nm (ε: 13.6 $mol^{-1}cm^{-1}$) by using the V550 Jasco spectrophotometer.

Mitochondrial network morphology

Cells were seeded onto 36mm-diameter dishes and mitochondrial morphology was assessed by staining cells with 10nM Mitotracker Red (Life Technologies) for 30 minutes at 37°C. Live-cell fluorescence images were captured with an inverted Nikon Eclipse Ti-U epifluorescence microscope equipped with a back-illuminated Photometrics Cascade CCD camera (Roper Scientific). Images were collected using a 63x/1.4 oil objective. Data were acquired and analyzed using the Metamorph software (Universal Imaging Corporation).

Cristae architecture

The samples used for transmission electron microscopy were processed using standard protocols (116). MEFs cells were seeded onto 36mm-diameter dishes and cultured/grown to 70-80% confluency. Cells were fixed with 2.5% glutaraldehyde in 0.1 M sodium cacodylate buffer (pH 7.4) at 37°C. Following fixation, samples were placed in 2% osmium tetroxide in 0.1 M sodium cacodylate buffer (pH 7.4), dehydrated in graded series of ethyl alcohol and embedded in Durcupan resin (Sigma-Aldrich, Saint-Louis, MO, USA). Ultrathin sections were cut with an ultramicrotome and placed on grids. Following

counterstaining, images were acquired with an AMT XR-60 CCD camera system (AMT, Woburn, MA, USA).

Images of mitochondrial ultrastructure morphology were used to score mitochondria into five categories: long mitochondria (1390-455nm) with dense matrix and normal *cristae* (class I), rond mitochondria (490 +/-20nm) with dense matrix and normal *cristae* (class II), mitochondria with clear matrix but normal *cristae* (class III), mitochondria with dense matrix but abnormal *cristae* (class IV), mitochondria with clear matrix and abnormal *cristae* (class V). 100-250 mitochondria per sample were analysed.

mtDNA content

Quantification of human mtDNA copy number relative to nuclear DNA were performed as previously described (172). Quantification of mouse mtDNA copy number relative to nuclear DNA was carried out amplifying both mt-Nd1 and β-Globin.

Primers used to amplify the mitochondrial ND1 gene were:

mND1F: AGCAGAAACAAACCGGGCCCC,

mND1R: TAACGCGAATGGGCCGGGTG.

Referent nuclear gene used to normalize mtDNA copy number was the Mus musculus β-Globin gene with the primers:

mB-GlobinF: TCACTTGGACAGCCTCCAGGGCA,

mB-GlobinR: CAGGGGAAGGAAACCCAGGAGGTG.

Using both analysis with a standard curve of a reference template and analysis of the difference in threshold amplification between mtDNA and nuclear DNA (ΔΔCt method). Both methods provided identical results.

mtDNA sequencing

Mitochondrial genome libraries were prepared from all the MEFs with Ion Xpress™ Plus Fragment Library Kit (Life Technologies) according to manufacturer instruction, using Long Extension PCR primers as in (173). The libraries were sequenced using the Ion Chef™ + Ion S5 XL Next-Generation Sequencing Systems for Targeted Sequencing (Life Technologies). Sequencing data were analyzed with a dedicated home-made pipeline integrating various modules for variant calling, annotation and priorization. The calling

module uses a consensus-based approach and integrates the prediction of 5 callers (GATK, VarScan, SNVer, LoFreq and Platypus). In parallel, a soft-clipping analysis was performed in order to predict deletion, insertion and duplication events.

Cellular viability

MEFs were seeded in 24-wells plates and after 24 hours washed with PBS and then incubated with the different media for the times indicated in the figures' legend. At the end of the incubation time, the medium was removed, and cells were fixed with DMEM containing 10% trichloroacetic acid at 4°C for 1h, then washed five times with water and dried at room temperature. 0,4% sulforhodamine B (SRB) in 1% acetic acid was added in each well and incubated for 30 minutes in the dark. After four washes in 1% acetic acid solution, the cells were solubilized with 10mM Tris pH 10.5. Absorbance at 564 nm was determined with a Multilabel Plate Reader (Victor3).

Western blotting

Cell lysates were prepared as previously described (11). Proteins were separated by 8% SDS–PAGE and transferred onto nitrocellulose membranes (Bio-Rad). The membranes were incubated overnight at 4°C with the primary antibodies, then visualized using horseradish peroxidase-conjugated secondary antibodies. The chemiluminescence signals were revealed by using an ECL Western blotting kit and measured with Gel Logic 1500 Imaging System, Biosense.

Respiratory supercomplexes analysis by BN-PAGE

Mitoplasts were isolated from 10^6 cells/mL using 50 µg/mL digitonin, suspended in PBS and protein content determined. After centrifugation, the pellet was suspended (5mg protein/ml) in 150mM K-acetate, 30mM HEPES pH 7.4, 10% glycerol, 1mM PMSF, 1% (w/v) digitonin and incubated on ice for 30min. Samples were centrifuged, and aliquots of supernatant were separated on the 3-12% gradient gel, after addition of 5% Serva G Blue in 750mM aminocaproic acid. Gels were analyzed for CI in-gel-activity (IGA) and western blot (174).

OPA1 oligomerization analysis by BN-PAGE

Cells (5×10^6) were harvested with the scraper in ice-cold PBS, centrifuged and resuspended in buffer H (Mannitol 220mM, Sucrose 70mM, Tris-HCl 10mM, pH 7.2) with protease inhibitor cocktail for 10min, then homogenized for ~50 strokes with a Dounce homogenizer at 4 °C. After centrifugation for 5 min at 1000g, and the supernatant was re-centrifuged for 20 min at 13000g. The resulting pellet (mitochondrial fraction) was resuspended in 6-Aminocaproic Acid 1.5M, Bis-Tris 75mM, pH 7, with protease inhibitor cocktail and protein quantified by Bradford. Aliquot were incubated with 5.63µM lauryl maltoside, gently stirred on a wheel for 10min at 4°C, then centrifuged for 20 min at 13000g. The supernatant was loaded on the 3-12% or 4-16% gradient gels, after addition of 5% Serva G Blue in 750mM aminocaproic acid. Gels were analyzed for western blot.

Reagents

Antibodies were: Drp1, Mfn1, Mfn2 (Abnova); SDHA CII, α subunits of CV (Mitosciences); OPA1 (BD Biosciences); tubulin (Sigma-Aldrich); VDAC (Biovision). Horseradish peroxidase-conjugated secondary antibodies were from Jackson ImmunoResearch or Alexafluor, the ECL western blotting kit from Biorad. All the other reagents were from Sigma-Aldrich.

Statistical analysis

All numerical data are expressed as mean ± SD or SEM, as indicated. Student's unpaired two-tail test was used for statistical analysis, unless otherwise indicated. Differences were considered statistically significant for $p < 0.05$.

RESULTS

We first analyzed skin fibroblasts derived from five healthy donors and seven patients carrying four different *OPA1* missense mutations. Among these mutations, three were selected on the basis of their known clinical phenotype, ranging from very mild, asymptomatic or associated with pure optic atrophy (I382M), to severe syndromic forms (G439V and R445H). The last mutation selected, the D603H, is a novel mutation here reported and fully characterized for the first time.

Each of the very same *OPA1* mutations present in patients' fibroblasts has been inserted in the OPA1 isoform 1, which has been then stably expressed in Opa1-/- MEFs, devoid of Opa1 protein (18). The MEF cell lines obtained express 100% of WT or mutated OPA1, allowing to analyze the changes without the compensatory effect due to the presence of the wt allele, as occurs in fibroblasts.

The mitochondrial dynamics machinery

Fusion and fission proteins

We evaluated the expression levels of the main proteins involved in the mitochondrial dynamics machinery, namely OPA1, MFN1, MFN2 and DRP1 in cellular lysates of both fibroblasts and MEFs by western blotting analysis.

In fibroblasts, mitofusins and DRP1 levels were similar in control and DOA patients, whereas the OPA1 amount was reduced in I382M, R445H and D603H mutants and slightly increased in fibroblasts bearing the G439V mutation (Figure 7A-C). The pattern of long and short forms was not influenced by the presence of the different mutations.

In WT MEFs, OPA1 exhibits the typical pattern with five bands, two for the long forms and three for the short ones, due to the presence of all the isoforms (four in mice, because of the absence of exon 4 splicing), and of their cleavage products. Conversely, ISO1 MEFs and all the mutants present only two bands, being expressed one long isoform with the S1 cleavage site only (Figure 7B).

As highlighted by the densitometry analysis, no significant difference was observed in OPA1 level and processing, while a tendency to overexpression was apparent in I382M and D603H mutant compared with ISO1 (Figure 7D). No difference was evidenced also in the level of the other proteins involved in mitochondrial dynamics.
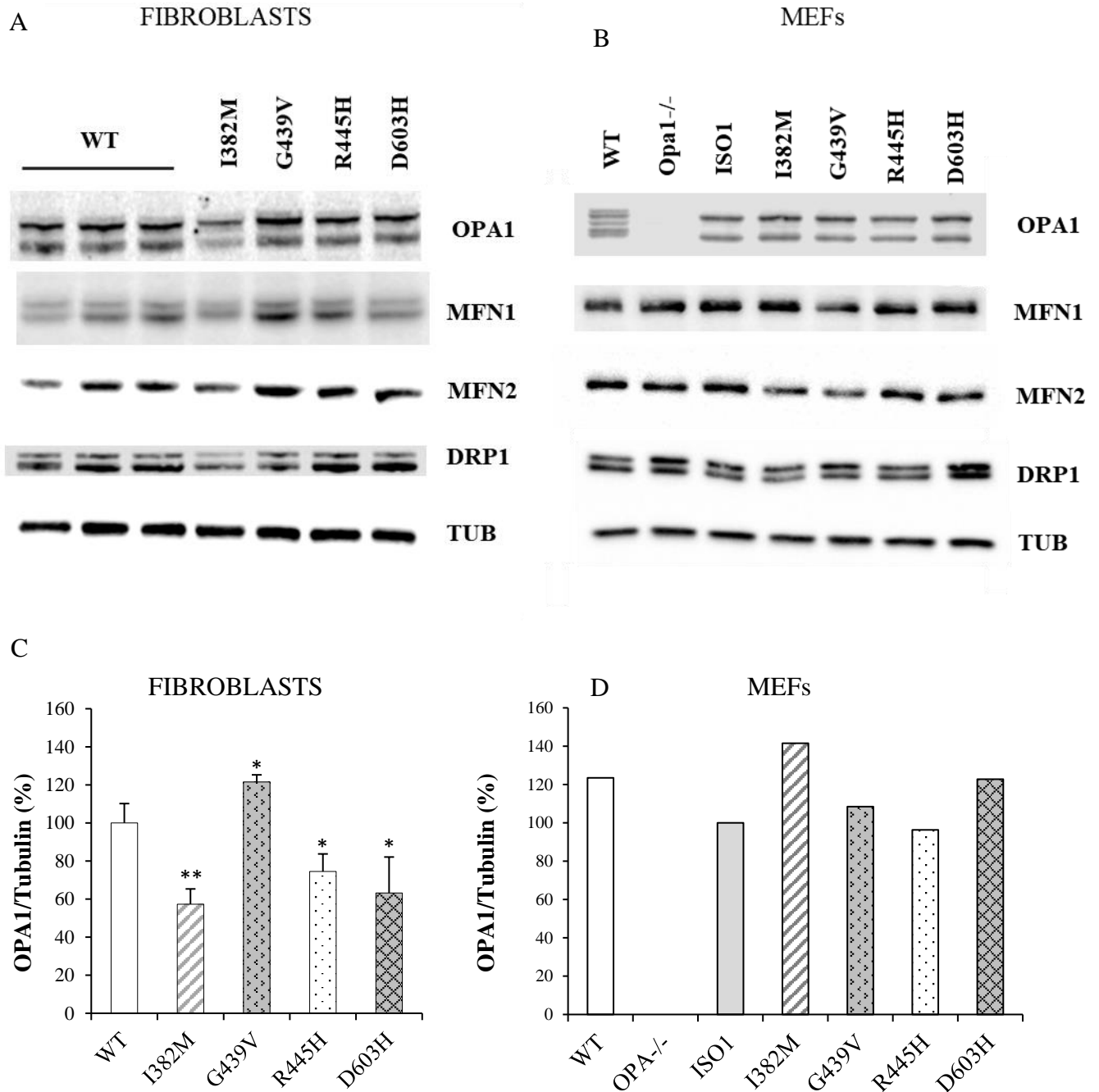

Figure 7. Representative western blot of proteins involved in the fusion/fission machinery in fibroblasts (A) and MEFs (B). Densitometric quantification was performed for each band against that of tubulin (C and D). Data are means ± SD of three independent experiments. *denotes $p < 0.05$ **$p < 0.01$

OPA1 oligomers

We decided to investigate whether the mutations affect the levels of OPA1 oligomers, by setting up a protocol of separation by blue native (BN)-PAGE. The experiments were carried out in MEFs only, due to the relatively huge amount of mitochondrial proteins necessary for the analysis. The results are reported in the representative blot shown in Figure 8A, where it is apparent that all cells presented a similar behavior, except the Opa1-/-. Two large bands were detected, one with an apparent molecular weight of ~180 kDa, suggested by (3) to be composed only by short forms, and the second with an apparent molecular weight between ~250 and ~440kDa, comprising at least a trimer of two long and one or two short forms (10). All the mutants showed a higher amount of oligomers compared to WT and ISO1 cells, indicating a stronger affinity, possibly as to a compensatory effect on reduced activity, and supporting the dominant negative mechanism hypothesis. However, among the mutants there are some differences, with the D603H showing the lower amount of oligomers when normalized to SDHA subunit of CII, as the loading control, as illustrated in figure 8B.
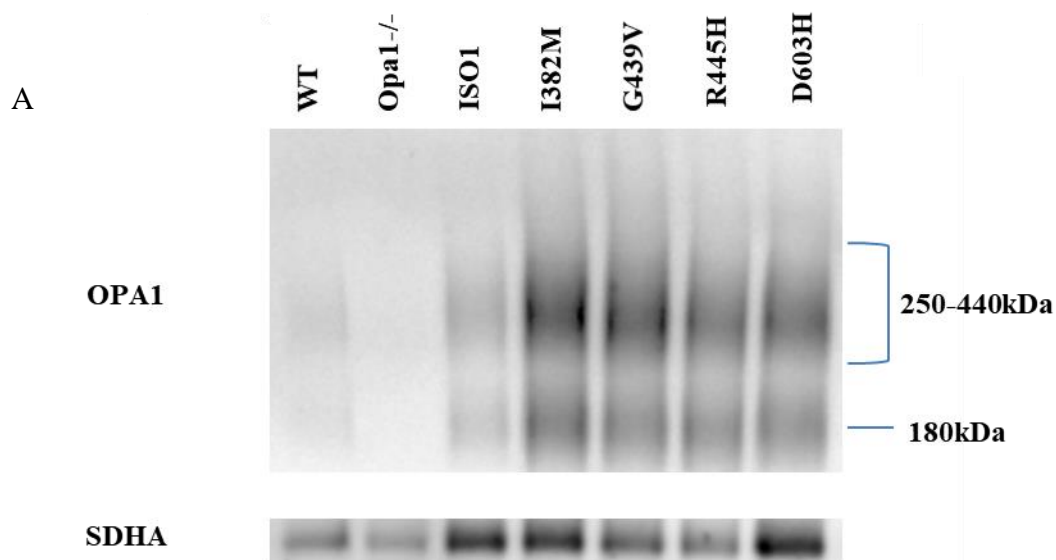
B
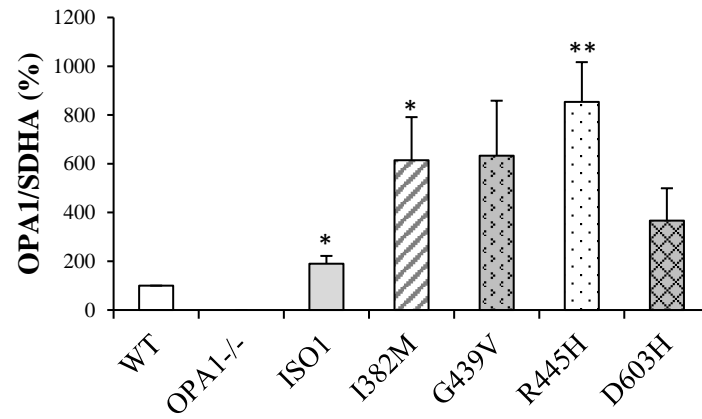
Figure 8. OPA1 oligomers in mitochondria isolated from the indicated MEFs, solubilized and separated by BN-PAGE and probed with anti-OPA1 antibody by western blot (A); densitometric bands quantification (B). Data are means ± SEM of four independent experiments. SDHA subunit of CII was used as loading loading control. *denotes $p < 0.05$ **$p < 0.01$

The mtDNA

Copy number

Considering the OPA1 involvement in mtDNA maintenance (13), we evaluated the mtDNA content in cells derived from DOA patients. As reported in Figure 9A, in fibroblasts with the I382M and D603H mutations the mtDNA copy number was similar to controls. Interestingly, the two DOA plus mutants behaved in opposite ways: in fact, while fibroblasts bearing the R445H mutation showed a significant reduction in the mtDNA content, fibroblasts with the G439V mutation displayed a significant increase (Figure 9A). In MEFs, the measurement of mtDNA copy number revealed that both the DOA-plus mutations were associated with a very low mtDNA content, similar to Opa1-/- MEFs, whereas the other two mutations were similar to WT MEFs and ISO1 cells (Figure 9B).
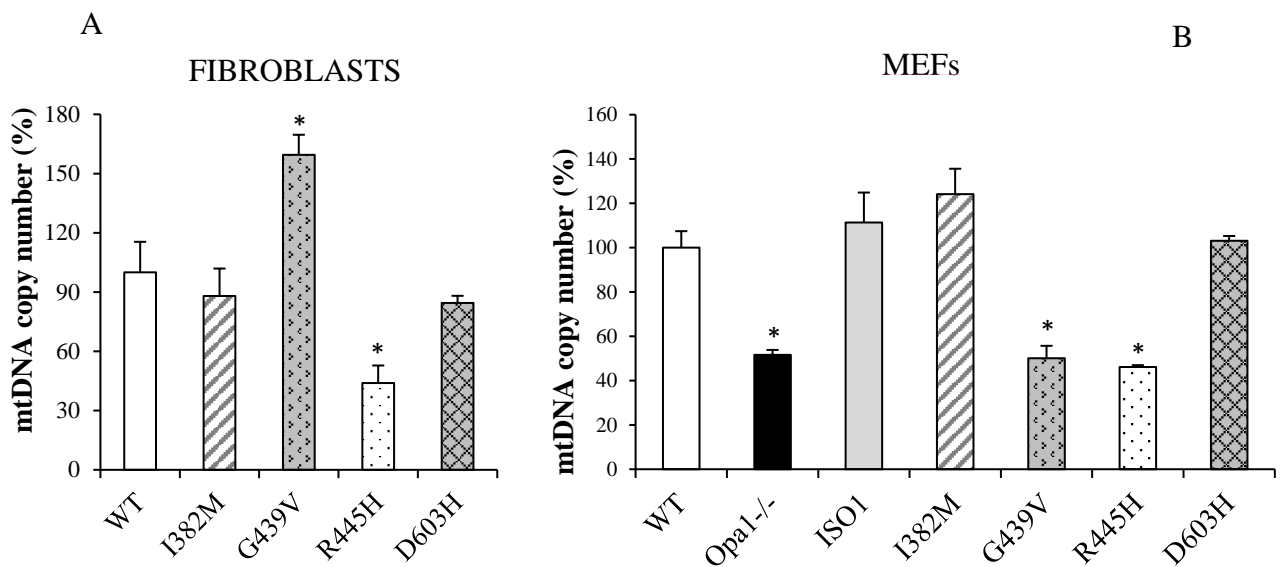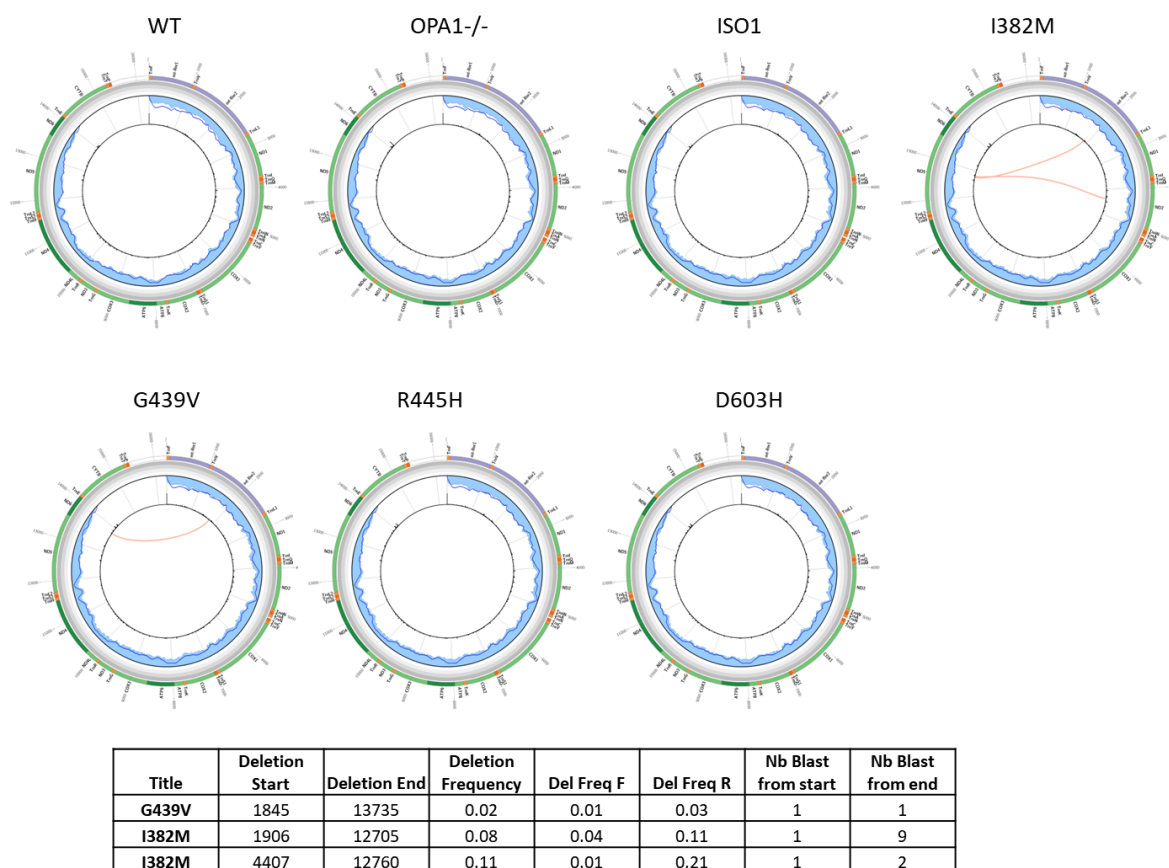

Figure 9. The mtDNA copy number of fibroblasts (A) and MEFs (B). Data are means ± SEM of at least three independent experiments. * denotes $p<0.05$.

NGS analysis

As mentioned above, OPA1 mutations could contribute to mtDNA instability, but mtDNA deletions accumulation was never reported in DOA patients' fibroblasts (78). Given the results of mtDNA content in MEFs, we decided to go deeper and, taking advantage of NGS, to evaluate the occurrence of major mutations both in terms of substitution and micro and/or macro insertion/deletion.

46

The analysis revealed the absence of homoplasmic mutation in the MEF cell lines, which all share the same mtDNA haplotype, with only minor heteroplasmic differences in terms of synonyms substitutions. Only the I382M and the G439V displayed two and one macro deletions respectively, but the frequency was so low to be not relevant (Figure 10).

Title	Deletion Start	Deletion End	Deletion Frequency	Del Freq F	Del Freq R	Nb Blast from start	Nb Blast from end
G439V	1845	13735	0.02	0.01	0.03	1	1
I382M	1906	12705	0.08	0.04	0.11	1	9
I382M	4407	12760	0.11	0.01	0.21	1	2

**Figure 10.** Results of bioinformatic analysis of MEFs mtDNA deep sequencing.

Mitochondrial morphology

Mitochondrial network morphology

The mitochondrial network morphology was then investigated by fluorescence microscopy. Fibroblasts were incubated in DMEM-glucose or in glucose-free DMEM containing galactose, a condition known to force cells to rely on OXPHOS for ATP synthesis. MEFs bearing the *OPA1* mutations were incubated in DMEM-glucose only. The cell phenotypes were scored into three categories on the basis of different mitochondrial morphology: cells with filamentous and interconnected network (filamentous), cells with short filamentous mitochondria (intermediate) and cells with fragmented mitochondria (fragmented). Representative images of the three categories for fibroblasts and MEFs are shown in Figure 11A and B, respectively.

Quantitative analysis of fibroblasts incubated in DMEM-glucose revealed that most cells exhibited a completely filamentous mitochondrial network in controls and in the I382M mutants, whereas the G439V, the R445H and D603H mutations induced a slight increase of cells with intermediate mitochondria (27%, 18% and 33%, respectively, Figure 11. C). In DMEM-galactose, the percentage of cells with fragmented mitochondria, quite undetectable in control fibroblasts, was variously increased in the presence of the four *OPA1* mutations, being more relevant in the G439V and R445H mutants (54% and 40%, respectively, Figure 11C).

In MEFs, the same analysis was performed in DMEM-glucose only, being the alterations in the network already apparent under this condition. Indeed, except for the I382M mutation, that behaved similarly to ISO1, the D603H showed a marked increase of cells with fragmented network and very few cells with filamentous network. Furthermore, MEFs bearing the two DOA "plus" mutations exhibited the complete fragmentation of the mitochondrial network, exactly as the Opa1-/- MEFs (Figure 11D).

A

B

DMEM

C

Fibroblasts

DMEM-galactose

D
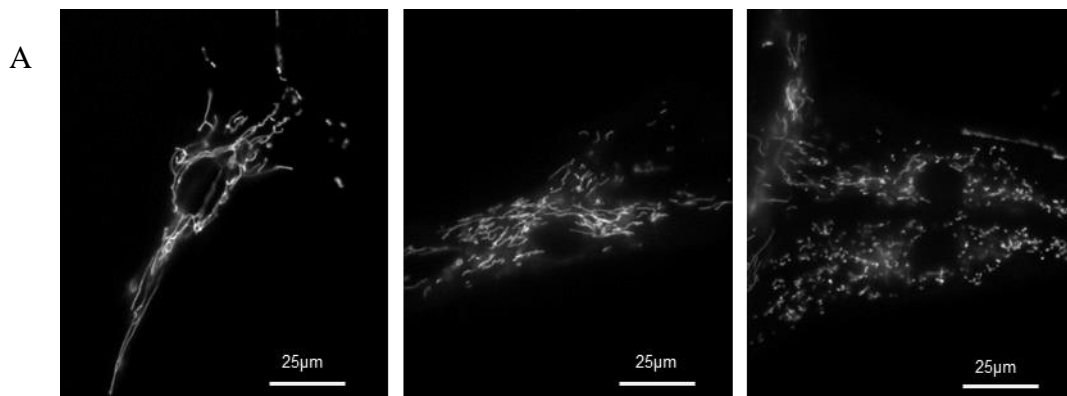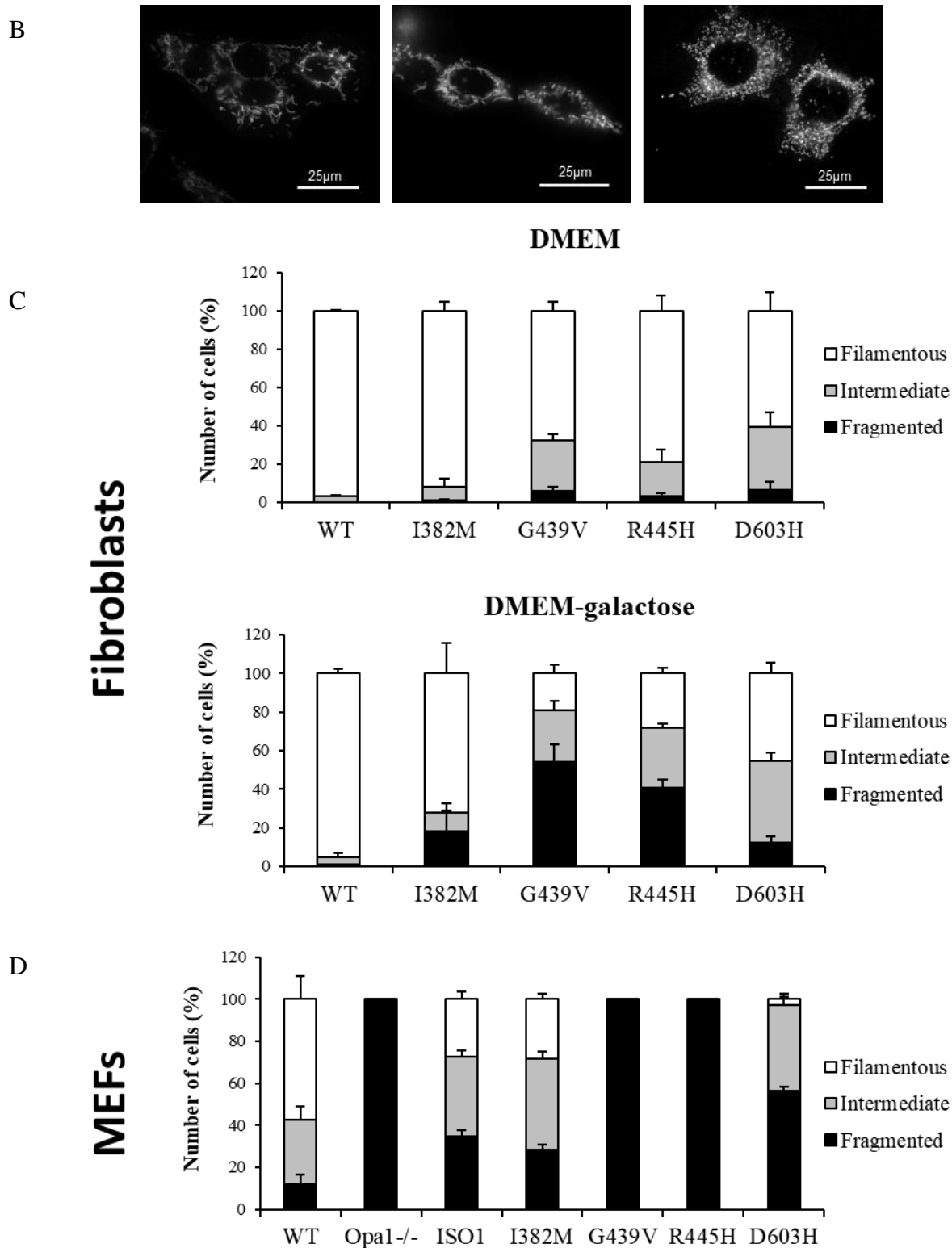
MEFs

Figure 11. Representative images of the three categories of fibroblasts (A) and MEFs (B), which were scored as: cells with filamentous and interconnected network (filamentous), cells with short filamentous mitochondria (intermediate) and cells with fragmented mitochondria (fragmented). Quantification of cells according to these categories in fibroblasts (C) and MEFs (D). 40-60 cells were scored for each cell line Data are means ± SEM of at least two independent experiments.

Cristae **architecture**

Ultrastructural defects in the *cristae* architecture of fibroblasts from DOA patients bearing different OPA1 mutations were already reported in previous studies (11,78).

Thus, we decided to evaluate the mitochondrial ultrastructure of mutant MEFs by electron microscopy (EM). The mitochondria were scored into five categories (Figure 12. A), on the basis of their shape, the *cristae* organization and the matrix density, as described in detail in Methods.

As reported in Figure 12B, the two DOA mutants showed a mitochondrial ultrastructure similar to ISO1 cells, whereas the two DOA plus mutants exhibited a drastic disorganization of *cristae* architecture and reduced matrix density, with the R445H mutant being the most severely affected with features similar to Opa1-/- MEFs.

A

Class I   Class II   Class III   Class IV   Class V
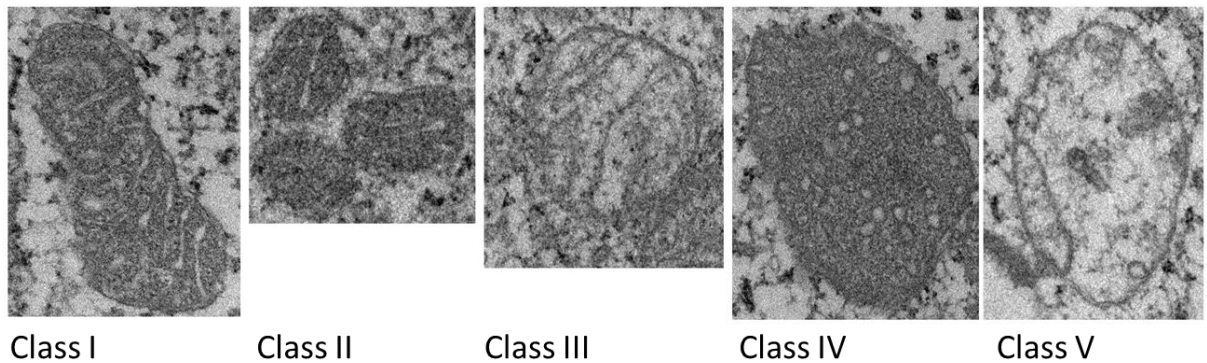
B
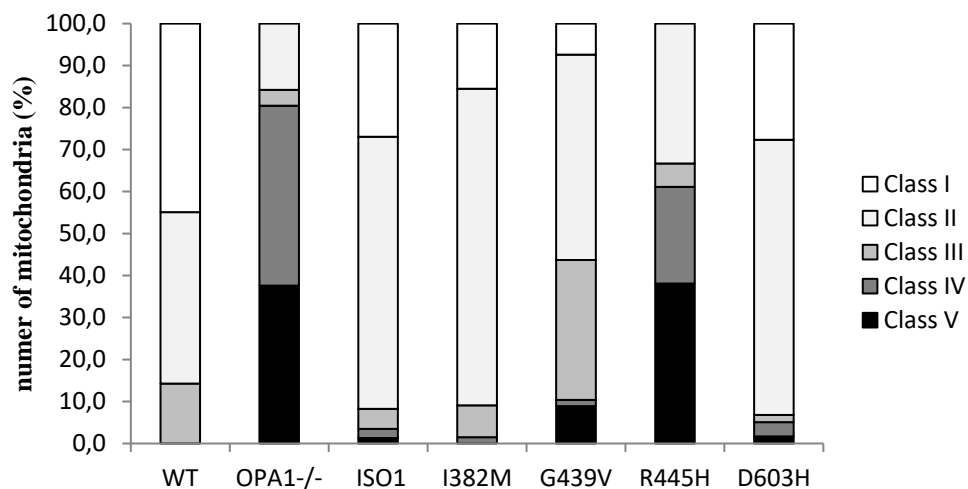
Figure 12. Representative EM images of the five classes in which the mitochondria were scored (A) and quantification (B).

Energetic profile

Cell viability

Previous studies showed that fibroblasts from patients bearing *OPA1* mutations causing haploinsufficiency exhibit the same proliferation rate of controls both in DMEM and in DMEM-galactose (11). Thus, we measured the growth of *OPA1* mutants MEFs under both normal and stressfull conditions.

In DMEM, all MEFs mutants were able to proliferate, without any statistically significant difference from WT cells (Figure 13. A). Conversely, when incubated in DMEM-galactose, the two DOA "plus" mutants were unable to grow, being significantly different from WT already after 24h, even if they did not undergo cell death. The D603 MEFs did grow as WT at 24h, but stopped growing at longer times, whereas the I382M MEFs were indistinguishable from WT (Figure 13B).

A   B
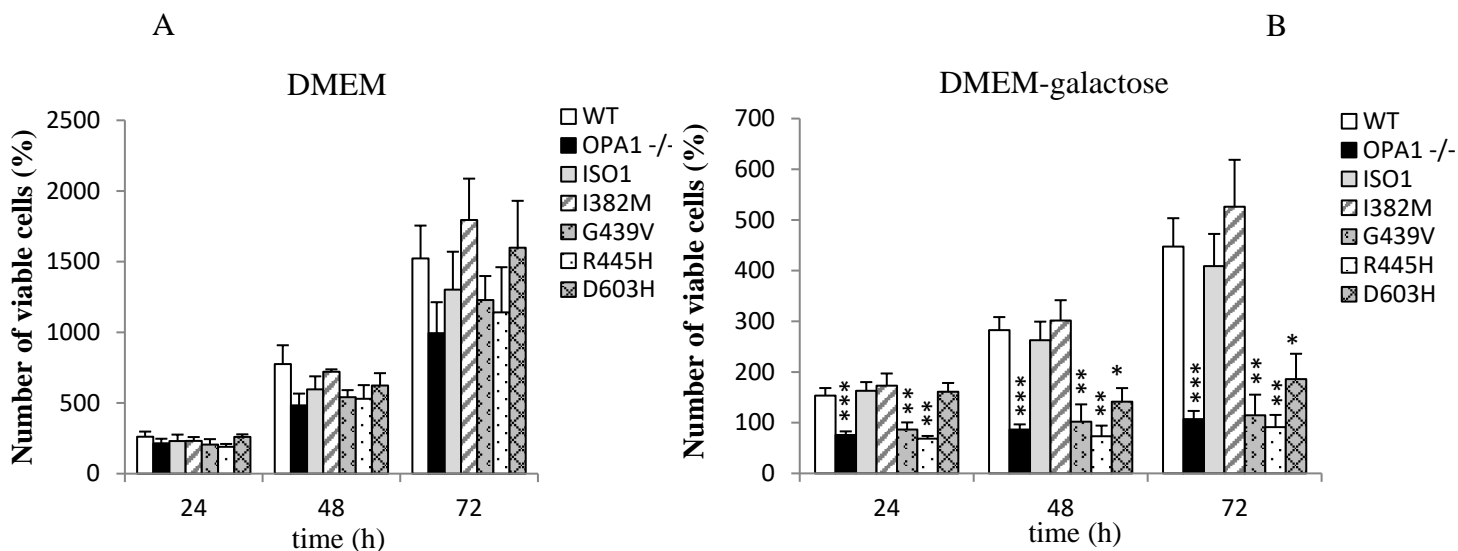

Figure 13. Viability of MEFs in DMEM (A) and DMEM-galactose (B). Data are expressed as % over the number of cells determined at time t=0, and are mean ± SEM of at least three independent experiments. *denotes p<0.05, **p<0.01 ***p<0.001.

Cellular ATP content

To evaluate the energetic competence of DOA patients' fibroblasts and MEFs (Figure 14 A and B, respectively), we measured the cellular ATP content during incubation in DMEM-galactose.

In agreement with previous reports(11), under these conditions WT cells shift from glycolytic to oxidative metabolism, with an increase in cellular ATP after 24h (+61.3 ±15%) which was maintained up to 48h (+38.9 ±16,7%). Conversely, all the mutant fibroblasts were unable to increase their ATP levels when forced to exploit exclusively the OXPHOS, with significant differences at 24h, being the D603H mutants the most severely affected (Figure 14A).

In MEFs, already after 16h incubation in DMEM-galactose, the two DOA "plus" mutants exhibited a marked reduction of ATP levels, which were similar to those of Opa1-/- MEFs, and further decreased after 24h, whereas MEFs with the other *OPA1* mutations behaved as WT (Figure 14B).
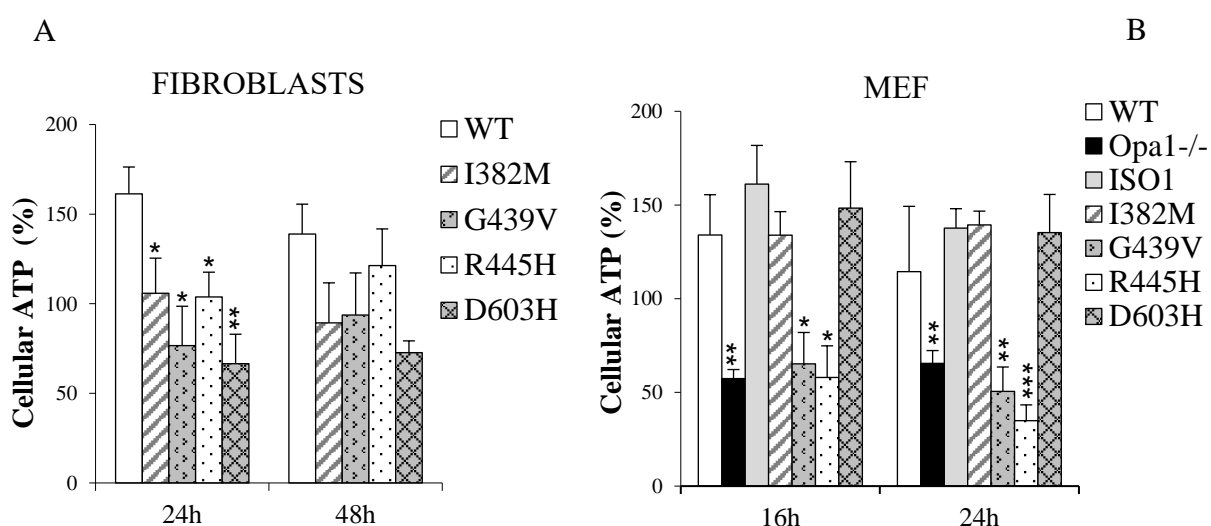

Figure 14. Cellular ATP content in fibroblasts (A) and MEFs (B) incubate for the indicated times in DMEM-galactose. Data are express as % of ATP content determined at t=0, and are means ± SEM of at least three independent experiments. *denotes $p < 0.05$, **$p < 0.01$, ***$p < 0.001$.

Mitochondrial ATP synthesis

Then we determined the rate of mitochondrial ATP synthesis in digitonin-permeabilized cells, supplying saturating concentrations of the substrates of CI, CII and glycerol-3-phosphate dehydrogenase (GPD). The data were normalized for the citrate synthase (CS) activity, an indicator of mitochondrial mass.

As reported in Figure 15A, the values of ATP synthesis rate showed a great variability in fibroblasts, with no correlation with the mutations' severity.

That was not the case of the MEFs. Indeed, only the OPA1-/- MEFs exhibited a marked reduction (about the 70%), whereas only a tendency toward reduction was apparent for the two DOA "plus" mutants and for the I382M, while the D603H mutant was similar to the ISO1 and WT, partially in accord with the cellular ATP content (Figure 15. B). It has to be noticed that we always determined higher CS activity in the I382M mutant.
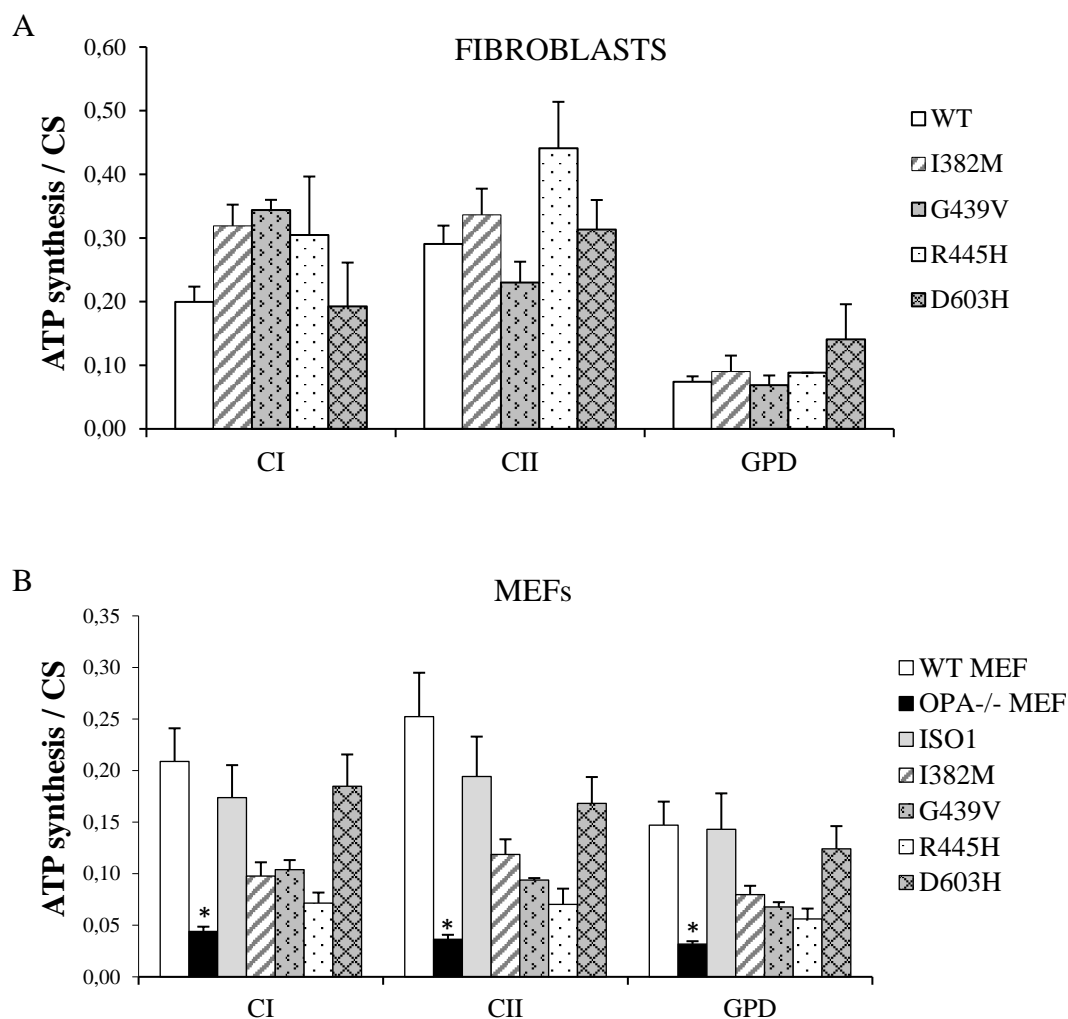
Figure 15. Mitochondrial ATP synthesis rates of fibroblasts (A) and MEFs (B) normalized for total protein content and CS activity. Data are the means ± SEM of at least three determinations. * denotes $p < 0.001$.

Organization of RCSs

Finally, we analyzed the supramolecular organization of CI-containing RCS in digitonin-solubilized mitoplasts after BN-PAGE, by determining the CI in gel activity (CI-IGA) as previously described (175). The assembly of complex V (CV) was determined in the same gels after western blot analysis using antibodies against the α subunit of CV.

In WT fibroblasts, the CI-IGA revealed three bands, corresponding to isolated CI, the CI+III$_2$ and the CI+III$_2$+IV supercomplexes. The intensity of bands corresponding to isolated CI and to CI+III$_2$ supercomplex was significantly decreased in mutants compared to controls, whereas the majority of CI-IGA was detected as a single band corresponding to the CI+III$_2$+IV supercomplex. It seems therefore that in fibroblasts the four mutations did not dramatically affect the supramolecular organization of OXPHOS complexes, but rather promoted the aggregation of the CI+III$_2$ and CI+III$_2$+IV supercomplexes.

Western blot analysis revealed a single band corresponding to the CV monomer, clearly indicating that the CV assembly was not influenced by any of the *OPA1* mutations (Figure 16A).

That is not the case of MEFs, where four bands were positive to the CI-IGA in the WT and ISO1 cells, as detailed in Figure 16B. Conversely, in the two DOA "plus" mutants, the bands corresponding to isolated CI, and CI+III$_2$ and CI+III$_2$+IV supercomplexes were much weaker, and that at higher molecular weight, corresponding to the CI+III$_2$+IV$_n$ supercomplex, was absent. A reduced activity was also apparent in the I382M mutant, whereas the D603H was more or less similar to ISO1 cells (Figure 16B).

Western blot analysis of CV revealed in G439V and R445H MEFs the presence of two bands at lower molecular weight, corresponding to the F$_1$ portion alone, in addition to the band corresponding to the monomeric holo-enzyme, similarly to Opa1-/- MEFs, indicating that CV is partially disassembled in sub-complexes (Figure 16. B). The amount of CII, used as loading control, did not significantly change.

In DOA "plus" MEFs, the defects in RCSs assembly are mirrored by a decreased amount of representative subunits of the OXPHOS complexes, as demonstrated by western blot on SDS-PAGE of total lysate in Figure 16C and D. This result is in line with the significant decrease on mtDNA content measured in these cell lines (see figure 9B)

A

Fibroblasts
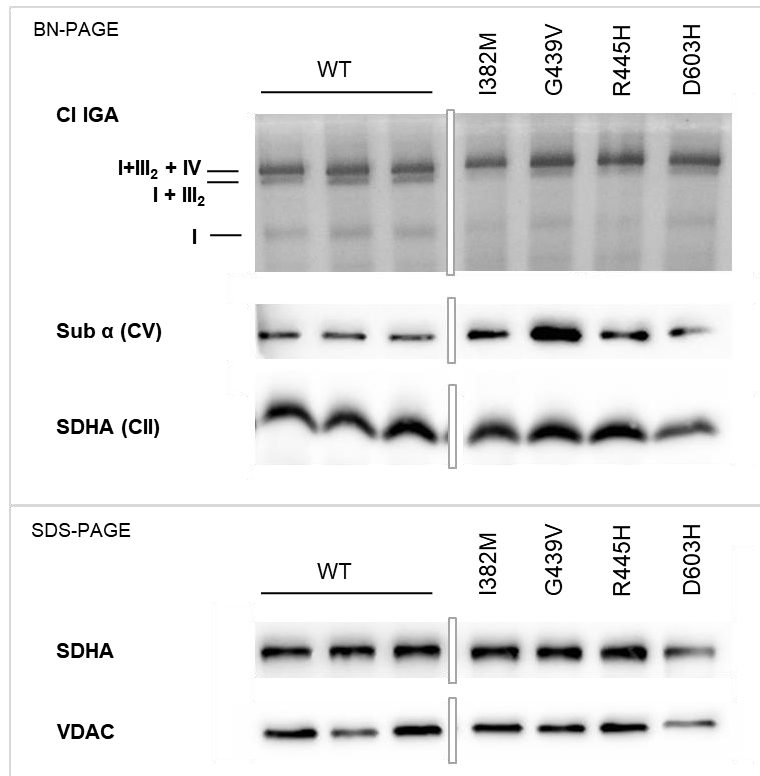
B

MEFs
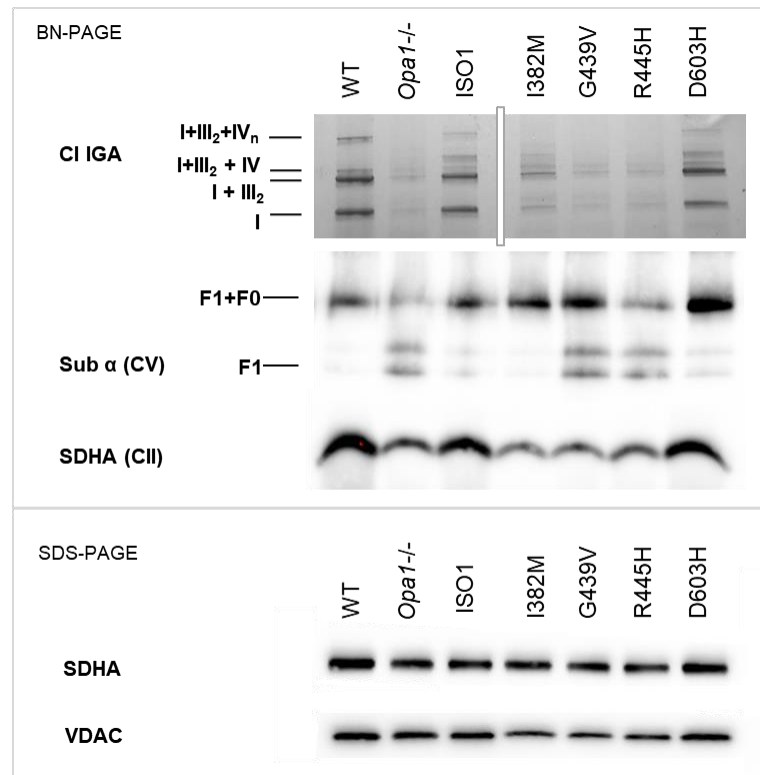
C
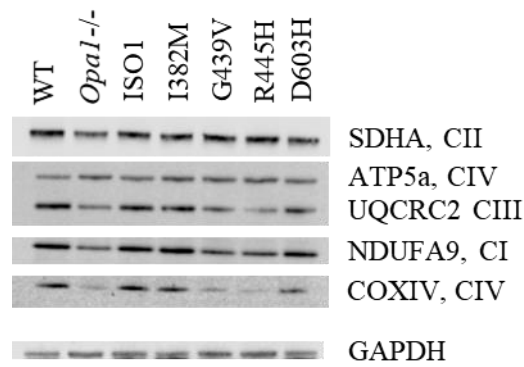
D
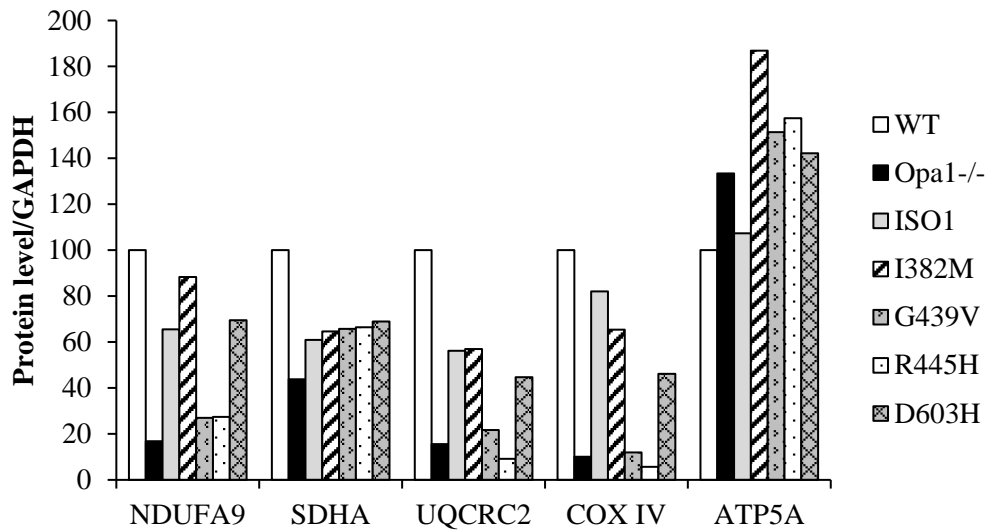
Figure 16. Respiratory supercomplexes and CV in fibroblasts (A) and MEFs (B). After BN-PAGE of digitonin-solubilized mitochondria, the CI in-gel activity (IGA) was measured. Western blot analysis was carried out using antibodies against NDUFA9 (CI), SDHA (CII), Core2 (CIII), sub α (CV). CII was used as a loading control. (C) Western blot of respiratory complexes subunits in MEFs, with densitometric quantification performed for each band against the band of GAPDH (D).

Other cell models of DOA by using CRISPR/Cas9 gene editing technology

The MEF model suffers of some experimental limitations, first because it is a mouse system, that can someway differ from the human counterpart, secondly because the *OPA1* nonsense mutations causing haploisufficiency could not be introduced in the MEFs, as the premature truncation of the mRNA causes the total absence of the protein product.

For these reasons we decided to generate a human cell model, expressing the physiological pattern of OPA1 isoforms, introducing the same mutations already analyzed in the MEFs, by using the CRISPR/Cas9 gene editing technology (REF).

The choice fell on SHSY5Y cells, a human neuroblastoma cell line, able to differentiate in neuronal cells after incubation with retinoic acid, allowing us obtaining a cell model closer to that specifically affected in DOA, where the pathological effects of *OPA1* mutations is disclosed. We also conducted the same experiments in parallel on HeLa cells, more resistant and already widely used in the study of OPA1.

We decided to introduce two of the *OPA1* mutations previously introduced into MEFs (the I382M and the DOA "plus" R445H mutations) and two other nonsense mutations that we were unable to study in the MEF model (the T449X and the V903X). We designed several guideRNAs for each mutation and, after introduction into a plasmid, containing the gene for the Cas9 protein and GFP as reporter gene, we tested the cutting efficiency on Hek293 cells. Those that were shown to cut at the desired site were selected and co-transfected in SHSY5Y and HeLa cells together with another plasmid, in which we subcloned the donor DNA. This genomic fragment was isolated and cloned from the genomic DNA of the fibroblasts of patients with the corresponding mutations, and it was supposed to serve as template for the cells to introduce the mutations within their DNA by homologous recombination (HR).

Both cell lines, however, not only demonstrated a very low transfection efficiency of our plasmids (<5%), as shown by fluorescence analysis for GFP expression, but even selecting only groups of GFP-positive cells using a cell sorter it was impossible to identify, among the hundreds of clones screened, cells that successfully introduced the selected mutations via HR (results not shown). The only clone we were able to isolate was a HeLa clone that introduced heterozygously a random mutation at the cutting site via non homologous end joining (NHEJ), adding three bases and then leaving the ORF in-frame, with the only

addition of a phenylalanine. However preliminary studies showed that this mutation did not impact on the mitochondrial network phenotype. While on the one hand both cell lines expressed low levels of HR compared to the NHEJ machinery, on the other hand the need to start from single clones led us to lose many of the isolated cells, especially for the SHSY5Y that hardly survived under this condition, tending to differentiate and stop growing in the absence of contacts with neighboring cells.

Therefore, although the CRISPR/Cas9 technology has proven to be a very powerful tool in recent years, it seems that, at least in our conditions, it is much more suitable for generating knockouts of genes rather than introducing specific point mutations.

Search for therapeutic molecules: the ORMs

One of the advantage of disposing a cell model bearing mutations causing a disease is the possibility to test the effects of bioactive molecules for therapy.

A number of "OPA1 Rescuing Molecules" (ORMs) were previously identified in a research project carried out in collaboration with Dr. Enrico Baruffini and his group, at the University of Parma. In a strain of *Saccaromyces Cerevisiae* depleted of the OPA1 orthologue Mgm1, chimeric constructs constituted by the N- terminal region of Mgm1 and portions of the wild type or mutated human *OPA1* gene were introduced (176). One of these chimeras was used to perform a screening of more than a thousand molecules from libraries of FDA-approved molecules. This screening identified some ORMs, which proved capable of restoring the wild-type phenotype in the yeast model.

Here I present a preliminary analysis, where the effects of three of these ORMs (ORM2, ORM11 and ORM12) were evaluated, by examining three parameters: the mitochondrial network morphology, the cell viability and the ATP content after metabolic stress.

Three MEF cell lines were employed, the ISO1 as control, those bearing the D603H mutation, representative of classic DOA and characterized by intermediate clinical severity, and those with the R445H, as representative of the most severe syndromic form DOA "plus".

Determination of ORMs dose-responses

First, we evaluated the effects of increasing concentrations of the three ORMs on the cell viability, after incubation in DMEM in the absence or presence of the indicated concentrations of the three ORMs, obtained by serial dilutions. For each cell line, the number of viable cells before (time 0) and after 48 hours of incubation was measured by using the SRB assay (Figure 17).

The ORM2 was already slightly toxic at 1μM in ISO1 and R445H, whereas it had a positive effect on D603H. ORM11 exhibited a mild effect on R445H and D603H only, except at the highest concentration tested (50μM). ORM12 had no positive effect in all cell lines, and become toxic at 50μM. On the basis of the results, we decided to use the concentrations of 1, 1 and 10μM for ORM2, ORM11 and ORM12, respectively.
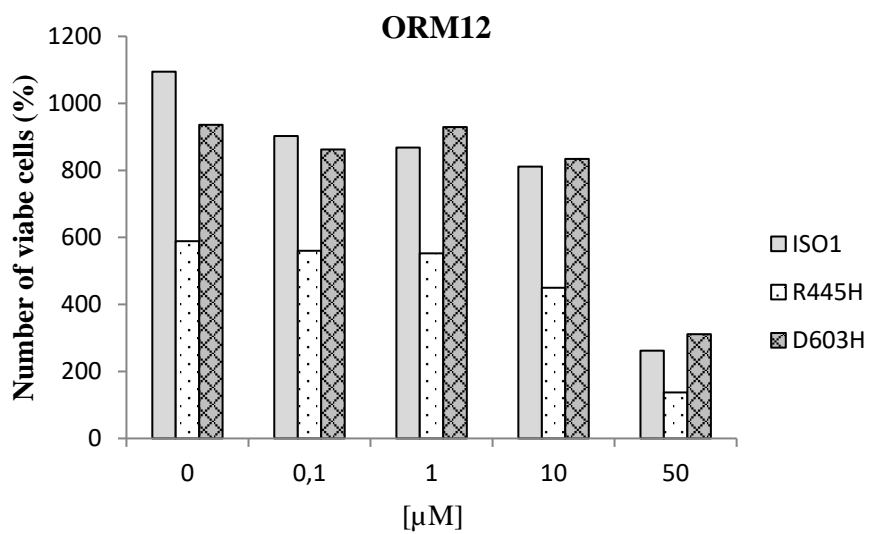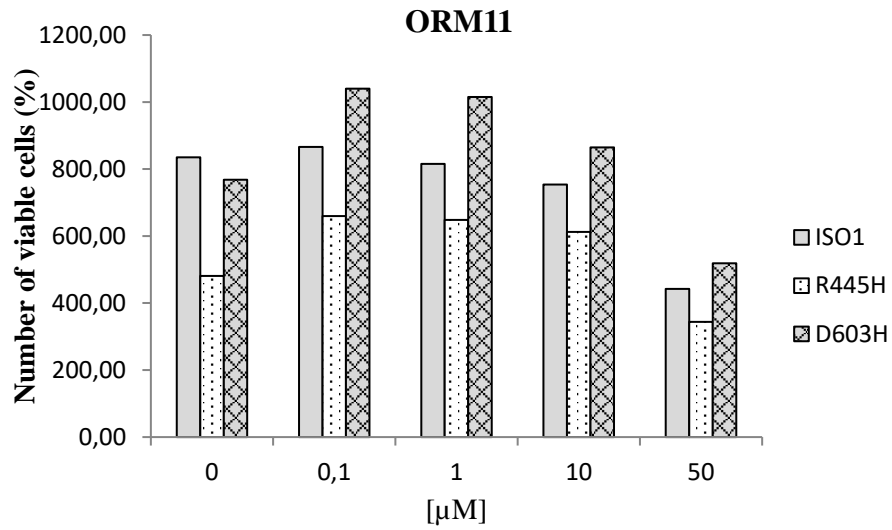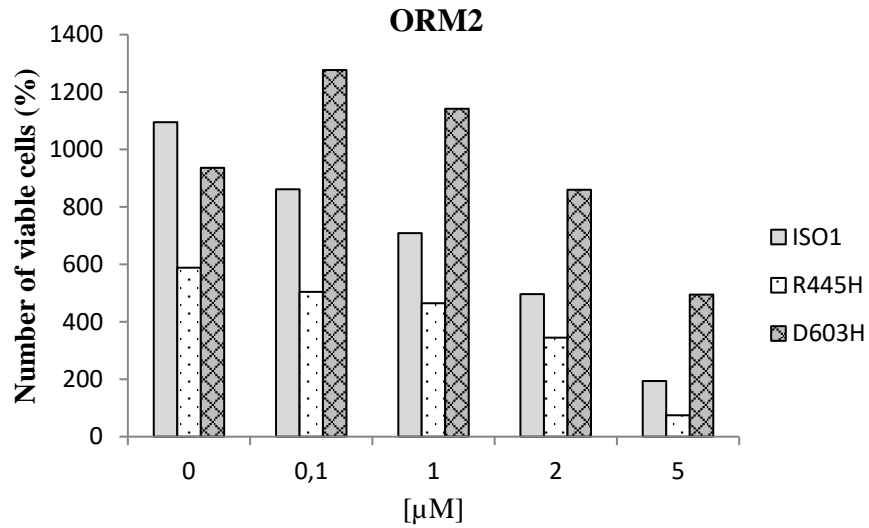
Figure 17. Number of viable ISO1, R445H and D603H cells after 48h incubation in the absence or presence of the indicated ORMs. Data are expressed as percentage compared to t=0.

Mitochondrial network morphology

The mitochondrial morphology was evaluated and quantified as previously described, after 24 and 48h of incubation in the absence or presence of the ORMs in both DMEM or DMEM-Galactose (Figure 18).

In ISO1 MEFs, slight positive effects were exhibited by ORM2 in both DMEM and DMEM-galactose at 24h incubation, being these effects lost at 48h in DMEM-galactose. Still, in this condition the ORM12 showed positive effects.

Conversely, no effects were evidenced in R445H, exhibiting a totally fragmented network in every condition. Finally, in D603H, only the ORM2 consistently incremented the number of cells with filamentous and intermediate network in DMEM and in particular in DMEM-galactose.
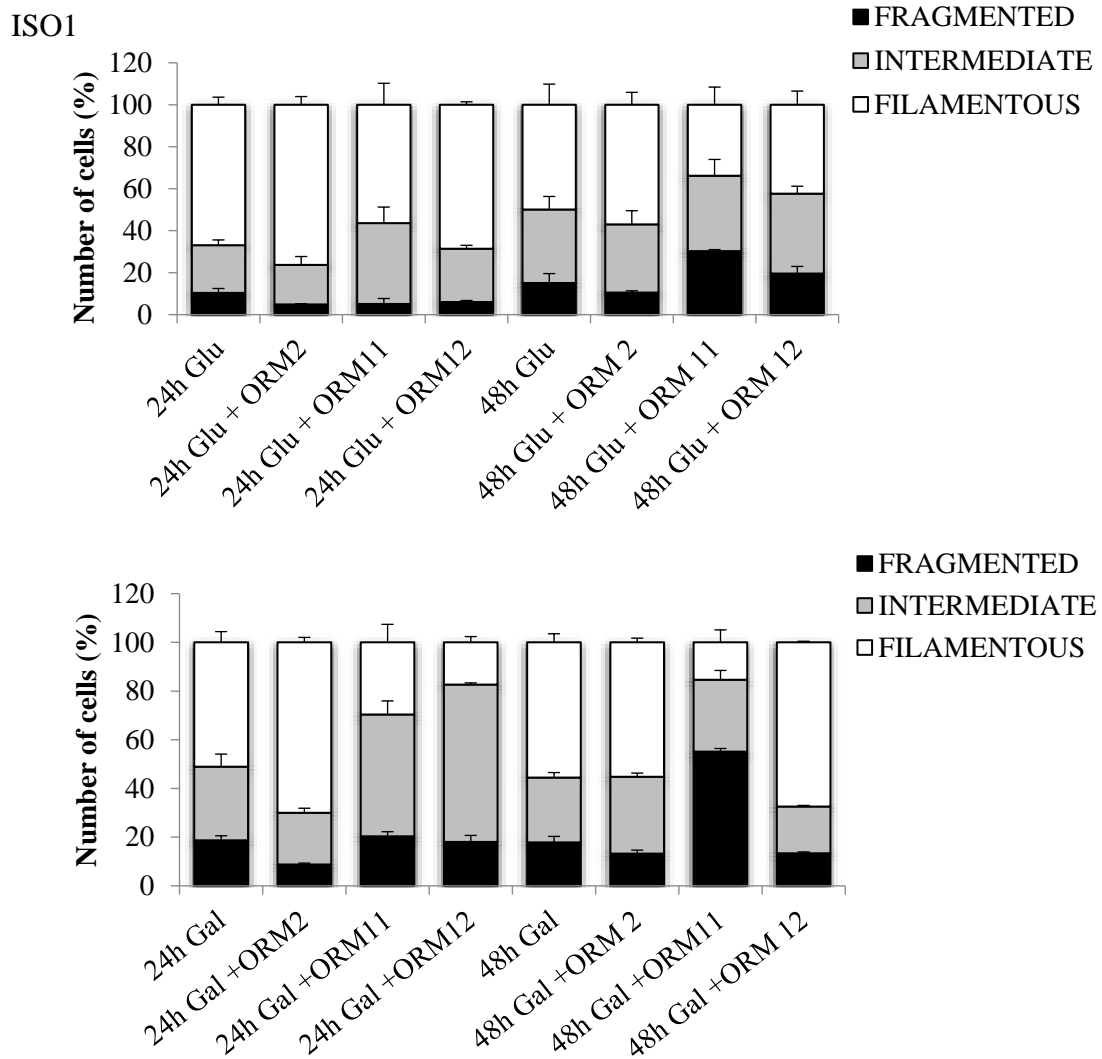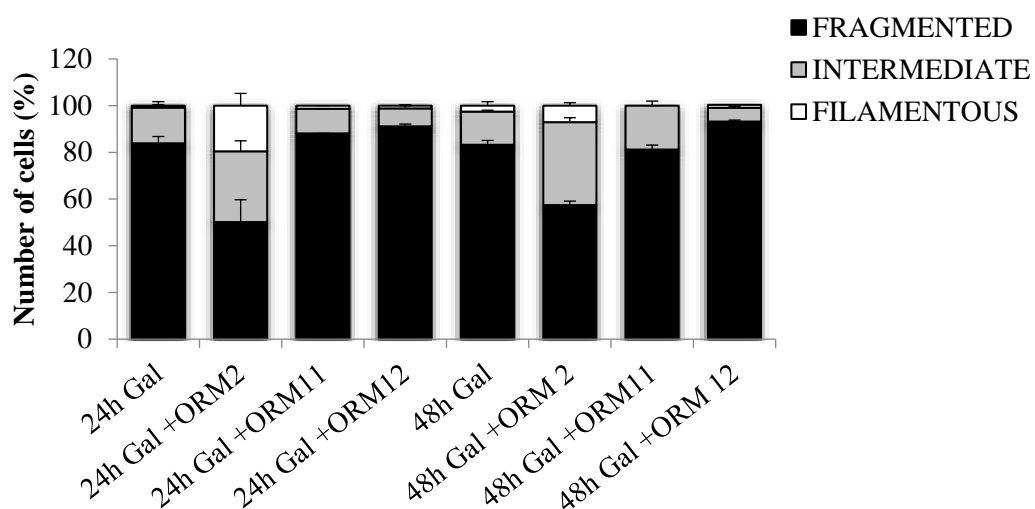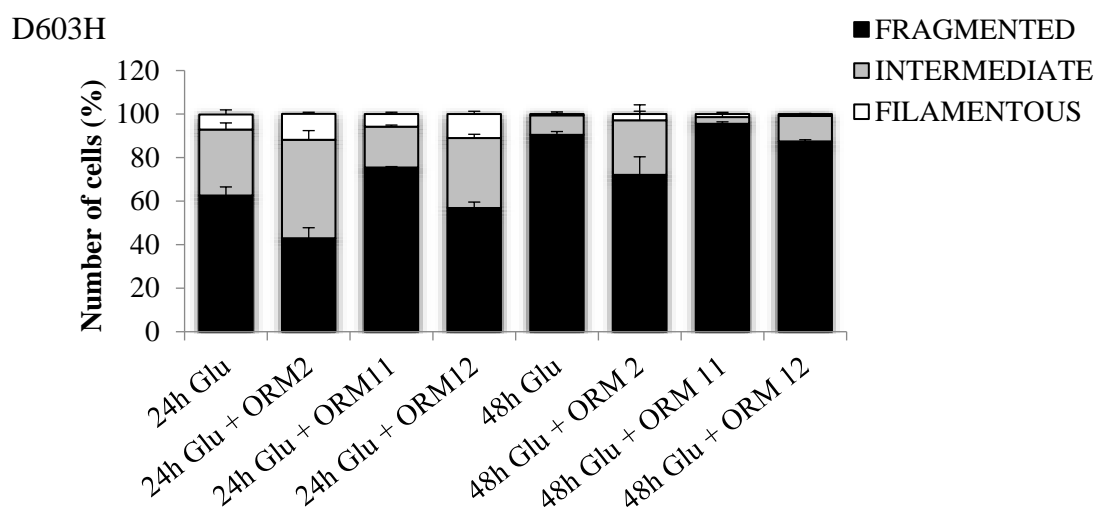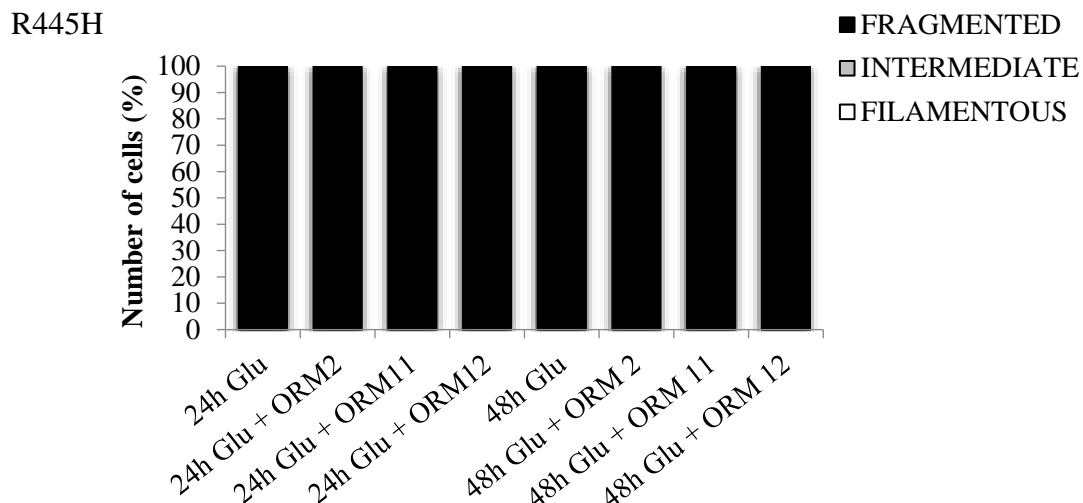
Figure 18. Effects of the three ORMs on mitochondrial network morphology of ISO1, R445H and D603H incubated in DMEM and DMEM-Galactose after 24 and 48h. Data are means ± SEM of at least two independent experiments.

Cellular viability after metabolic stress

 Then we evaluated the effects of ORMs on the viability of cells incubated in DMEM-galactose, a condition of metabolic stress, as previously described. After 24h of incubation, the ORM12 exhibited a positive effect on all cell lines, significant on both the mutants. In the D603H mutant, a minor positive effect was obtained also by the ORM2, which persisted after 48h. The ORM12 was indeed effective on all three the cell lines, even if not statistically significant. The ORM2 showed some efficacy in ISO1 and D603H, but not in the R445H mutant (Figure 19).
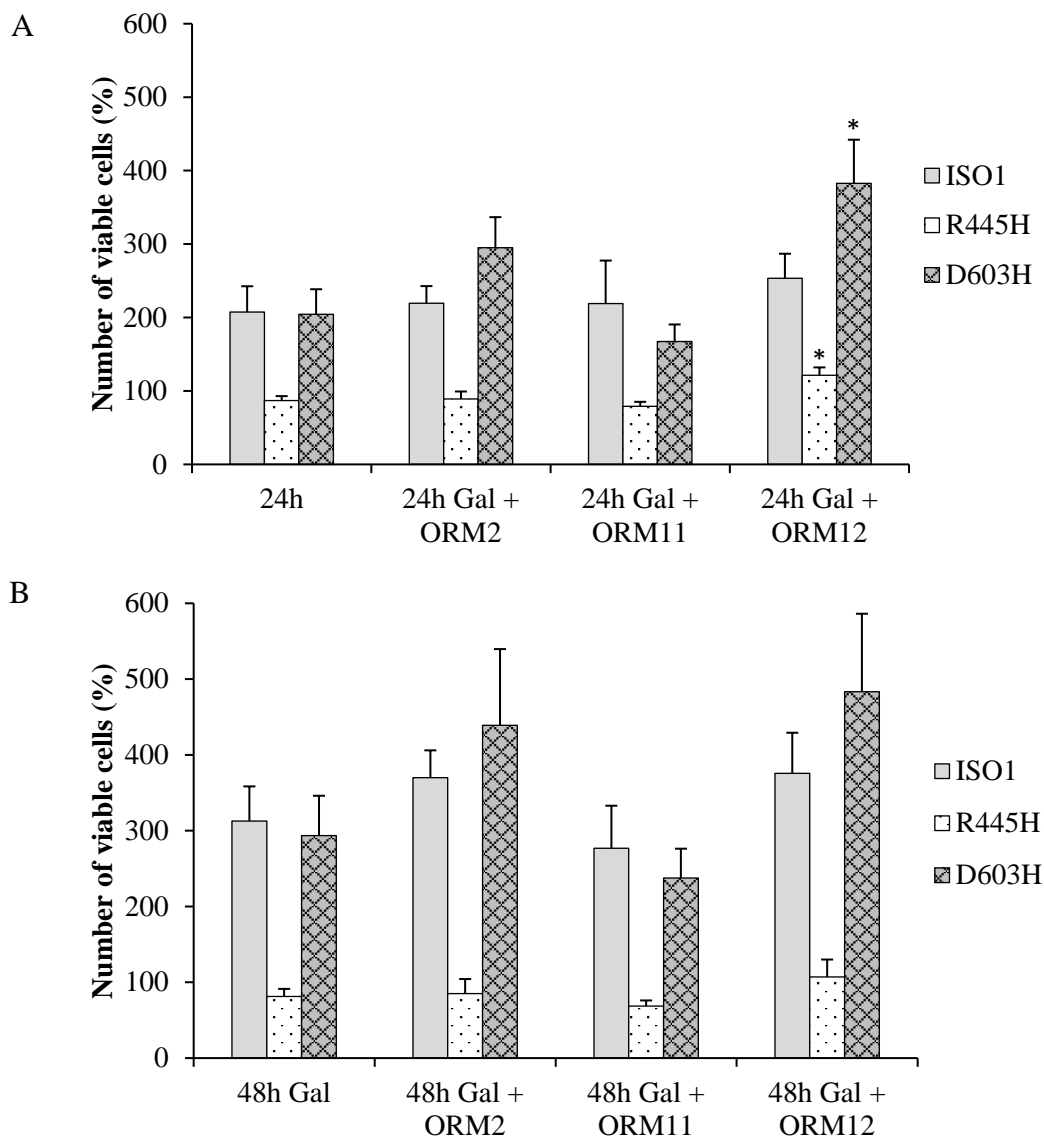
Figure 19. Viability of ISO1, R445H and D603H cells after 24 (A) and 48h (B) incubation in DMEM-galactose in the absence or presence of the ORMs. Data are expressed as percentage compared to t=0. Data are the means ± SEM of at least three determinations. * denotes $p<0.05$.

Cellular ATP content

Finally, to confirm the effects of the ORMs on mitochondrial energetic efficiency, we evaluated the cellular ATP content after the metabolic stress induced by incubation in DMEM-galactose. Cells were incubated in the absence or presence of the three ORMs in DMEM-galactose for 16 and 24h. It could be noticed that the ORMs had no effects in ISO1 and D603H cell lines, which did not exhibit any decrease of ATP levels under stress condition. Conversely, in the R445H mutant that experienced a significant decrease of the cellular ATP already after 16h under stress medium, ORM2 and ORM12, increased the ATP content, this effect persisting also at 24h (Figure 20), in agreement with results obtained in the viability experiments.
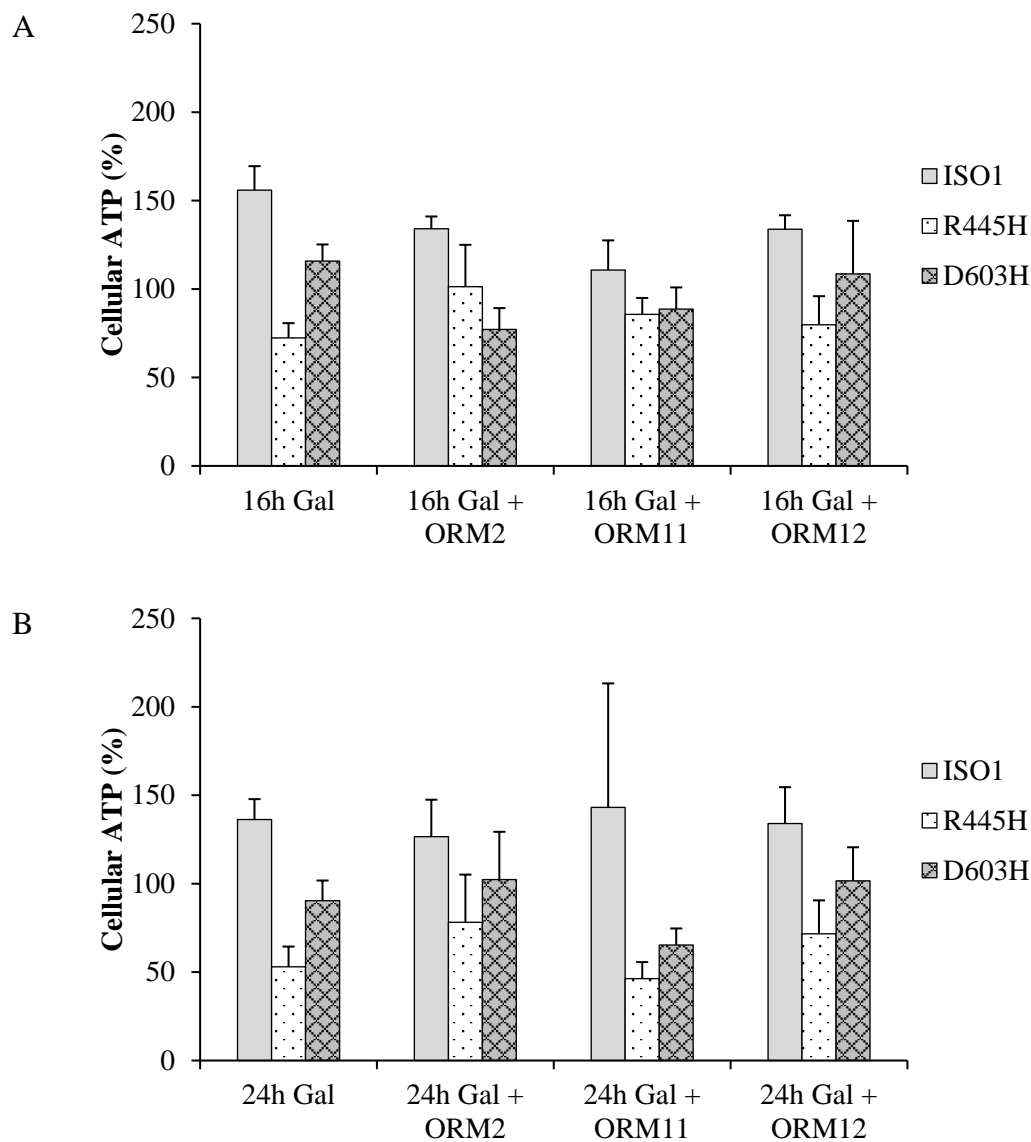
Figure 20. ATP content of ISO1, R445H and D603H cells after 16 (A) and 24h (B) of incubation in the absence or presence of the ORMs in DMEM-galactose. Data are expressed as percentage compared to t=0. Data are the means ± SEM of at least three determinations.

DISCUSSION AND CONCLUSIONS

Although DOA was initially described as a homogenous clinical phenotype characterized by optic neuropathy, in the last years the scenario has become much more complex. The two main entities, the DOA and the DOA "plus", due to mutations that cause haploinsufficiency and negative dominance respectively, were flanked by a broad spectrum of neurodegenerative diseases in which OPA1 was directly implicated (multiple sclerosis-like syndrome, spastic paraplegia, Behr-like syndrome, syndromic parkinsonism and dementia). On the other side, much more severe syndromic forms were characterized by a biallelic mode of inheritance (both hetero and homozygous).

Nevertheless, till now we have no knowledge of an unique relationship between the position of the mutation within the protein and the severity of the related phenotype, and in some cases the same mutation was found associated with DOA or DOA "plus" alternately (96,155). So far, one of the most widely used model in this sense has been the patients' fibroblasts, that anyway presents some limitations. In fact, this model suffers from a great biological variability due to the different nuclear and mitochondrial genetic background from patient to patient and it is also influenced by the patient's age at the time of biopsy. Fibroblasts have a rather slow growth, undergo senescence after a number of divisions and often show very mild phenotypes when compared to the patient's clinical status. Furthermore, the results obtained on mtDNA depletion or deletion are often conflicting according to the study considered.

The need of alternative models suitable for establishing the potential pathogenicity of a mutation within a standard context is therefore evident.

The model *ad hoc* generated and described in the present study is relatively easy to obtain and manage, allowing for evaluation of different OPA1 mutations in a standardized nuclear and mitochondrial background, and for quick definition of the mutation pathogenicity. Thus, it could represent a usefully tool for patients' diagnosis and also for testing the pathogenicity of new mutations. In fact, alongside the three previously characterized mutations chosen on the basis of their clinical phenotype, ranging from very mild, asymptomatic or associated with pure optic atrophy (I382M), to severe syndromic forms (G439V and R445H), we fully characterized the novel D603H mutation.

The analysis of the same *OPA1* mutations in parallel in the MEF models and in patients' fibroblasts proved useful, in addition to pathogenicity prediction, also for shedding some light on their mechanistic effects.

The three main phenotypes analyzed in fibroblasts comprise mtDNA content, energetic competence and network morphology. Only the two DOA "plus" mutants showed some

alterations in the mtDNA content, but despite the similarity of the clinical picture of the patients, the directions of these alterations were totally opposite. Indeed, the mtDNA content of fibroblasts bearing the R445H mutation was significantly reduced, whereas it increased in those with the G439V mutation. These results are discordant with those previously reported in muscle biopsies of DOA patients (42), in which the mtDNA content was similar to controls for the G439V mutation and slightly increased for the R445H mutation, but seem to be related with the alterations found in the OPA1 protein level. Both the features may be patient specific, and the augmented protein level in the G439V mutant could represent an attempt of compensation of the lowered efficiency of OPA1, while the decreased OPA1 levels of the other mutants may be due to an increased turnover of the defective protein. However, neither the altered mtDNA content nor the OPA1 protein levels seem to directly impact on the energetic features. In fact, while all the mutant fibroblasts fail to increase their ATP levels switching from glycolysis to oxidative metabolism, their capacity to synthetize ATP from the exogenous substrates of CI and CII is variable, with the differences being neither significant nor ascribable to the different mutation.

Moreover, all the mutants seem to share the same tendency toward the aggregation of the CI-containing supercomplexes to the higher molecular weight supercomplex $CI+III_2+IV$. Again, this could be explained by a compensatory effect in the attempt to maintain the energetic functions. In this regard it would be interesting to evaluate whether the OPA1 oligomers profile is also perturbed in WT and mutant fibroblasts.

Finally, a more convincing genotype/phenotype correlation is apparent in fibroblasts only when analyzing the mitochondrial morphology under stress conditions. In fact, the three mutants (the two DOA "plus" and the new D603H) exhibited only a slight increase of cells with intermediate network morphology in high glucose DMEM. However, under stress conditions, i.e. DMEM-galactose, the percentage of cells with fragmented mitochondria, quite undetectable in control fibroblasts, was variously increased by the presence of all the four *OPA1* mutations, being more relevant in the G439V and R445H.

Taken together, these results highlight once more how the albeit useful fibroblast model shows some major limitations in the definition of the pathogenicity of a new mutation.

In this regard, the MEF model provided some useful details.

Although the level of mutant OPA1 protein, the processing into long and short forms, and the OPA1 oligomerization pattern were similar, all the mutants exhibited a significant increase in the amounts of oligomers compared with both WT and ISO1 cells. Noticeably, the amount of total protein compared to the ISO1 cells was similar, as proved by the western

blot on the SDS-PAGE. It was initially proposed that OPA1 oligomers comprise two long and one short OPA1 form (10), although it has to be considered that oligomerization could also involve other protein complexes required for cristae formation, as revealed by SILAC-based interaction screens such as subunits of the MICOs complex (mitofilin and CHCHD3), the ATP synthase, prohibitin, Sam50 and the adenonucleotide transporters (76). In this later study, it was demonstrated in WT MEFs that OPA1 oligomerization increased after starvation and was rapidly decreased following addition of respiratory substrates. Furthermore, OPA1 oligomers were associated with maintenance of *cristae* width and assembly of the ATP synthase. In contrast with our results, MEFs bearing the Q297V OPA1 mutation in the GTPase domain did not exhibit increased oligomerization (76). The reason for this different behavior is not known.

We can only speculate that the increased oligomerization described in the present study may be due to a stronger affinity of the mutant proteins, supporting the dominant negative mechanism hypothesis. Indeed, the presence of an OPA1 mutant protein cohort with impaired GTPase activity and increased formation of oligomeric complexes, could explain how these mutant proteins prevent the wild type allele from having an attenuation effect against the mutation, as in the case of the haploinsufficiency mutations, with the formation of inactive wt/mutant hetero-oligomers. In this regard, the lack of a suitable assay for measuring the GTPase in-gel-activity of oligomers in the BN-gel hinders the possibility to verify this hypothesis, even if *in vitro* experiments demonstrated a reduced GTP hydrolysis activity for the two DOA plus mutations (65).

Since the OPA1 3D-structure has not been resolved experimentally yet (for example by X-ray crystallography or NMR spectroscopy), we do not know how every mutation could impact on the oligomers formation, even if the residue R445 was supposed to form a hydrogen bond with the N404 on another OPA1 protein (44).

It is of interest the finding that MEFs bearing the DOA "plus" mutations exhibited a drastic depletion of mtDNA, to levels comparable with those of Opa1-/- MEFs, while the other two mutants were comparable to controls. This is in contrast with what observed in fibroblasts. Given that all MEF cell lines share the same haplotype, as confirmed by the NGS analysis, and reveal no accumulation of micro or macro deletions, it seems that the mutations impact only on the quantity of mtDNA (in the most severe mutations) and not on its quality.

Nevertheless, this reduced mtDNA copy number caused a decreased expression of the mitochondria-encoded subunits of the respiratory complexes, mirrored by a lower amount

of assembled RCSs and partial disassembly of CV in the G439V and R445H mutants. It is hard to say if this reduced amount of assembled RCSs is only due to the reduced amount of protein or can be ascribed also to the partial disruption of the *cristae* architecture that these two mutants exhibit, since we previously reported a similar perturbation of RCSs organization in MEFs bearing the uncleavable form of isoform1, which exhibited a partial disruption of *cristae* architecture but no mtDNA depletion (20). Both the RCSs disassembly and the *cristae* disruption likely play a role in the manifest energetic dysfunctions associated with these mutations, mostly evidenced under conditions of metabolic stress.

The mitochondrial network morphology proved to be linearly correlated with the patients' clinical pictures, but in this case without being exposed to stressful conditions. In fact, while the two DOA mutations exhibited different percentage of cells with network fragmentation, with a more severe picture for the D603H, the two DOA "plus" mutants exhibited a totally fragmented network, in line with the patients' disease severity. The phenotype caused by the two DOA "plus" mutations located in the GTPase domain in close proximity to the nucleotide binding site, may involve the disruption of the GTPase activity, with a direct effect on the fusogenic capacity, as we previously proved to be for the G300E mutation (20).

Thus, considering all the phenotypes, the two DOA plus mutants, G439V and R445H, always showed a very severe phenotype whereas the mild DOA mutant, I382M, did not exhibit any significant dysfunction. In this regard, the new D603H DOA mutation presented only a few altered features, with no mtDNA perturbation, with weak energetic impairment but significantly fragmented mitochondrial network, exhibiting an intermediate phenotype, thus proving to well mirroring the patient clinical picture and being able to predict the mutation pathogenicity.

The therapeutic options for diseases linked to OPA1 mutations are still very limited.

Although DOA may be a good candidate for gene therapy, given the main ophthalmic manifestation of the symptoms, by now the only treatment showing some improvement in patients is that with idebenone, a short chain analogue of coenzyme Q10 already approved for the treatment of LHON (177). The need for new approaches is apparent.

In an attempt to develop a suitable therapeutic strategy for DOA, we characterized three "OPA1 Rescuing Molecules" or ORMs, taking advantage of the MEF model with OPA1 pathogenic mutations. These ORMs have been previously identified though a screening on a large library of bioactive molecules already FDA approved, performed on a yeast OPA1-Mgm1 chimaera(176).

The chemical entity of these molecules cannot be disclosed here for constraints due to intellectual property. Their chemical structures are not related, a common characteristic being the rather high hydrophobicity.

While the ORM11 failed to cause any positive effect on the biochemical features here investigated, the other two ORMs provided some interesting results, which deserve some comments.

Indeed, the ORM2 exhibited positive effects on the mitochondrial morphology and viability in both ISO1 and D603H, and slightly increased the ATP levels under stress conditions in the R445H and D603H mutant cells. Conversely, ORM12 showed no significant effect on mitochondrial morphology and ATP content, but significantly increased the viability under stress conditions in the two mutant cell lines. These results are clearly still preliminary, and more experiments are in progress to identify their molecular mechanisms, however it may be promising that both ORMs ameliorate the viability, ORM2 acting mostly at the level of network morphology, differently from ORM12. In particular, the improved viability may be due to an increase in OPA1 protein level or to changes in the long/short balance. In alternative activation of the mitochondrial biogenesis and mtDNA content might be involved. Other ORMs have been recently identified in yeast and their efficacy will be tested in the next future. These results are encouraging, suggesting that our cell model seems very suitable for the screening of active molecules with a therapeutic perspective.

In conclusion, we can state that, despite the large number of studies conducted on OPA1 since its discovery, to date not only we are not able to define a clear pathogenetic mechanism associated with the single mutation, but we are not even able to predict *a priori* the impact that a new mutation may have on the function of the protein on the basis of its position. Moreover, the lack of an efficient assay for the GTPase activity in native conditions, together with the deficiency of experimental resolution of the three-dimension structure, although partial computational models exist, do not allow to speculate too much on the possible implications of a mutation on OPA1 oligomerization status, which seems to be crucial for its function.

The MEF model here characterized, proved to be quick and relatively easy to obtain, can overcome some of the major fibroblasts limits, in particular reducing the biological variability, allowing to analyze the mutations in the same nuclear and mitochondrial genetic background. We present here evidence that this model exhibits a nice genotype/phenotype correlation with several mitochondrial dysfunctions in parallel with the severity of the

clinical phenotype of patients. Studies are ongoing to evaluate a number of other *OPA1* mutations, in order to further validate its efficacy in pathogenicity prediction.

Furthermore, this cellular model seems helpful to test the effectiveness of molecules against the pathology, as supported by our preliminary study here presented. Indeed we were able to observe some phenotype improvements due to treatment with a few ORMs, previously identified in a yeast hight throuput screeneng. Although premilinary, our results are encouraging and will be soon followed by further analyses, both in terms of biochemical phenotypes and of number of molecules analyzed. Indeed we are currently processing the data obtained from a metabolomic analysis, which hopefully may shed some more light on the pathogenic mechanisms behind OPA1 mutations.

BIBLIOGRAPHY

1. Eiberg H, Kjer B, Kjer P, Rosenberg T. Dominant optic atrophy (OPA1) mapped to chromosome 3q region. I. Linkage analysis. Hum Mol Genet. 1994 Jun;3(6):977–80.

2. Olichon A, Emorine LJ, Descoins E, Pelloquin L, Brichese L, Gas N, et al. The human dynamin-related protein OPA1 is anchored to the mitochondrial inner membrane facing the inter-membrane space. FEBS Lett. 2002 Jul 17;523(1–3):171–6.

3. Satoh M, Hamamoto T, Seo N, Kagawa Y, Endo H. Differential sublocalization of the dynamin-related protein OPA1 isoforms in mitochondria. Biochemical and Biophysical Research Communications. 2003 Jan;300(2):482–93.

4. Alexander C, Votruba M, Pesch UE, Thiselton DL, Mayer S, Moore A, et al. OPA1, encoding a dynamin-related GTPase, is mutated in autosomal dominant optic atrophy linked to chromosome 3q28. Nat Genet. 2000 Oct;26(2):211–5.

5. Delettre C, Lenaers G, Griffoin JM, Gigarel N, Lorenzo C, Belenguer P, et al. Nuclear gene OPA1, encoding a mitochondrial dynamin-related protein, is mutated in dominant optic atrophy. Nat Genet. 2000 Oct;26(2):207–10.

6. Kjer P. Infantile optic atrophy with dominant mode of inheritance: a clinical and genetic study of 19 Danish families. Acta Ophthalmol Suppl. 1959;164(Supp 54):1–147.

7. Misaka T, Miyashita T, Kubo Y. Primary Structure of a Dynamin-related Mouse Mitochondrial GTPase and Its Distribution in Brain, Subcellular Localization, and Effect on Mitochondrial Morphology. Journal of Biological Chemistry. 2002 May 3;277(18):15834–42.

8. Olichon A, Elachouri G, Baricault L, Delettre C, Belenguer P, Lenaers G. OPA1 alternate splicing uncouples an evolutionary conserved function in mitochondrial fusion from a vertebrate restricted function in apoptosis. Cell Death Differ. 2007 Apr;14(4):682–92.

9. Olichon A, Baricault L, Gas N, Guillou E, Valette A, Belenguer P, et al. Loss of OPA1 Perturbates the Mitochondrial Inner Membrane Structure and Integrity, Leading to Cytochrome *c* Release and Apoptosis. Journal of Biological Chemistry. 2003 Mar 7;278(10):7743–6.

10. Frezza C, Cipolat S, Martins de Brito O, Micaroni M, Beznoussenko GV, Rudka T, et al. OPA1 Controls Apoptotic Cristae Remodeling Independently from Mitochondrial Fusion. Cell. 2006 Jul;126(1):177–89.

11. Zanna C, Ghelli A, Porcelli AM, Karbowski M, Youle RJ, Schimpf S, et al. OPA1 mutations associated with dominant optic atrophy impair oxidative phosphorylation and mitochondrial fusion. Brain. 2008 Feb;131(2):352–67.

12. Cogliati S, Frezza C, Soriano ME, Varanita T, Quintana-Cabrera R, Corrado M, et al. Mitochondrial Cristae Shape Determines Respiratory Chain Supercomplexes Assembly and Respiratory Efficiency. Cell. 2013 Sep;155(1):160–71.

13. Elachouri G, Vidoni S, Zanna C, Pattyn A, Boukhaddaoui H, Gaget K, et al. OPA1 links human mitochondrial genome maintenance to mtDNA replication and distribution. Genome Research. 2011 Jan 1;21(1):12–20.

14. Delettre C, Griffoin J-M, Kaplan J, Dollfus H, Lorenz B, Faivre L, et al. Mutation spectrum and splicing variants in the OPA1 gene. Human Genetics. 2001 Dec;109(6):584–91.

15. Belenguer P, Pellegrini L. The dynamin GTPase OPA1: more than mitochondria? Biochim Biophys Acta. 2013 Jan;1833(1):176–83.

16. Akepati VR, Müller E-C, Otto A, Strauss HM, Portwich M, Alexander C. Characterization of OPA1 isoforms isolated from mouse tissues. Journal of Neurochemistry. 2008 Jul;106(1):372–83.

17. MacVicar T, Langer T. OPA1 processing in cell death and disease – the long and short of it. Journal of Cell Science. 2016 Jun 15;129(12):2297–306.

18. Song Z, Chen H, Fiket M, Alexander C, Chan DC. OPA1 processing controls mitochondrial fusion and is regulated by mRNA splicing, membrane potential, and Yme1L. The Journal of Cell Biology. 2007 Aug 27;178(5):749–55.

19. Rainbolt TK, Lebeau J, Puchades C, Wiseman RL. Reciprocal Degradation of YME1L and OMA1 Adapts Mitochondrial Proteolytic Activity during Stress. Cell Reports. 2016 Mar;14(9):2041–9.

20. Del Dotto V, Mishra P, Vidoni S, Fogazza M, Maresca A, Caporali L, et al. OPA1 Isoforms in the Hierarchical Organization of Mitochondrial Functions. Cell Reports. 2017 Jun;19(12):2557–71.

21. Ryu S-W, Han EC, Yoon J, Choi C. The Mitochondrial Fusion-Related Proteins Mfn2 and OPA1 are Transcriptionally Induced during Differentiation of Bone Marrow Progenitors to Immature Dendritic Cells. Molecules and Cells [Internet]. 2014 [cited 2017 Nov 2]; Available from: http://www.molcells.org/journal/view.html?doi=10.14348/molcells.2015.2285

22. Nan J, Hu H, Sun Y, Zhu L, Wang Y, Zhong Z, et al. TNFR2 Stimulation Promotes Mitochondrial Fusion via Stat3- and NF-kB–Dependent Activation of OPA1 ExpressionNovelty and Significance. Circulation Research. 2017 Aug 4;121(4):392–410.

23. Parra V, Verdejo HE, Iglewski M, Del Campo A, Troncoso R, Jones D, et al. Insulin stimulates mitochondrial fusion and function in cardiomyocytes via the Akt-mTOR-NFκB-Opa-1 signaling pathway. Diabetes. 2014 Jan;63(1):75–88.

24. Müller-Rischart AK, Pilsl A, Beaudette P, Patra M, Hadian K, Funke M, et al. The E3 Ligase Parkin Maintains Mitochondrial Integrity by Increasing Linear Ubiquitination of NEMO. Molecular Cell. 2013 Mar;49(5):908–21.

25. Laforge M, Rodrigues V, Silvestre R, Gautier C, Weil R, Corti O, et al. NF-κB pathway controls mitochondrial dynamics. Cell Death Differ. 2016 Jan;23(1):89–98.

26. Carrascoso I, Alcalde J, Sánchez-Jiménez C, González-Sánchez P, Izquierdo JM. T-Cell Intracellular Antigens and Hu Antigen R Antagonistically Modulate Mitochondrial Activity and Dynamics by Regulating Optic Atrophy 1 Gene Expression. Molecular and Cellular Biology. 2017 Sep 1;37(17):e00174-17.

27. Ishihara N, Fujita Y, Oka T, Mihara K. Regulation of mitochondrial morphology through proteolytic cleavage of OPA1. The EMBO journal. 2006;25(13):2966–2977.

28. Cipolat S, Rudka T, Hartmann D, Costa V, Serneels L, Craessaerts K, et al. Mitochondrial Rhomboid PARL Regulates Cytochrome c Release during Apoptosis via OPA1-Dependent Cristae Remodeling. Cell. 2006 Jul;126(1):163–75.

29. Koppen M, Langer T. Protein degradation within mitochondria: versatile activities of AAA proteases and other peptidases. Crit Rev Biochem Mol Biol. 2007 Jun;42(3):221–42.

30. Ehses S, Raschke I, Mancuso G, Bernacchia A, Geimer S, Tondera D, et al. Regulation of OPA1 processing and mitochondrial fusion by *m* -AAA protease isoenzymes and OMA1. The Journal of Cell Biology. 2009 Dec 28;187(7):1023–36.

31. Head B, Griparic L, Amiri M, Gandre-Babbe S, van der Bliek AM. Inducible proteolytic inactivation of OPA1 mediated by the OMA1 protease in mammalian cells. The Journal of Cell Biology. 2009 Dec 28;187(7):959–66.

32. Griparic L, Kanazawa T, van der Bliek AM. Regulation of the mitochondrial dynamin-like protein Opa1 by proteolytic cleavage. The Journal of Cell Biology. 2007 Aug 27;178(5):757–64.

33. Anand R, Wai T, Baker MJ, Kladt N, Schauss AC, Rugarli E, et al. The *i* -AAA protease YME1L and OMA1 cleave OPA1 to balance mitochondrial fusion and fission. The Journal of Cell Biology. 2014 Mar 17;204(6):919–29.

34. Kowno M, Watanabe-Susaki K, Ishimine H, Komazaki S, Enomoto K, Seki Y, et al. Prohibitin 2 Regulates the Proliferation and Lineage-Specific Differentiation of Mouse Embryonic Stem Cells in Mitochondria. Akagi T, editor. PLoS ONE. 2014 Apr 7;9(4):e81552.

35. Merkwirth C, Dargazanli S, Tatsuta T, Geimer S, Lower B, Wunderlich FT, et al. Prohibitins control cell proliferation and apoptosis by regulating OPA1-dependent cristae morphogenesis in mitochondria. Genes & Development. 2008 Feb 15;22(4):476–88.

36. Samant SA, Zhang HJ, Hong Z, Pillai VB, Sundaresan NR, Wolfgeher D, et al. SIRT3 Deacetylates and Activates OPA1 To Regulate Mitochondrial Dynamics during Stress. Molecular and Cellular Biology. 2014 Mar 1;34(5):807–19.

37. Stafa K, Tsika E, Moser R, Musso A, Glauser L, Jones A, et al. Functional interaction of Parkinson's disease-associated LRRK2 with members of the dynamin GTPase superfamily. Hum Mol Genet. 2014 Apr 15;23(8):2055–77.

38. Praefcke GJK, McMahon HT. The dynamin superfamily: universal membrane tubulation and fission molecules? Nature Reviews Molecular Cell Biology. 2004 Feb;5(2):133–47.

39. Niemann HH, Knetsch ML, Scherer A, Manstein DJ, Kull FJ. Crystal structure of a dynamin GTPase domain in both nucleotide-free and GDP-bound forms. EMBO J. 2001 Nov 1;20(21):5813–21.

40. Dadgar S, Hagens O, Dadgar SR, Haghighi EN, Schimpf S, Wissinger B, et al. Structural model of the OPA1 GTPase domain may explain the molecular consequences of a novel mutation in a family with autosomal dominant optic atrophy. Experimental Eye Research. 2006 Sep;83(3):702–6.

41. Low HH, Löwe J. A bacterial dynamin-like protein. Nature. 2006 Dec 7;444(7120):766–9.

42. Amati-Bonneau P, Valentino ML, Reynier P, Gallardo ME, Bornstein B, Boissiere A, et al. OPA1 mutations induce mitochondrial DNA instability and optic atrophy 'plus' phenotypes. Brain. 2008 Feb 1;131(2):338–51.

43. Chappie JS, Mears JA, Fang S, Leonard M, Schmid SL, Milligan RA, et al. A pseudoatomic model of the dynamin polymer identifies a hydrolysis-dependent powerstroke. Cell. 2011 Sep 30;147(1):209–22.

44. Namba K, Mutai H, Takiguchi Y, Yagi H, Okuyama T, Oba S, et al. Molecular impairment mechanisms of novel OPA1 mutations predicted by molecular modeling in patients with autosomal dominant optic atrophy and auditory neuropathy spectrum disorder. Otology & Neurotology. 2016;37(4):394–402.

45. Danino D, Hinshaw JE. Dynamin family of mechanoenzymes. Curr Opin Cell Biol. 2001 Aug;13(4):454–60.

46. Landes T, Leroy I, Bertholet A, Diot A, Khosrobakhsh F, Daloyau M, et al. OPA1 (dys)functions. Seminars in Cell & Developmental Biology. 2010 Aug;21(6):593–8.

47. Yamaguchi R, Lartigue L, Perkins G, Scott RT, Dixit A, Kushnareva Y, et al. Opa1-Mediated Cristae Opening Is Bax/Bak and BH3 Dependent, Required for Apoptosis, and Independent of Bak Oligomerization. Molecular Cell. 2008 Aug;31(4):557–69.

48. Varanita T, Soriano ME, Romanello V, Zaglia T, Quintana-Cabrera R, Semenzato M, et al. The Opa1-Dependent Mitochondrial Cristae Remodeling Pathway Controls Atrophic, Apoptotic, and Ischemic Tissue Damage. Cell Metabolism. 2015 Jun;21(6):834–44.

49. Glytsou C, Calvo E, Cogliati S, Mehrotra A, Anastasia I, Rigoni G, et al. Optic Atrophy 1 Is Epistatic to the Core MICOS Component MIC60 in Mitochondrial Cristae Shape Control. Cell Reports. 2016 Dec;17(11):3024–34.

50. Ding C, Wu Z, Huang L, Wang Y, Xue J, Chen S, et al. Mitofilin and CHCHD6 physically interact with Sam50 to sustain cristae structure. Sci Rep. 2015 Nov 4;5:16064.

51.   Takahashi K, Ohsawa I, Shirasawa T, Takahashi M. Optic atrophy 1 mediates coenzyme Q-responsive regulation of respiratory complex IV activity in brain mitochondria. Experimental Gerontology. 2017 Nov;98:217–23.

52.   Boissan M, Montagnac G, Shen Q, Griparic L, Guitton J, Romao M, et al. Nucleoside diphosphate kinases fuel dynamin superfamily proteins with GTP for membrane remodeling. Science. 2014 Jun 27;344(6191):1510–5.

53.   Huang G, Massoudi D, Muir AM, Joshi DC, Zhang C-L, Chiu SY, et al. WBSCR16 Is a Guanine Nucleotide Exchange Factor Important for Mitochondrial Fusion. Cell Rep. 2017 Jul 25;20(4):923–34.

54.   Schlattner U, Tokarska-Schlattner M, Ramirez S, Tyurina YY, Amoscato AA, Mohammadyani D, et al. Dual function of mitochondrial Nm23-H4 protein in phosphotransfer and intermembrane lipid transfer: a cardiolipin-dependent switch. J Biol Chem. 2013 Jan 4;288(1):111–21.

55.   Lang A, Anand R, Altinoluk-Hambüchen S, Ezzahoini H, Stefanski A, Iram A, et al. SIRT4 interacts with OPA1 and regulates mitochondrial quality control and mitophagy. Aging (Albany NY). 2017 Oct 29;9(10):2163–89.

56.   Norton M, Ng AC-H, Baird S, Dumoulin A, Shutt T, Mah N, et al. ROMO1 is an essential redox-dependent regulator of mitochondrial dynamics. Sci Signal. 2014 Jan 28;7(310):ra10.

57.   An H-J, Cho G, Lee J-O, Paik S-G, Kim YS, Lee H. Higd-1a interacts with Opa1 and is required for the morphological and functional integrity of mitochondria. Proceedings of the National Academy of Sciences. 2013 Aug 6;110(32):13014–9.

58.   Chen M, Chen Z, Wang Y, Tan Z, Zhu C, Li Y, et al. Mitophagy receptor FUNDC1 regulates mitochondrial dynamics and mitophagy. Autophagy. 2016;12(4):689–702.

59.   Kieper N, Holmström KM, Ciceri D, Fiesel FC, Wolburg H, Ziviani E, et al. Modulation of mitochondrial function and morphology by interaction of Omi/HtrA2 with the mitochondrial fusion factor OPA1. Experimental Cell Research. 2010 Apr;316(7):1213–24.

60.   Cipolat S, de Brito OM, Dal Zilio B, Scorrano L. OPA1 requires mitofusin 1 to promote mitochondrial fusion. Proceedings of the National Academy of Sciences of the United States of America. 2004;101(45):15927–15932.

61.   Griparic L, van der Wel NN, Orozco IJ, Peters PJ, van der Bliek AM. Loss of the Intermembrane Space Protein Mgm1/OPA1 Induces Swelling and Localized Constrictions along the Lengths of Mitochondria. Journal of Biological Chemistry. 2004 Apr 30;279(18):18792–8.

62.   Misaka T, Murate M, Fujimoto K, Kubo Y. The dynamin-related mouse mitochondrial GTPase OPA1 alters the structure of the mitochondrial inner membrane when exogenously introduced into COS-7 cells. Neurosci Res. 2006 Jun;55(2):123–33.

63. Civiletto G, Varanita T, Cerutti R, Gorletta T, Barbaro S, Marchet S, et al. Opa1 Overexpression Ameliorates the Phenotype of Two Mitochondrial Disease Mouse Models. Cell Metabolism. 2015 Jun;21(6):845–54.

64. Lee H, Smith SB, Yoon Y. The short variant of the mitochondrial dynamin OPA1 maintains mitochondrial energetics and cristae structure. Journal of Biological Chemistry. 2017 Apr 28;292(17):7115–30.

65. Ban T, Heymann JAW, Song Z, Hinshaw JE, Chan DC. OPA1 disease alleles causing dominant optic atrophy have defects in cardiolipin-stimulated GTP hydrolysis and membrane tubulation. Human Molecular Genetics. 2010 Jun 1;19(11):2113–22.

66. Ban T, Ishihara T, Kohno H, Saita S, Ichimura A, Maenaka K, et al. Molecular basis of selective mitochondrial fusion by heterotypic action between OPA1 and cardiolipin. Nat Cell Biol. 2017 Jul;19(7):856–63.

67. Sun Y, Xue W, Song Z, Huang K, Zheng L. Restoration of Opa1-long isoform inhibits retinal injury-induced neurodegeneration. J Mol Med. 2016 Mar;94(3):335–46.

68. Wai T, García-Prieto J, Baker MJ, Merkwirth C, Benit P, Rustin P, et al. Imbalanced OPA1 processing and mitochondrial fragmentation cause heart failure in mice. Science. 2015 Dec 4;350(6265):aad0116.

69. Frey TG, Mannella CA. The internal structure of mitochondria. Trends Biochem Sci. 2000 Jul;25(7):319–24.

70. Amutha B, Gordon DM, Gu Y, Pain D. A novel role of Mgm1p, a dynamin-related GTPase, in ATP synthase assembly and cristae formation/maintenance. Biochem J. 2004 Jul 1;381(Pt 1):19–23.

71. Alavi MV, Bette S, Schimpf S, Schuettauf F, Schraermeyer U, Wehrl HF, et al. A splice site mutation in the murine Opa1 gene features pathology of autosomal dominant optic atrophy. Brain. 2007 Apr;130(Pt 4):1029–42.

72. Davies VJ, Hollins AJ, Piechota MJ, Yip W, Davies JR, White KE, et al. Opa1 deficiency in a mouse model of autosomal dominant optic atrophy impairs mitochondrial morphology, optic nerve structure and visual function. Hum Mol Genet. 2007 Jun 1;16(11):1307–18.

73. Sarzi E, Angebault C, Seveno M, Gueguen N, Chaix B, Bielicki G, et al. The human OPA1delTTAG mutation induces premature age-related systemic neurodegeneration in mouse. Brain. 2012 Dec;135(12):3599–613.

74. Williams PA, Piechota M, von Ruhland C, Taylor E, Morgan JE, Votruba M. Opa1 is essential for retinal ganglion cell synaptic architecture and connectivity. Brain. 2012 Feb 1;135(2):493–505.

75. Song Z, Ghochani M, McCaffery JM, Frey TG, Chan DC. Mitofusins and OPA1 mediate sequential steps in mitochondrial membrane fusion. Molecular biology of the cell. 2009;20(15):3525–3532.

76. Patten DA, Wong J, Khacho M, Soubannier V, Mailloux RJ, Pilon-Larose K, et al. OPA1-dependent cristae modulation is essential for cellular adaptation to metabolic demand. EMBO J. 2014 Nov 18;33(22):2676–91.

77. Gomes LC, Di Benedetto G, Scorrano L. During autophagy mitochondria elongate, are spared from degradation and sustain cell viability. Nat Cell Biol. 2011 May;13(5):589–98.

78. Agier V, Oliviero P, Lainé J, L'Hermitte-Stead C, Girard S, Fillaut S, et al. Defective mitochondrial fusion, altered respiratory function, and distorted cristae structure in skin fibroblasts with heterozygous OPA1 mutations. Biochimica et Biophysica Acta (BBA) - Molecular Basis of Disease. 2012 Oct;1822(10):1570–80.

79. Amati-Bonneau P, Guichet A, Olichon A, Chevrollier A, Viala F, Miot S, et al. OPA1 R445H mutation in optic atrophy associated with sensorineural deafness. Ann Neurol. 2005 Dec;58(6):958–63.

80. Chevrollier A, Guillet V, Loiseau D, Gueguen N, de Crescenzo M-AP, Verny C, et al. Hereditary optic neuropathies share a common mitochondrial coupling defect. Ann Neurol. 2008 Jun;63(6):794–8.

81. Van Bergen NJ, Crowston JG, Kearns LS, Staffieri SE, Hewitt AW, Cohn AC, et al. Mitochondrial oxidative phosphorylation compensation may preserve vision in patients with OPA1-linked autosomal dominant optic atrophy. PLoS ONE. 2011;6(6):e21347.

82. Lodi R, Tonon C, Valentino ML, Iotti S, Clementi V, Malucelli E, et al. Deficit of in vivo mitochondrial ATP production in OPA1-related dominant optic atrophy. Ann Neurol. 2004 Nov;56(5):719–23.

83. Lodi R, Tonon C, Valentino ML, Manners D, Testa C, Malucelli E, et al. Defective mitochondrial adenosine triphosphate production in skeletal muscle from patients with dominant optic atrophy due to OPA1 mutations. Arch Neurol. 2011 Jan;68(1):67–73.

84. Chen H, Chomyn A, Chan DC. Disruption of fusion results in mitochondrial heterogeneity and dysfunction. J Biol Chem. 2005 Jul 15;280(28):26185–92.

85. Lee H, Yoon Y. Transient Contraction of Mitochondria Induces Depolarization through the Inner Membrane Dynamin OPA1 Protein. Journal of Biological Chemistry. 2014 Apr 25;289(17):11862–72.

86. Santo-Domingo J, Giacomello M, Poburko D, Scorrano L, Demaurex N. OPA1 promotes pH flashes that spread between contiguous mitochondria without matrix protein exchange. EMBO J. 2013 Jul 3;32(13):1927–40.

87. Rosselin M, Santo-Domingo J, Bermont F, Giacomello M, Demaurex N. L-OPA1 regulates mitoflash biogenesis independently from membrane fusion. EMBO reports. 2017 Mar;18(3):451–63.

88. Richter-Dennerlein R, Korwitz A, Haag M, Tatsuta T, Dargazanli S, Baker M, et al. DNAJC19, a mitochondrial cochaperone associated with cardiomyopathy, forms a

complex with prohibitins to regulate cardiolipin remodeling. Cell Metab. 2014 Jul 1;20(1):158–71.

89. Korwitz A, Merkwirth C, Richter-Dennerlein R, Tröder SE, Sprenger H-G, Quirós PM, et al. Loss of OMA1 delays neurodegeneration by preventing stress-induced OPA1 processing in mitochondria. The Journal of Cell Biology. 2016 Jan 18;212(2):157–66.

90. Jones BA, Fangman WL. Mitochondrial DNA maintenance in yeast requires a protein containing a region related to the GTP-binding domain of dynamin. Genes Dev. 1992 Mar;6(3):380–9.

91. Pelloquin L, Belenguer P, Menon Y, Ducommun B. Identification of a fission yeast dynamin-related protein involved in mitochondrial DNA maintenance. Biochem Biophys Res Commun. 1998 Oct 29;251(3):720–6.

92. Bogenhagen DF, Rousseau D, Burke S. The layered structure of human mitochondrial DNA nucleoids. J Biol Chem. 2008 Feb 8;283(6):3665–75.

93. Spelbrink JN. Functional organization of mammalian mitochondrial DNA in nucleoids: history, recent developments, and future challenges. IUBMB Life. 2010 Jan;62(1):19–32.

94. Youle RJ, Van Der Bliek AM. Mitochondrial fission, fusion, and stress. Science. 2012;337(6098):1062–1065.

95. Carelli V, Chan DC. Mitochondrial DNA: impacting central and peripheral nervous systems. Neuron. 2014 Dec 17;84(6):1126–42.

96. Hudson G, Amati-Bonneau P, Blakely EL, Stewart JD, He L, Schaefer AM, et al. Mutation of OPA1 causes dominant optic atrophy with external ophthalmoplegia, ataxia, deafness and multiple mitochondrial DNA deletions: a novel disorder of mtDNA maintenance. Brain. 2008 Feb;131(2):329–37.

97. Yu-Wai-Man P, Griffiths PG, Burke A, Sellar PW, Clarke MP, Gnanaraj L, et al. The prevalence and natural history of dominant optic atrophy due to OPA1 mutations. Ophthalmology. 2010 Aug;117(8):1538–1546, 1546.e1.

98. Kim JY, Hwang J-M, Ko HS, Seong M-W, Park B-J, Park SS. Mitochondrial DNA content is decreased in autosomal dominant optic atrophy. Neurology. 2005 Mar 22;64(6):966–72.

99. Wong ED, Wagner JA, Gorsich SW, McCaffery JM, Shaw JM, Nunnari J. The dynamin-related GTPase, Mgm1p, is an intermembrane space protein required for maintenance of fusion competent mitochondria. J Cell Biol. 2000 Oct 16;151(2):341–52.

100. Lee Y, Jeong S-Y, Karbowski M, Smith CL, Youle RJ. Roles of the mammalian mitochondrial fission and fusion mediators Fis1, Drp1, and Opa1 in apoptosis. Mol Biol Cell. 2004 Nov;15(11):5001–11.

101. Olichon A, Landes T, Arnauné-Pelloquin L, Emorine LJ, Mils V, Guichet A, et al. Effects of OPA1 mutations on mitochondrial morphology and apoptosis: Relevance to ADOA pathogenesis. Journal of Cellular Physiology. 2007 May;211(2):423–30.

102. Cornille K, Milea D, Amati-Bonneau P, Procaccio V, Zazoun L, Guillet V, et al. Reversible optic neuropathy with OPA1 exon 5b mutation. Ann Neurol. 2008 May;63(5):667–71.

103. Scorrano L, Ashiya M, Buttle K, Weiler S, Oakes SA, Mannella CA, et al. A distinct pathway remodels mitochondrial cristae and mobilizes cytochrome c during apoptosis. Dev Cell. 2002 Jan;2(1):55–67.

104. Alavi MV, Fuhrmann N. Dominant optic atrophy, OPA1, and mitochondrial quality control: understanding mitochondrial network dynamics. Molecular neurodegeneration. 2013;8(1):32.

105. Landes T, Emorine LJ, Courilleau D, Rojo M, Belenguer P, Arnauné-Pelloquin L. The BH3-only Bnip3 binds to the dynamin Opa1 to promote mitochondrial fragmentation and apoptosis by distinct mechanisms. EMBO Rep. 2010 Jun;11(6):459–65.

106. Ott M, Zhivotovsky B, Orrenius S. Role of cardiolipin in cytochrome c release from mitochondria. Cell Death Differ. 2007 Jul;14(7):1243–7.

107. Kushnareva Y, Seong Y, Andreyev AY, Kuwana T, Kiosses WB, Votruba M, et al. Mitochondrial dysfunction in an Opa1(Q285STOP) mouse model of dominant optic atrophy results from Opa1 haploinsufficiency. Cell Death Dis. 2016 Jul 28;7:e2309.

108. Barrera M, Koob S, Dikov D, Vogel F, Reichert AS. OPA1 functionally interacts with MIC60 but is dispensable for crista junction formation. FEBS Letters. 2016 Oct;590(19):3309–22.

109. Tsujimoto Y, Shimizu S. Another way to die: autophagic programmed cell death. Cell Death Differ. 2005 Nov;12 Suppl 2:1528–34.

110. Schweichel JU, Merker HJ. The morphology of various types of cell death in prenatal tissues. Teratology. 1973 Jun;7(3):253–66.

111. Kroemer G, Galluzzi L, Vandenabeele P, Abrams J, Alnemri ES, Baehrecke EH, et al. Classification of cell death: recommendations of the Nomenclature Committee on Cell Death 2009. Cell Death Differ. 2009 Jan;16(1):3–11.

112. White KE, Davies VJ, Hogan VE, Piechota MJ, Nichols PP, Turnbull DM, et al. OPA1 Deficiency Associated with Increased Autophagy in Retinal Ganglion Cells in a Murine Model of Dominant Optic Atrophy. Investigative Opthalmology & Visual Science. 2009 Jun 1;50(6):2567.

113. Burté F, Carelli V, Chinnery PF, Yu-Wai-Man P. Disturbed mitochondrial dynamics and neurodegenerative disorders. Nat Rev Neurol. 2015 Jan;11(1):11–24.

114. Twig G, Elorza A, Molina AJA, Mohamed H, Wikstrom JD, Walzer G, et al. Fission and selective fusion govern mitochondrial segregation and elimination by autophagy. EMBO J. 2008 Jan 23;27(2):433–46.

115. Moulis MF, Millet AM, Daloyau M, Miquel M-C, Ronsin B, Wissinger B, et al. OPA1 haploinsufficiency induces a BNIP3-dependent decrease in mitophagy in neurons: relevance to Dominant Optic Atrophy. Journal of Neurochemistry. 2017 Feb;140(3):485–94.

116. Kane MS, Alban J, Desquiret-Dumas V, Gueguen N, Ishak L, Ferre M, et al. Autophagy controls the pathogenicity of *OPA1* mutations in dominant optic atrophy. Journal of Cellular and Molecular Medicine. 2017 Oct;21(10):2284–97.

117. Liao C, Ashley N, Diot A, Morten K, Phadwal K, Williams A, et al. Dysregulated mitophagy and mitochondrial organization in optic atrophy due to OPA1 mutations. Neurology. 2017;88(2):131–142.

118. Fülöp L, Szanda G, Enyedi B, Várnai P, Spät A. The effect of OPA1 on mitochondrial Ca 2+ signaling. PLoS One. 2011;6(9):e25199.

119. Fülöp L, Rajki A, Maka E, Molnár MJ, Spät A. Mitochondrial Ca2+ uptake correlates with the severity of the symptoms in autosomal dominant optic atrophy. Cell Calcium. 2015 Jan;57(1):49–55.

120. Kushnareva YE, Gerencser AA, Bossy B, Ju WK, White AD, Waggoner J, et al. Loss of OPA1 disturbs cellular calcium homeostasis and sensitizes for excitotoxicity. Cell Death & Differentiation. 2013;20(2):353–365.

121. Dayanithi G, Chen-Kuo-Chang M, Viero C, Hamel C, Muller A, Lenaers G. Characterization of Ca $^{2+}$ Signalling in Postnatal Mouse Retinal Ganglion Cells: Involvement of OPA1 in Ca $^{2+}$ Clearance. Ophthalmic Genetics. 2010 Jun;31(2):53–65.

122. Cho D-H, Nakamura T, Fang J, Cieplak P, Godzik A, Gu Z, et al. S-Nitrosylation of Drp1 Mediates β-Amyloid-Related Mitochondrial Fission and Neuronal Injury. Science. 2009 Apr 3;324(5923):102–5.

123. Manev H, Favaron M, Guidotti A, Costa E. Delayed increase of Ca2+ influx elicited by glutamate: role in neuronal death. Molecular pharmacology. 1989;36(1):106–112.

124. Randall RD, Thayer SA. Glutamate-induced calcium transient triggers delayed calcium overload and neurotoxicity in rat hippocampal neurons. Journal of Neuroscience. 1992;12(5):1882–1895.

125. Abramov AY, Duchen MR. Impaired mitochondrial bioenergetics determines glutamate-induced delayed calcium deregulation in neurons. Biochim Biophys Acta. 2010 Mar;1800(3):297–304.

126. Budd SL, Nicholls DG. Mitochondria, calcium regulation, and acute glutamate excitotoxicity in cultured cerebellar granule cells. J Neurochem. 1996 Dec;67(6):2282–91.

127. Ullian E., Barkis W., Chen S, Diamond J., Barres B. Invulnerability of retinal ganglion cells to NMDA excitotoxicity. Molecular and Cellular Neuroscience. 2004 Aug;26(4):544–57.

128. Jahani-Asl A, Pilon-Larose K, Xu W, MacLaurin JG, Park DS, McBride HM, et al. The Mitochondrial Inner Membrane GTPase, Optic Atrophy 1 (Opa1), Restores Mitochondrial Morphology and Promotes Neuronal Survival following Excitotoxicity. Journal of Biological Chemistry. 2011 Feb 11;286(6):4772–82.

129. Nguyen D, Alavi MV, Kim K-Y, Kang T, Scott RT, Noh YH, et al. A new vicious cycle involving glutamate excitotoxicity, oxidative stress and mitochondrial dynamics. Cell Death and Disease. 2011 Dec;2(12):e240.

130. Dutta R, Trapp BD. Mechanisms of neuronal dysfunction and degeneration in multiple sclerosis. Progress in Neurobiology. 2011 Jan;93(1):1–12.

131. Maltecca F, De Stefani D, Cassina L, Consolato F, Wasilewski M, Scorrano L, et al. Respiratory dysfunction by AFG3L2 deficiency causes decreased mitochondrial calcium uptake via organellar network fragmentation. Human Molecular Genetics. 2012 Sep 1;21(17):3858–70.

132. Chao de la Barca JM, Simard G, Sarzi E, Chaumette T, Rousseau G, Chupin S, et al. Targeted Metabolomics Reveals Early Dominant Optic Atrophy Signature in Optic Nerves of *Opa1* [delTTAG/+] Mice. Investigative Opthalmology & Visual Science. 2017 Feb 3;58(2):812.

133. Son JM, Sarsour EH, Kakkerla Balaraju A, Fussell J, Kalen AL, Wagner BA, et al. Mitofusin 1 and optic atrophy 1 shift metabolism to mitochondrial respiration during aging. Aging Cell. 2017 Oct;16(5):1136–45.

134. Tezze C, Romanello V, Desbats MA, Fadini GP, Albiero M, Favaro G, et al. Age-Associated Loss of OPA1 in Muscle Impacts Muscle Mass, Metabolic Homeostasis, Systemic Inflammation, and Epithelial Senescence. Cell Metabolism. 2017 Jun;25(6):1374–1389.e6.

135. Kita T, Nishida H, Shibata H, Niimi S, Higuti T, Arakaki N. Possible Role of Mitochondrial Remodelling on Cellular Triacylglycerol Accumulation. Journal of Biochemistry. 2009 Dec 1;146(6):787–96.

136. Wikstrom JD, Mahdaviani K, Liesa M, Sereda SB, Si Y, Las G, et al. Hormone-induced mitochondrial fission is utilized by brown adipocytes as an amplification pathway for energy expenditure. The EMBO Journal. 2014 Jan;n/a-n/a.

137. Pidoux G, Witczak O, Jarn\a ess E, Myrvold L, Urlaub H, Stokka AJ, et al. Optic Atrophy 1 is an A-kinase anchoring protein on lipid droplets that mediates adrenergic control of lipolysis. The EMBO journal. 2011;30(21):4371–4386.

138. Quirós PM, Ramsay AJ, Sala D, Fernández-Vizarra E, Rodríguez F, Peinado JR, et al. Loss of mitochondrial protease OMA1 alters processing of the GTPase OPA1 and causes obesity and defective thermogenesis in mice. The EMBO journal. 2012;31(9):2117–2133.

139. Carelli V, Ross-Cisneros FN, Sadun AA. Mitochondrial dysfunction as a cause of optic neuropathies. Prog Retin Eye Res. 2004 Jan;23(1):53–89.

140. Delettre C, Lenaers G, Pelloquin L, Belenguer P, Hamel CP. OPA1 (Kjer Type) Dominant Optic Atrophy: A Novel Mitochondrial Disease. Molecular Genetics and Metabolism. 2002 Feb;75(2):97–107.

141. Lenaers G, Hamel C, Delettre C, Amati-Bonneau P, Procaccio V, Bonneau D, et al. Dominant optic atrophy. Orphanet J Rare Dis. 2012 Jul 9;7:46.

142. Barboni P, Savini G, Parisi V, Carbonelli M, La Morgia C, Maresca A, et al. Retinal nerve fiber layer thickness in dominant optic atrophy measurements by optical coherence tomography and correlation with age. Ophthalmology. 2011 Oct;118(10):2076–80.

143. Barboni P, Savini G, Cascavilla ML, Caporali L, Milesi J, Borrelli E, et al. Early macular retinal ganglion cell loss in dominant optic atrophy: genotype-phenotype correlation. Am J Ophthalmol. 2014 Sep;158(3):628–636.e3.

144. Milea D, Sander B, Wegener M, Jensen H, Kjer B, Jørgensen TM, et al. Axonal loss occurs early in dominant optic atrophy. Acta Ophthalmol. 2010 May;88(3):342–6.

145. Chen H, Chan DC. Critical dependence of neurons on mitochondrial dynamics. Curr Opin Cell Biol. 2006 Aug;18(4):453–9.

146. Bertholet AM, Millet AME, Guillermin O, Daloyau M, Davezac N, Miquel M-C, et al. OPA1 loss of function affects in vitro neuronal maturation. Brain. 2013 May;136(Pt 5):1518–33.

147. Williams PA, Morgan JE, Votruba M. Opa1 deficiency in a mouse model of dominant optic atrophy leads to retinal ganglion cell dendropathy. Brain. 2010 Oct;133(10):2942–51.

148. Ferré M, Caignard A, Milea D, Leruez S, Cassereau J, Chevrollier A, et al. Improved locus-specific database for OPA1 mutations allows inclusion of advanced clinical data. Hum Mutat. 2015 Jan;36(1):20–5.

149. Pesch UE, Leo-Kottler B, Mayer S, Jurklies B, Kellner U, Apfelstedt-Sylla E, et al. OPA1 mutations in patients with autosomal dominant optic atrophy and evidence for semi-dominant inheritance. Hum Mol Genet. 2001 Jun 15;10(13):1359–68.

150. Konigsmark BW, Knox DL, Hussels IE, Moses H. Dominant congenital deafness and progressive optic nerve atrophy. Occurrence in four generations of a family. Arch Ophthalmol. 1974 Feb;91(2):99–103.

151. Ozden S, Düzcan F, Wollnik B, Cetin OG, Sahiner T, Bayramoğlu I, et al. Progressive autosomal dominant optic atrophy and sensorineural hearing loss in a Turkish family. Ophthalmic Genet. 2002 Mar;23(1):29–36.

152. Amati-Bonneau P, Odent S, Derrien C, Pasquier L, Malthiéry Y, Reynier P, et al. The association of autosomal dominant optic atrophy and moderate deafness may be

due to the R445H mutation in the OPA1 gene. Am J Ophthalmol. 2003 Dec;136(6):1170–1.

153. Shimizu S, Mori N, Kishi M, Sugata H, Tsuda A, Kubota N. A novel mutation in the OPA1 gene in a Japanese patient with optic atrophy. Am J Ophthalmol. 2003 Feb;135(2):256–7.

154. Payne M, Yang Z, Katz BJ, Warner JEA, Weight CJ, Zhao Y, et al. Dominant optic atrophy, sensorineural hearing loss, ptosis, and ophthalmoplegia: a syndrome caused by a missense mutation in OPA1. Am J Ophthalmol. 2004 Nov;138(5):749–55.

155. Yu-Wai-Man P, Griffiths PG, Gorman GS, Lourenco CM, Wright AF, Auer-Grumbach M, et al. Multi-system neurological disease is common in patients with OPA1 mutations. Brain. 2010 Mar;133(3):771–86.

156. Leruez S, Milea D, Defoort-Dhellemmes S, Colin E, Crochet M, Procaccio V, et al. Sensorineural hearing loss in OPA1-linked disorders. Brain. 2013 Jul;136(Pt 7):e236.

157. Milone M, Younge BR, Wang J, Zhang S, Wong L-J. Mitochondrial disorder with OPA1 mutation lacking optic atrophy. Mitochondrion. 2009 Jul;9(4):279–81.

158. Verny C, Loiseau D, Scherer C, Lejeune P, Chevrollier A, Gueguen N, et al. Multiple sclerosis-like disorder in OPA1-related autosomal dominant optic atrophy. Neurology. 2008 Mar 25;70(13 Pt 2):1152–3.

159. Marelli C, Amati-Bonneau P, Reynier P, Layet V, Layet A, Stevanin G, et al. Heterozygous OPA1 mutations in Behr syndrome. Brain. 2011 Apr;134(Pt 4):e169; author reply e170.

160. Carelli V, Musumeci O, Caporali L, Zanna C, La Morgia C, Del Dotto V, et al. Syndromic parkinsonism and dementia associated with *OPA 1* missense mutations: *OPA1* Mutations. Annals of Neurology. 2015 Jul;78(1):21–38.

161. Bonifert T, Karle KN, Tonagel F, Batra M, Wilhelm C, Theurer Y, et al. Pure and syndromic optic atrophy explained by deep intronic OPA1 mutations and an intralocus modifier. Brain. 2014 Aug 1;137(8):2164–77.

162. Bonneau D, Colin E, Oca F, Ferré M, Chevrollier A, Guéguen N, et al. Early-onset Behr syndrome due to compound heterozygous mutations in OPA1. Brain. 2014 Oct;137(Pt 10):e301.

163. Carelli V, Sabatelli M, Carrozzo R, Rizza T, Schimpf S, Wissinger B, et al. 'Behr syndrome' with OPA1 compound heterozygote mutations. Brain. 2015 Jan;138(Pt 1):e321.

164. Schaaf CP, Blazo M, Lewis RA, Tonini RE, Takei H, Wang J, et al. Early-onset severe neuromuscular phenotype associated with compound heterozygosity for OPA1 mutations. Mol Genet Metab. 2011 Aug;103(4):383–7.

165. Lee J, Jung S-C, Hong YB, Yoo JH, Koo H, Lee JH, et al. Recessive optic atrophy, sensorimotor neuropathy and cataract associated with novel compound heterozygous mutations in OPA1. Mol Med Rep. 2016 Jul;14(1):33–40.

166. Rubegni A, Pisano T, Bacci G, Tessa A, Battini R, Procopio E, et al. Leigh-like neuroimaging features associated with new biallelic mutations in OPA1. Eur J Paediatr Neurol. 2017 Jul;21(4):671–7.

167. Spiegel R, Saada A, Flannery PJ, Burté F, Soiferman D, Khayat M, et al. Fatal infantile mitochondrial encephalomyopathy, hypertrophic cardiomyopathy and optic atrophy associated with a homozygous OPA1 mutation. J Med Genet. 2016 Feb;53(2):127–31.

168. Nasca A, Rizza T, Doimo M, Legati A, Ciolfi A, Diodato D, et al. Not only dominant, not only optic atrophy: expanding the clinical spectrum associated with OPA1 mutations. Orphanet J Rare Dis. 2017 May 12;12(1):89.

169. Chen H, Detmer SA, Ewald AJ, Griffin EE, Fraser SE, Chan DC. Mitofusins Mfn1 and Mfn2 coordinately regulate mitochondrial fusion and are essential for embryonic development. J Cell Biol. 2003 Jan 20;160(2):189–200.

170. Zanna C, Ghelli A, Porcelli AM, Martinuzzi A, Carelli V, Rugolo M. Caspase-independent death of Leber's hereditary optic neuropathy cybrids is driven by energetic failure and mediated by AIF and Endonuclease G. Apoptosis. 2005 Oct;10(5):997–1007.

171. Bradford MM. A rapid and sensitive method for the quantitation of microgram quantities of protein utilizing the principle of protein-dye binding. Anal Biochem. 1976 May 7;72:248–54.

172. Giordano C, Iommarini L, Giordano L, Maresca A, Pisano A, Valentino ML, et al. Efficient mitochondrial biogenesis drives incomplete penetrance in Leber's hereditary optic neuropathy. Brain. 2014 Feb;137(Pt 2):335–53.

173. Melov S, Hinerfeld D, Esposito L, Wallace DC. Multi-organ characterization of mitochondrial genomic rearrangements in ad libitum and caloric restricted mice show striking somatic mitochondrial DNA rearrangements with age. Nucleic Acids Res. 1997 Mar 1;25(5):974–82.

174. Ghelli A, Tropeano CV, Calvaruso MA, Marchesini A, Iommarini L, Porcelli AM, et al. The cytochrome b p.278Y>C mutation causative of a multisystem disorder enhances superoxide production and alters supramolecular interactions of respiratory chain complexes. Hum Mol Genet. 2013 Jun 1;22(11):2141–51.

175. Porcelli AM, Angelin A, Ghelli A, Mariani E, Martinuzzi A, Carelli V, et al. Respiratory complex I dysfunction due to mitochondrial DNA mutations shifts the voltage threshold for opening of the permeability transition pore toward resting levels. J Biol Chem. 2009 Jan 23;284(4):2045–52.

176. Nolli C, Goffrini P, Lazzaretti M, Zanna C, Vitale R, Lodi T, et al. Validation of a MGM1/OPA1 chimeric gene for functional analysis in yeast of mutations associated with dominant optic atrophy. Mitochondrion. 2015 Nov;25:38–48.

177. Barboni P, Valentino ML, La Morgia C, Carbonelli M, Savini G, De Negri A, et al. Idebenone treatment in patients with OPA1-mutant dominant optic atrophy. Brain. 2013 Feb;136(Pt 2):e231.